Thermodynamic Analysis of Hybrid Molten Carbonate Fuel Cell Systems

by

Ramin Rashidi

A Thesis Submitted in Partial Fulfillment

of the Requirements for the Degree of

Master of Applied Science

in

The Faculty of Engineering and Applied Science

Mechanical Engineering Program

University of Ontario Institute of Technology

December 2008

Abstract

This study deals with the thermodynamic analysis of a molten carbonate fuel cell (MCFC) hybrid system to determine its efficiencies, irreversibilities and performance. The analysis includes a performance investigation of a typical molten carbonate fuel cell stack, an industrial MCFC hybrid system, and an MCFC hybrid system deployed by Enbridge. A parametric study is performed to examine the effects of varying operating conditions on the performance of the system. Furthermore, thermodynamic irreversibilities in each component are determined and an optimization of the fuel cell is conducted. Finally, a simplified and novel method is used for the cost analysis of the Enbridge MCFC hybrid system.

An exergy analysis of the hybrid MCFC systems demonstrates that overall efficiencies of up to 60 % are achievable. The maximum exergy destruction was found in components in which chemical reactions occur. In addition, the turboexpander is one of the major contributors to the overall exergy destruction of the system.

The cost analysis of the Enbridge system illustrates that by merging the importance of “green” energy and rising costs of carbon offsets, this new technology could be a promising solution and substitute for future energy supply.

Keywords: *Molten Carbonate Fuel Cell, energy, exergy, optimization, efficiency, combined system, cost analysis.*

Acknowledgments

It is a pleasure to thank the many people who made this thesis possible.

Firstly, I would like to express my deep and sincere gratitude to my supervisors Dr. Ibrahim Dincer and Dr. Peter Berg for their constructive support and guidance. Their thoughtful advice from the very first days have always motivated me and gave me the confidence to tackle my studies successfully. Moreover, the financial support from Enbridge Inc. and NSERC is appreciated.

I would like to thank the exam committee members, for their time in revising my thesis and their helpful recommendations.

Also, I would like to express my great appreciations to the faculty and staff of the Faculty of Engineering and Applied Science at UOIT. Their great assistance and support is always appreciated.

Moreover, the encouraging company of Prof. Dincer’s research group, especially Yousef Haseli, David MacPhee, Calin Zamfirescu and Fatih Orhan, made my research more interesting.

I am indebted to my many student colleagues, Masoud Charkhabi, Hassan Nojoumi, Pooya Saneipour and Payam Bahadorani for having provided an educational, fun and simulating environment for me.

Lastly, but most importantly, I would like to thank my family. Without their encouragement and understanding it would have been impossible for me to finish this work. To them I dedicate this thesis.

Table of Contents

List of Tables

List of Figures

Nomenclature

b	cell active surface area width, m
$\bar{C}_p$	molar heat capacity, kJ/kmol K
d	pore diameter, m
dx	differential length of the cell, m
E	voltage, V
E^0	Nernst potential, V
F	Faraday constant, C/mol
$\Delta\bar{g}_f$	molar Gibbs free energy of formation, kJ/kmol
$\bar{h}$	molar absolute enthalpy, kJ/kmol
I	current, A
i	current density, A/cm^2
L	total length of the cell, m
LHV	fuel lower heating value, kJ/kg
$\dot{m}$	mass flow rate, kg/s
$\dot{n}$	molar flow rate, mol/s
n	number of single cells in a fuel cell stack
P	pressure, Pa
$\dot{Q}$	rate of heat transfer, W
R	universal gas constant (8.3145 kJ/kmol K)
r	pressure coefficient
S	entropy, kJ/kg K
$\bar{s}$	molar entropy, kJ/kmol K

S/C	steam to carbon ratio
T	temperature, K
U	utilization factor
$\dot{W}$	power, W
X	mole fraction
x_k	optimization variable at the kth iteration
Y	optimization variable
z	number of electrons transferred per molecule of fuel

Greek Letters

α	heat transfer coefficient, $W/m^2 K$
δ	optimization variable
ε	tolerance
η	overpotential (re-scaled), $\Omega . m^2$
η_{energy}	energy efficiency
η_{exergy}	exergy efficiency
θ	contact angle of the electrolyte, ^{o}
μ_o	optimization variable
σ	interfacial surface tension, N/m
$\bar{\Psi}$	molar exergy, kJ/kmol
$\bar{\Psi}^{chemical}$	molar chemical availability, kJ/kmol

Subscripts

a	anode
act	activation
AN	anode
atm	atmospheric
c	cathode
C	compressor
CA	cathode
CB	catalytic burner
conc	concentration
ch	chemical
des	destruction
e	electrolyte
eq	equilibrium
FC	fuel cell
HEX	heat exchanger
i	species
in	inlet
k	k^{th} number in the optimization process
MC	mixing chamber
n	number of electrons transferred per molecule of fuel
ohm	ohmic
out	outlet

RHE	regenerative heat exchanger
T	turbine
TE	turbo-expander
tot	total
0	standard reference state (P=1 atm, T_0=298.15 K)

Acronyms

CHP	Combined Heat and Power
DCSS	Distillation Condensation Sub System
DIR	Direct Internal Reforming
EDS	Energy Dispersive X-ray Spectrometer
ER	External Reforming
GHG	Greenhouse Gas
HRR	Heat Recovery Ratio
HRVG	Heat Recovery Vapor Generator
IIR	Indirect Internal Reforming
IR	Internal Resistance
MCFC	Molten Carbonate Fuel Cell
PEMFC	Proton Exchange Membrane Fuel Cell
SEM	Scanning Electron Microscope
SOFC	Solid Oxide Fuel Cell
TPBR	Triple Phase Boundary Region

Chapter 1: INTRODUCTION

Currently, the annual global population growth rate is about 2 % while rising even more sharply in many countries [1]. Consequently, global energy services demand is expected to increase up to 10 fold and primary energy demands by 1.5-3 fold over the next five decades or so [2, 3]. Therefore, there is a need for renewable and environmentally benign power production substitutes in order to resolve the inevitable energy crisis. With substantial investments by both the private and public sectors, fuel cell technology is rapidly advancing. Due to their high energy efficiency and clean environmental performance, fuel cells are regarded as a potential reliable future source of energy supply. Fuel cells are electrochemical energy conversion devices which typically run on hydrogen, methane or methanol and produce electricity, heat and benign emissions (water and, in the case of methane and methanol, CO_2). However, the large initial capital costs of fuel cell technology have offset the advantages they offer and slowed down their adoption for widespread use. The main reasons for using fuel cells in power generation can be characterized as the need for pollution reduction, back-up power, diversification of energy supply and, hence, a reduction of foreign energy dependency (e.g. [4]).

One technology with great promise is the molten carbonate fuel cell (MCFC). The present demonstration and research projects of MCFC stacks and systems show a wide range of power output. Power ranges from a few kilowatts to several megawatts are achievable. Due to the high operating temperature of an MCFC, it is particularly suitable for stationary co-generation of electrical power and heat [5]. Hospitals, hotels, office buildings and industrial applications could be the place of choice to test these projects. Despite numerous research on MCFC systems, there are still many opportunities for further improvements of this technology. Enhancing the component durability to achieve the goal of a 40,000 h life time, increasing the cell performance and reducing costs in order to make the systems economically viable in the power producing market are the main targets in competitive improvements.

1.1 Motivation and objectives

Fuel cell technology is a new and promising alternative for producing green energy. Currently, there is a great demand for research and optimization of fuel cell systems. Lowering the costs and increasing the lifetime of the fuel cell are the main two goals of researchers in this area.

This thesis concentrates solely on the performance investigation of MCFC stack and hybrid systems. Two industrial MCFC hybrid systems are used for the analyses performed in this study. Figure 1 demonstrates the outline of the work done in this thesis.

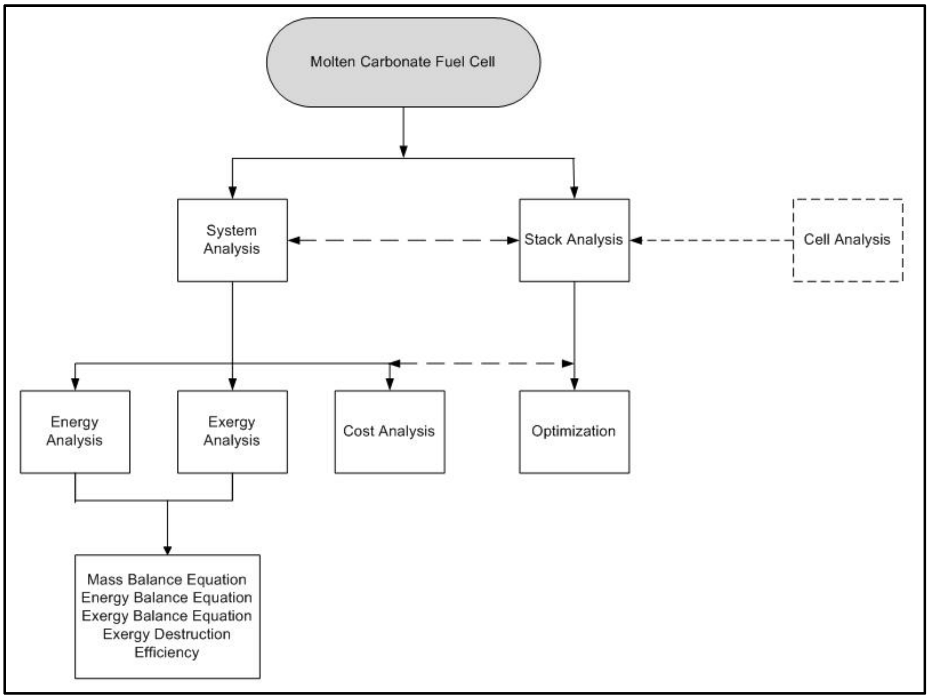

Figure 1: Outline of the thesis.

The main objectives met in this project are as follows:

- Energy investigation of an industrial MCFC system and an Enbridge system
- Exergy investigation of an industrial MCFC system and an Enbridge system
- Parametric study to investigate the enhancement of the system performance by varying the operating conditions such as:
    - Ambient temperature and pressure
    - Operating pressure, temperature and MCFC current
    - Hydrogen utilization
- Seeking the quantities and location of exergy destruction in the hybrid MCFC systems
- Optimization to seek the optimum
    - Operating temperature
    - Operating pressure
    - Fuel cell current
- Cost analysis of the Enbridge hybrid system to determine the amortization period, considering the variation in natural gas and electricity costs

Chapter 2: LITERATURE REVIEW

2.1 General MCFC aspects

Molten carbonate fuel cell technology was established about 30 years ago and it has developed fast in the USA, Korea, Japan and Europe during the last decade or so. Using MCFC in combined heat and power (CHP) production has emerged as a new and highly efficient source of energy supply. This fuel cell which was only used as an interesting laboratory object for demonstration purposes during the last several years, has now reached the commercialization stage due to its essentially “no emission” performance as well as its high efficiency compared to conventional methods of power production [6].

There have been several attempts to illustrate the advantages of molten carbonate fuel cells in operation during the several last decades (e.g. [6-9]).

Bischoff [6] presented a general review of MCFC operation and its market. He discussed mostly aspects of their development and especially the progress made on MCFCs at MTU CFC Solutions GmbH, the German leader of MCFC projects. “Hot module” system design as the most advanced technology for MCFC is being developed in a collaborative effort at FuelCellEnergy Inc. and MTU CFC Solutions. Although several demonstration modules have been manufactured and tested, this does not mean that the technology is readily available at this point. Manufacturing difficulties and cost issues are the main barriers that must be overcome before commercialization can occur. Furthermore, the commercial life time target of 40,000 hours is seemingly unlikely to be met which further delays the progress.

Nanotechnology used for manufacturing of fuel cell compartments, such as the anode, has improved the performance of MCFCs in recent times [8]. Introducing new micro-composite electrodes might increase the durability, conductivity and most importantly, the life time of the electrodes during fuel cell operation. Commercialization of MCFC systems in the current competitive market, where the material and design innovation are much easier to be achieved for other types of fuel cells, requires a thorough understanding of the new technology and it emerges as a wide area of research to be completed [9].

2.2 General exergy applications

This section summarizes the projects and studies that have considered exergetic analyses for industrial applications.

Exergy can be defined as the maximum amount of work that can be obtained during a process that brings the system into equilibrium [10, 11]. Therefore, exergy is a property of both the system and the reference environment and its value demonstrates the deviation of the system from its reference environment.

Exergy analysis is an effective tool to achieve efficient energy utilization with reduced environmental impact which can be used for design and optimization of energy systems. Exergy analysis, in general, can be used for any application involving heat and work transfer. Exergetic efficiency shows the actual effectiveness of the system. Moreover, exergy analysis could be used in conjunction with life cycle assessment to obtain even more useful results. Dincer et al. [12] conducted an exergetic life cycle assessment of hydrogen production from renewables. The economic effectiveness, exergetic efficiency and environmental impact of producing hydrogen using wind and solar energy versus the conventional utilization of fossil fuels were compared. The results obtained suggest that a theoretical increase of a vehicle’s engine efficiency of about

100 % is achievable when implementing a hydrogen fuel cell instead of an internal combustion engine. Moreover, when substituting gasoline with “renewable” hydrogen from wind or solar energy, a greenhouse gas (GHG) emissions reduction of 12-23 or 5-8 times the conventional method are achievable, respectively.

Nevertheless, depending on the operating conditions, the costs of electricity from wind, solar or hydrogen are significantly higher than the cost of electricity produced from natural gas.

Many studies have been performed to analyze and improve fuel cell systems performance using an exergy analysis [13-15].

Hussain et al. [15] performed an energy and exergy analysis on an integrated SOFC power system. The location, type and magnitude of waste and losses were obtained. Their results suggest that by utilizing the heat produced from the SOFC to preheat the air and fuel instead of rejecting it to the environment, a substantial increase in energy and exergy efficiencies of the SOFC power system are attainable. Kazim [13] performed an exergy analysis of a 10 kW PEM fuel cell at variable operating temperature, pressure, air stoichiometry and cell voltage. In order to include a wider range of operating conditions, a fuel cell with operating voltages of 0.5 and 0.6 V, air stoichiometics of 2, 3 and 4, temperature ratios (i.e. T_{FC}/T_0) of 1 to 1.25, and pressure ratios (P_{FC}/P_0) ranging from 1-3 were used for his study. The results suggest that the exergetic efficiency of the fuel cell can be enhanced by increasing the operating pressure, temperature, average cell voltage and air stoichiometry. However, air stoichiometries of more than 4 may not be suitable because it does not maintain the required fuel cell humidity.

Yaling et al. [14] also conducted an exergetic analysis of fuel cells. Their model developed expressions for electrical and thermal exergetic efficiencies and total exergetic efficiency of a direct methanol fuel cell. Their proposed model helped to obtain the effects of parameters such as methanol concentration, current density, operating pressure and temperature on the fuel cell efficiency. They concluded that operating at high current density, high operating temperature and low methanol concentration improves the exergetic efficiency of the system significantly.

A general study on analyzing power cycles using exergy analysis is being conducted by Kanoglu et al. [16]. Co-generation cycles, geothermal power cycles and vapor and gas power cycles were examined from an energetic and exergetic point of view. This study proves the importance and diversity of applications in which exergy analysis could be used. Since it is not easy to have a common efficiency definition for all energy systems and because it is also important that the efficiency provides a true insight into the economic issues of the system, it is essential to use exergetic efficiency in calculations.

Exergy analysis can also be used in drying processes. Dincer et al. [17] performed a thermodynamic analysis of a drying process using an exergy analysis. In their study, mass, energy and exergy balance equations have been used and efficiencies were derived as functions of heat and mass transfer parameters. The results obtained show that increasing the humidity ratio of drying air, moisture content of the product and specific exergy of the inlet drying air decreases the system exergetic efficiency. Hence, this study proves that exergy analysis could be used as a helpful tool in design and optimization of drying processes.

2.3 Cell level model

Molten carbonate single cell modeling is initiated mainly by the work of Wolf et al. [18]. The model produced is a non-isothermal steady-state model. Their study was a two-dimensional investigation which took into account the conductive heat transfer normal to the cell hardware and heat transfer by the bulk streams. Different geometries such as co-flow, cross-flow and counter-flow were used for their study. The main results obtained from this investigation showed that increasing the cell active area to more than 1 m^2 generates a temperature distribution field which might have a variation of up to 200 K. This study provides a great insight into the heat transfer phenomenon in MCFC systems.

To investigate the effects of the cell shape on the performance of MCFC, Bosio et al. [19] used square and rectangular shape cells. The results of the cell model were used for an empirical three-dimensional stack model. The results obtained show that the rectangular shape cell where the cell direction traversed by the cathodic gas is shorter than the anodic side enhances the heat transfer performance in the stack and that results in obtaining higher efficiencies. As a result, the pressure drop in the channels remains within an acceptable level while the oxidant flow rate is increased. Their model was also used to optimize the thermal and pressure drop management when reformed natural gas, as well as coal gas, were used as fuel.

Bosio et al. [20] also investigated the scaling up process of molten carbonate fuel cell reactors. They developed an empirical two-dimensional model. A rectangular shape cell was being used for the analysis in which the oxidant was supplied at the longer side of the cell and the fuel flow was by cross-flow arrangement. The main novel feature of this work was the inclusion of the micro modeling of the electrode-kinetics into the macroscopic model, as well as studying the effects of cross-flow of the reactants through the electrolyte.

Chung et al. [21] investigated the effects of fuel internal reforming on the MCFC temperature distribution and the fuel cell performance. They developed a mathematical two-dimensional cell model with cross-flow fuel and oxidant arrangement. The model includes the water-gas shift reaction as well as the methane-reforming reaction which occur simultaneously. They concluded that the best results are obtained when the steam to methane ratio is maintained at 2:1. Moreover, the conversion of methane to hydrogen, considering thermodynamic equilibrium, reaches 99 %. Increasing the molar ratio of water-gas to methane at a fixed total flow rate decreases the voltage. Additionally, the temperature is more evenly distributed in comparison to an externally reformed MCFC because of the endothermic nature of the reforming reaction.

Standaert et al. [22] developed an analytical co-flow isothermal cell model which could be applied to any type of fuel cell. The external load resistance and the amount of fuel supply to produce the maximum current were taken into consideration as independent variables. For an MCFC with high fuel utilizations, linearization of the Nernst potential (i.e. the analytical solution) agreed well with the results from the non-linearized Nernst equations. Moreover, their model suggested that MCFCs could operate at high fuel utilizations without any abrupt decrease of cell voltage or power.

Standaert et al. [23] further developed their earlier model to include the behavior of a non-isothermal fuel cell with co-flow arrangement. The model generated a simplified relationship between the local temperature and the fuel utilization. The results from this approach showed a small deviation compared to the numerically computed cell voltage.

2.4 Stack level model

Yoshiba et al. [24] developed a three-dimensional numerical analysis for a MCFC stack. Their model can calculate the current, temperature profile and voltage of each single cell in the MCFC stack. Five gas flow types were tested in their experiments. The results showed that the highest net output power can be obtained by a co-flow type stack only when considering a uniform gas distribution in the two-dimensional cell plane. The model predicted that the temperature of the cathode outlet gas is equal to the maximum temperature of the fuel cell and the thermal management of the stack is much easier when the co-flow arrangement is employed.

Yoshiba et al. [25] also investigated the effects of internal resistance and fuel flow rate on the fuel cell performance using their model. As a result, they concluded that an insufficient supply of fuel gas to particular cells or parts of the active area of a cell increases the IR (i.e. Internal Resistance) over-potential which causes a voltage gradient. They validated their result by performing experiments on a 100-kW class stack and their result suggested that the discrepancies in the cell voltage were mainly due to insufficient fueling.

Bosio et al. [20] developed an empirical three-dimensional stack model to investigate MCFC stacks scale-up. The overall stack simulation in their study demonstrated how the gas cross-over phenomena at the cell level may deteriorate the overall performance and damages the materials of the MCFC stack. Therefore, while a thermodynamic equilibrium should be established under open circuit conditions, unreacted fuel passed through the electrolyte which causes short-circuit currents within the cell, being the main reason for irreversibilites.

Bosio et al. [26] further investigated the effects of gas diffusion limitations on the overall performance of the fuel cell. The new model was validated by experimental work when high reactant utilization factors were used and the results showed that the mass transport limitations affect the performance of the stack significantly.

Koh et al. [27, 28] investigated the effect of various stack parameters on temperature and pressure distributions in molten carbonate fuel cell stacks. The authors [27] developed a mathematical stack model to predict the temperature rise at a constant-load and average voltage operation of molten carbonate fuel cell stacks. The results from the model were validated by experimental data from a 5-kW test stack. The results obtained suggested that the cathode gas flow dominates the temperature distribution in the stack, and the inlet stream temperature does not affect the maximum temperature inside the stack significantly. Therefore, controlling the pressure of the cathode stream in order to maintain a thermal balance is necessary.

Koh et al. [28] developed a three-dimensional stack model based on heat and mass transfer, thereby predicting the temperature and pressure distributions in a co-flow MCFC. The model was further used to gauge the maximum temperature rise and average cell potential when the stack was scaled up. The main assumption made in order to simplify the model in this investigation was that the current density was assumed to be uniform and the mass balance equations for the gas phase were solved, based on this assumption. They concluded that the scale-up process has a significant effect on the stack temperature while no impact on the average cell voltage was observed. Moreover, Koh et al. [29] performed a theoretical study on a molten carbonate fuel cell stack for pressurized operation. The two-dimensional model was used for a co-flow arrangement and the effects of varying the system pressure and gas utilization on the temperature distribution and stack performance at a constant load were investigated. They figured that the lack of stack cooling results in hot spots near the stack outlet. However, an isothermal temperature distribution forms from the cathode inlet towards the outlet when sufficient cooling is provided. They also concluded that with operating pressures in the range of 1-5 atm, higher system pressure results in a decrease of pressure drop of the gas streams and consequently, the increase of cathode flow rate stabilizes the stack operation.

Koh et al. [30] also used CFD in order to predict the heat transfer and temperature distribution in the stack. They used the commercial software PHOENICS (v2.2) for computation of the fuel cell stack model. All gas properties except the anode gas heat capacity were kept constant in their model. The results showed that thermal radiation does not affect the heat balance model significantly. Effects of varying the number of meshing grids for the channels depth were also included in their study.

Li et al. [31] conducted a study on the start-up and performance analysis of a kW class MCFC stack. A 52-cell stack was assembled with inorganic adhesive under a suitable stacking pressure. After the start-up period, the stacking pressure dropped with elevating temperature. They observed that the thermal-electrical efficiency of the MCFC decreases by increasing current density. However, increasing the pressure of the reactants enhanced the efficiency.

An interesting study by Freni et al. [32] was conducted in order to investigate the feasibility of running an internal reformed ethanol molten carbonate fuel cell. Their model included the energy and mass balances which were determined by thermodynamic calculations. The results obtained from calculation of thermodynamic efficiencies suggested that these systems may be a promising solution in the near future.

2.5 System level model

A molten carbonate fuel cell has a high operating pressure and temperature. Therefore, a bottoming cycle consisting of a turbine helps to increase the power output and efficiency of the overall system. There are significant interests in such systems due to their higher efficiencies compared to conventional coal power plants. The basic advantage of such systems is that the necessary power required for the compressor could be supplied by the turbine which is a key part of the bottoming cycle. Introducing the bottoming cycle into the fuel cell power plant could be achieved in two ways: A) Combination with a gas turbine; B) Combination with a steam turbine. The latter is a more common and feasible approach because the exhaust cathode flow has a temperature of about 650^{o}C that can be used for steam generation.

Power generation by combining a MCFC with a steam turbine is an innovative idea. Varbanov et al. [33] conducted a performance analysis of a combined MCFC system in which the waste heat of the MCFC was utilized in steam generation. They also estimated the prospective power cost for the production from the combined system. Their result demonstrated that combining a 46.4 % efficient MCFC with a steam generation power system maintains an overall efficiency of up to nearly 70 %. Moreover, power production from a properly designed fuel cell combined cycle is more economical than contemporary fossil fuel power stations.

Bocci et al. [34] also investigated the performance of a MCFC combined micro-turbine power plant. A 500 kW MCFC combined with a 100kW turbine was modeled and analyzed in their work. Numerical models for a reformer, burner, turbine, compressor and the fuel cell were developed and implemented in Fortran 90 and Chemcad ©. The results showed that a global electrical efficiency of 50-55 % and a co-generative efficiency of about 75 % can be achieved. Therefore, it was suggested that the micro-turbine that produced the required power to run the compressor played a crucial part in enhancing the performance of the power plant. One of the successful projects using this technology is being built and operated in Santa Clara, California.

Analysis of a hybrid MCFC close-loop gas turbine plant is being performed by Desideri et al. [35]. Their work included the analysis of a basic plant configuration in which the main working parameters such as the plant performance, chemical properties, and streams and components temperature were determined. Moreover, they modified the plant configuration and the arrangement to better use the waste heat. Different bottoming cycles when using argon, air and carbon dioxide as working fluids were used in a comparative study to maximize the plant power output. The results obtained showed that the global electrical efficiency of the plant could be increased from 59 % for the basic system arrangement to 67 % for the combined MCFC and gas turbine system.

Lobachyov et al. [36] investigated the feasibility of enhancing the performance and efficiency of a 2MW power plant by adding a bottoming cycle to the original system. Employing several components such as steam turbines, heat exchangers and condensers could help to utilize the cathode exhaust energy. As a result, efficiencies of up to 70 % are achievable.

A possible approach studied by Lobachyov et al. [36] was to add a Kalina bottoming cycle to the original power plant. A Kalina cycle simply uses a heat recovery vapor generator (HRVG) and a distillation condensation subsystem (DCSS) to utilize the hot depleted cathode exhaust. However, a more efficient and cost optimized method is to replace or improve the components in which the maximum exergy destruction occurs. Therefore, the proposed bottoming cycle had a heat exchanger network to maximally reduce the exergy loss because of the heat transfer, a preheating system to preheat the incoming air in order to reduce the exergy loss in the burner, and a steam bottoming cycle to recover the useful work from the cathode exhaust stream. Analyses of these systems suggested that reducing the exergy loss of the components by improving or replacing them is more advantageous than other methods, both economically and efficiency-wise.

Simon et al. [37] investigated the performance of a non-internal reforming pressurized MCFC with a bottoming-cycle turbo-compressor. The cooling of their system was mainly done by the high cathode inlet stream while this is considered as one of the engineering difficulties is such systems. The results of this experimental work were obtained by utilizing a customized Aspen plus^{TM} block. Therefore, from a 60 % efficient MCFC and 12 % efficient bottoming cycle, a 50-60 % global electrical efficiency was achieved. However, the cogeneration efficiency remained near 75 %. They also conducted a sensitivity study and the results showed that by increasing the steam to methane ratio and pressure, and decreasing the air feed rate, the electrical efficiency of the system could be further enhanced.

Kang et al. [38] studied the effects of system components and configuration on the overall combined power plant efficiency. Their study included an experimental investigation of a 25 kW MCFC system and its efficiency. Moreover, the results were used to investigate the effects of the operating conditions on the performance of a 100 kW MCFC system. In order to analyze the effect of the system configuration on the overall system efficiency, four systems with different designs were studied. The results showed that the combined turbocharger-MCFC power plant has the highest efficiency between the four configurations studied. The main reason for the enhanced efficiency was the proper thermal integration between the operating units and the use of the turbocharger to produce the power required for the compressor without a need for external power sources. They suggested that the MCFC offers an enhanced performance when used as a combined power cycle. In addition, increasing the efficiency of the unit operators, fuel utilization, oxidant utilization, fuel cell capacity and the cathode recycle ratio increased the overall system efficiency.

Improvements and optimization of molten carbonate fuel cell power plants have also attracted a lot of interests by many researchers (e.g. [39, 40]). Braun et al. [40] proposed an exergy analysis to improve the performance of a molten carbonate fuel cell power plant. They used exergy and pinch analysis in order to pinpoint and quantify the inefficiencies of a 2 MW MCFC power plant. The exergetic efficiency of the system was found to be 53 % and the main source of inefficiency was the catalytic burner with 17 % of the total exergy destruction. The second most inefficient component of the power plant was the fuel cell with 14 %. System reconfiguration and heat transfer management of the whole system (i.e. pinch analysis) significantly improved the system second law efficiency to about 70 %.

Lunghi et al. [39] performed a parametric study on a hybrid MCFC, indirectly heated gas turbine system. The fuel cell section size and fuel utilization coefficient were optimized. Aspen plus^{TM} software was used for the calculations of a one-dimensional

MCFC stack model that they developed. The results showed that the optimum fuel cell parameters for standalone operation were not necessarily the optimum for the use in the hybrid cycle. Moreover, the combined fuel cell-gas turbine system achieved global electrical efficiency of 58 % at a fuel utilization of 70 %.

2.6 Cost analysis

Varbanov et al. [33] studied the performance and cost analysis of a MCFC-combined steam generating system. From their base case study (i.e. stand-alone MCFC), the fuel cell was marginally competitive with alternative options. However, including the bottoming cycle such as a heat recovery and steam generation cycle made the system a more economically competitive candidate. The results obtained from the cost analysis were based on an assumed capital cost for the fuel cell. Due to the fact that the available quotes for the fuel cell capital costs were not reliable, they conducted a sensitivity study to investigate the variation of fuel cell costs. To obtain a more reliable cost estimate, the obtained results were combined with the data collected from the steam cycle performance subsequently. The cost estimation illustrated that under the current economic conditions, a fuel cell combined cycle could produce power with a cost as low as 40 $/MWh. The main reason for such a low power cost can be explained by the fact that there is not any additional primary fuel cost for the bottoming cycle.

Another thermoeconomic analysis of a MCFC power plant was conducted by Lobachyov et al. [36]. They analyzed the feasibility of increasing the overall efficiency of a MCFC power plant by adding a bottoming cycle in order to utilize the energy of the exhaust cathode stream. Based on their assumptions made for materials, labor and capital costs, the proposed model for the MCFC power plant, which was combined with steam generation and a heat exchanger network, demonstrated a greater economical significance compared to the other configurations studied. The suggested modified system had the lowest capital investment requirements and the rate of return was the highest on a unit capacity basis.

A feasibility study of a co-generation system with a direct internal-reforming molten carbonate fuel cell for residual use was investigated by Sugiura et al. [41]. Their study included two analyses. Heat and material balance equations were used to study the base system in which the fuel cell temperature was kept constant (about $650^{o}C$) without any external heat supply. As a result, a model for a residential house using a direct internal-reforming MCFC co-generation system, taking into account the number of family members and the number of electric appliances, room layouts and consumption of electric power in Osaka, was assembled. Using the results obtained from the calculation of the electric power and hot water demand and supply, the scale of the co-generation system was optimized. Finally, the cost analysis of the optimized system running on city gas or propane gas was performed. Direct internal-reforming MCFC benefits from a more compact size and easier heat management compared to external-reforming system and that makes the direct internal-reforming MCFC co-generation system suitable for residential purposes. MCFC systems which use propane gas for an apartment and using city gas for a house, were the best options according to the results.

The cost analysis was based on the amount of gas, water, power and buying electric power during the shortage. The results showed that, although the gas consumption rate of the co-generation system was more than the amount of the gas used traditionally, the lighting and heating expenses were similar. The main advantage of the co-generation system was that it benefited from selling the excess electric power to Electric Power Corporation when the demand was low. As a result, the co-generation MCFC system was a feasible and profitable option for heating and lighting in residential use.

Silveira et al. [42] investigated the feasibility of having a MCFC as a co-generation system to produce electricity and cold water. Their study included an energy, exergy, and economic analysis of a fuel cell co-generation system. Results indicate that a global efficiency as high as 86 % is possible. The fuel cell unit and the absorption refrigeration system had the highest amount of exergy destruction and, therefore, they require to be optimized to enhance the overall efficiency. The main reasons for such inefficiencies were the chemical reaction involved and high temperature difference between the streams of these components. The cost analysis demonstrated that the investment of 1000-1500 US$/kW for the fuel cell system could be paid back in a period of 3 to 5 years.

In a similar study, Silveira et al. [43] investigated the feasibility of a fuel cell co-generation system used for the dairy industry. The considered dairy system demands of 8,500 kg/h of saturated steam ($P = 1.08$ MPa), 2,725 kW of cold water and 2,100kW of electricity. The co-generation system could be used to utilize the waste heat to produce hot and cold water and air for the dairy industry. They investigated two system configurations. Firstly, producing steam by using a heat recovery steam generator for the co-generation system. Secondly, using an absorption refrigeration system to produce cold water. The results obtained were similar to the work done by Silveira et al. [42] and the estimated payback period was calculated to be within 4 to 5 years of operation.

Chapter 3: BACKGROUND AND THEORY

3.1 Background

MCFCs typically operate at 600-650 K and produce a current density between 0.3 and 1 A/cm^2. In spite of public perception, to the contrary MCFCs have already reached a commercial scale during the last 10 years by offering cells of 1 m^2 electrodes and megawatt-capacity stacks. Technical and economical aspects of MCFCs have also improved remarkably during this period [8, 28].

In order to improve the performance of a MCFC, several single cells are usually connected in series to form a stack and as a result, the stack performance will depend on the performance of individual cells available in the stack. Connecting the cells in series and placing them in a stack "module" is a typical approach in MCFC manufacturing. Figure 2 is the schematic of a co-flow MCFC stack with its different compartments.

Therefore, the half-cell reactions of the MCFC are:

At the anode: $2H_2 + 2CO_3^{2-} \rightarrow 2H_2O + 2CO_2 + 4e^-$ (3.1)

At the cathode: $O_2 + 2CO_2 + 4e^- \rightarrow 2CO_3^{2-}$ (3.2)

Combining the half-cell reactions of the anode and the cathode gives the overall reaction of the fuel cell: $2H_2 + O_2 \rightarrow 2H_2O$ (3.3)

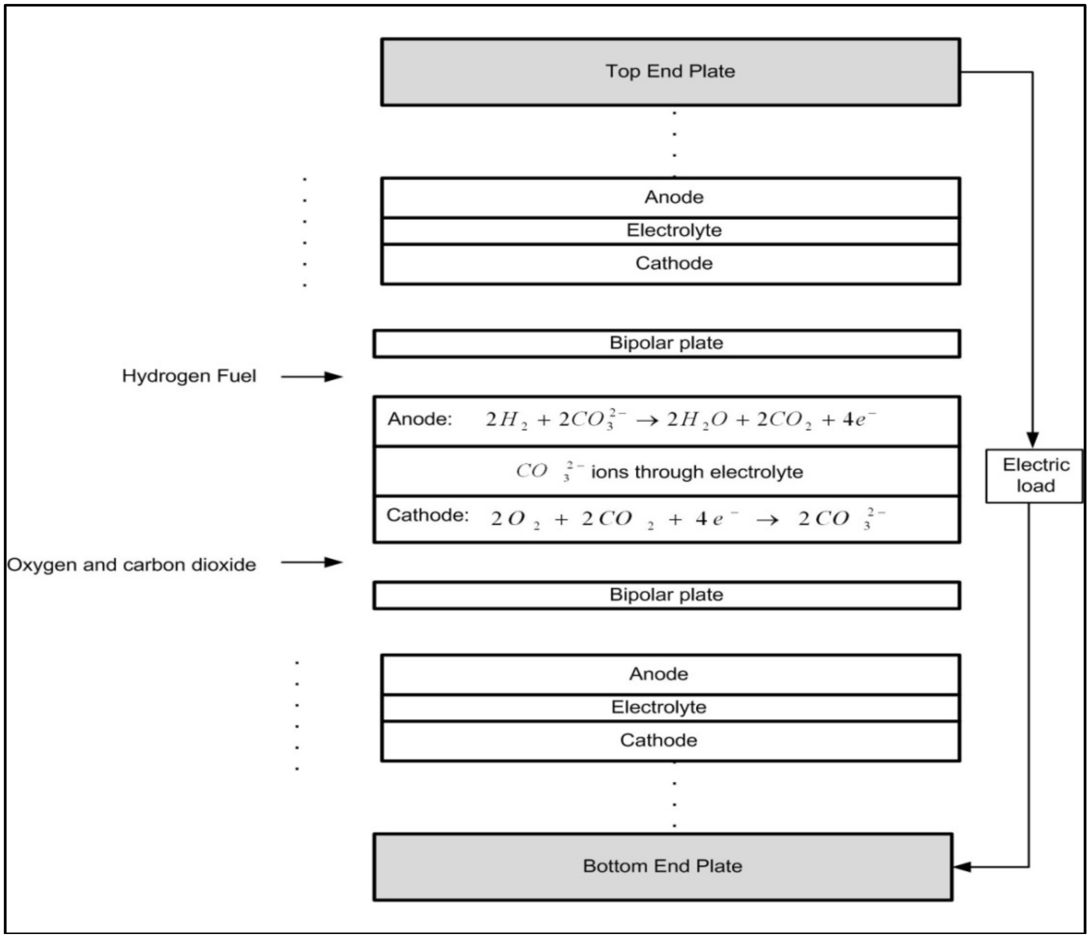

Figure 2: Schematic of a co-flow MCFC stack with its different compartments.

Top and bottom end plates are the last bipolar plates of the stack which are usually thicker than the other plates. They are used to gather the entire current of the stack and hold the cells in place by exerting pressure upon them.

One of the advantages of MCFC over other types of fuel cells is that the reactant required by the fuel cell is not limited to hydrogen. CO can also act as a fuel through the following electrochemical reaction at the anode,

$$2CO + 2CO_3^{2-} \rightarrow 4CO_2 + 4e^- \qquad (3.4)$$

The cathode reaction would be the same as when hydrogen is supplied to the anode.

Moreover, CO could be used to produce more hydrogen and carbon dioxide through the water-gas shift reaction which is given by

$$CO + H_2O \rightleftharpoons CO_2 + H_2 \tag{3.5}$$

The water-gas shift reaction can also occur is a separate external reformer and the products are supplied to the fuel cell. Internal and external reforming procedures are further discussed later in this chapter.

3.2 Cell compartments

A typical MCFC consists of three main compartments similar to all other types of fuel cells: a cathode, an anode and an electrolyte. The chemical energy of the reactants is converted into heat, water and, most importantly, electrical energy through the electrochemical half-cell reactions. However, MCFC reactions only take place where the ion-conducting phase, electron-conducting phase and void space occupied by reactant gases (i.e. triple phase boundary regions (TPBRs)) are present. Therefore, to obtain the maximum amount of energy from the fuel cell, a sophisticated design and optimization of fuel cell compartments are necessary.

3.2.1 Electrolyte

The electrolyte used for MCFCs is a molten mixture of potassium carbonate (K_2CO_3) and lithium carbonate (Li_2CO_3). In order to improve the pore size distribution and performance of the electrolyte, a small amount of sodium carbonate (Na_2CO_3) and carbonate of earth-alkaline metals are added to the mixture. Varying the composition of constitutes present in the electrolyte helps to reduce the Ohmic losses, electrolyte evaporation and cathode and anode dissolution in the electrolyte and, therefore, an optimization of the solution composition is essential.

A porous electrolyte matrix made out of ceramic powder such as lithium aluminate ($LiAlO_2$) is required to hold the molten electrolyte in place. The molten carbonate-filled matrix prevents cross-over of reactant gases; it conducts carbonate ions (CO_3^{2-}) and insulates against electron transfer.

Management of the molten carbonate electrolyte in the matrix is performed by a completely different procedure compared to all other types of fuel cells because of its liquid characteristics. Therefore, in order to establish the interface between the electrode and the electrolyte, and prevent the flow of electrolyte from one cell compartment to another, a balance in capillary pressures within the pores (diameter *d*) of the anode and cathode is required. Figure 3 illustrates the dynamic equilibrium in porous MCFC cell elements.

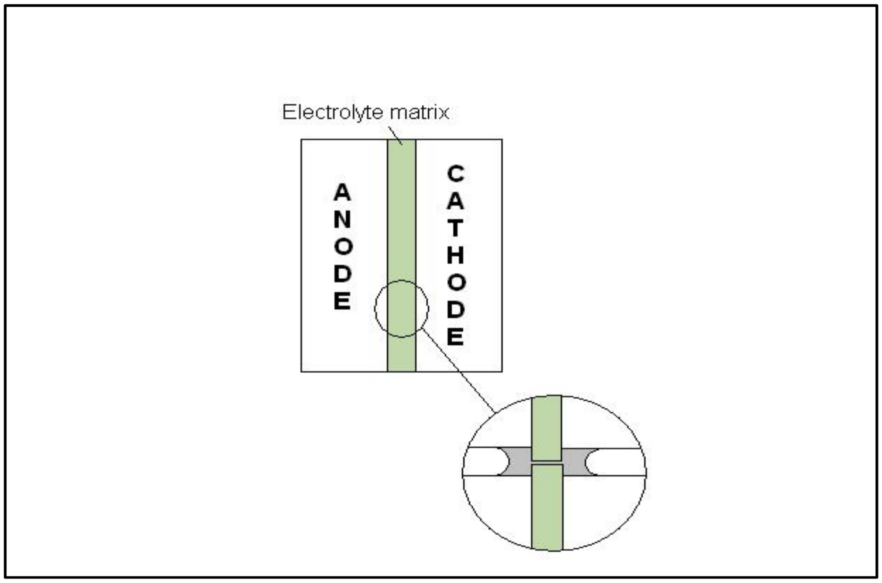

Figure 3: Dynamic equilibrium in a porous MCFC cell.

The largest pore size in each of the porous cell components, which are filled by the liquid electrolyte, are determined by [44]:

$$(\frac{\sigma \cos\theta}{d})_{cathode} = (\frac{\sigma \cos\theta}{d})_{electrolyte} = (\frac{\sigma \cos\theta}{d})_{anode} \qquad (3.6)$$

where ‘σ’ is the interfacial surface tension, ‘θ’ is the contact angle of the electrolyte and ‘d’ is the pore diameter. A fine balance needs to be stuck between pore sizes and contact angles so as to optimize and stabilize the electrolyte distribution.

There are two well-known methods used to manufacture the electrolyte tile: 1) Hot-pressing technique; 2) Tape-casting fabrication. The hot-pressing technique is a simple fabrication method which requires compression of $LiAlO_2$ under a pressure of around 5,000 psi and at temperatures as high as the melting point of the carbonate. The resulting tile would be too thick and has a poor microstructure. As a result, the size and shape of the matrices built are limited.

In the latter technique, $LiAlO_2$ particles with organic binders are dispersed in an organic solvent. Additives and plasticizers are subsequently added to enhance the manufacturing quality. The mixture is then casted over a smooth surface and thin layers of the matrix are produced. The cast is then dried and installed on the electrodes. Subsequently, the binder is burnt out and the matrix is formed. The main advantage of this method is that manufacturing of very thin matrices with large surface areas is possible.

A thinner electrolyte assembly results in lower ohmic losses which is one of the main contributors to the overall MCFC irreversibilities.

3.2.2 Cathode

The MCFC cathode must be a stable conductor that can withstand a corrosive and oxidizing environment. The performance of the cathode deteriorates as it is in the vicinity of an extremely corrosive carbonate environment and oxygen oxidizing area. Semiconducting oxides such as lithiated nickel oxide are the best materials that can be used for the cathode of MCFC at present. Lithiated nickel oxide is formed from simultaneous lithiation and oxidation of porous nickel particles during the initial cell operation. The big pores (macropores) remain empty to provide the path for the reactant gases to the three-phase zone. The smaller pores are filled with electrolyte and they provide carbonate ions to the three-phase zone which is the key area for electrochemical reactions in the fuel cell. The degree of cathode filling by the electrolyte depends on the macropores, gas channels and micropores distribution. Cathodic polarization could be reduced by any improvements in design of the pores. Therefore, to avoid the flooding of the cathode by the electrolyte, it is necessary that the distribution of the pores is correctly designed and controlled.

The thickness of the cathode affects the cathodic polarization. A thicker cathode results in higher gas diffusion losses. Moreover, increasing the cathode thickness increases the ohmic losses. However, increasing the small pore area increases the kinetic activation and enhances the liquid diffusion which results in lower losses. Therefore, an optimum cathode design requires an optimum cathode thickness.

The major problem with a NiO cathode is its solubility in the electrolyte. At high CO_2 partial pressures, Ni^{2+} ions are formed due to the reaction:

$$NiO + CO_2 \rightarrow Ni^{2+} + CO_3^{2-} \qquad (3.7)$$

Hence, Ni^{2+} ions are precipitated in the electrolyte and provide a path for other nickel ions towards the anode. This would result in fuel cell performance deterioration because of the electronic short-circuit caused by the metallic nickel ions.

3.2.3 Anode

The materials used for the anode must withstand a reducing environment. Copper, cobalt and nickel with additives such as aluminum or chromium are suitable as electro-catalyst for hydrogen oxidation at the anode. Additives increase the life time and stability of the anode while it is subjected to sintering and creeping under the stack's compressive forces.

Currently, a state-of-the-art anode is made of a porous sintered Ni-Cr/Ci-Al alloy with a thickness of 0.4-0.8 mm and a porosity of between 55 % and 75 %. Manufacturing of the anode involves the hot pressing of a powder or tape casting a slurry which needs to be sintered finally. In order to limit the degree of sintering, a small amount of Chromium is added to the slurry. However, chromium reacts with the lithium from the electrolyte and that results in the loss of electrolyte. Moreover, added chromium might result in mechanical deformation of the cell, loss of surface area, growth in pore sizes and redistribution of carbonate from the electrolyte. As a result, anode polarization increases and the fuel cell performance drops dramatically. One solution to solve such problems is to add a small amount of aluminum which resists the electrolyte loss and the fuel cell creep.

Since the electrochemical reactions at the anode side happens relatively fast, the anode area could be partially used as a reservoir for molten carbonate. Partial flooding of the anode with the electrolyte reduces the gas cross-over and helps to replenish carbonate when necessary. This is only possible when the MCFC anode is designed with an accurate pore distribution.

3.2.4 Separator plates

Separator plates are the fuel cell compartment that divide and separate the flow of fuel and oxidant to the cathode and the anode. They are exposed to both the reducing and oxidizing environments. Moreover, damage to the plates by the corrosive electrolyte through creepage and evaporation must be limited by suitable coatings.

Materials and fabrication of separator plates are a major part of the total cost of a MCFC and there exists ongoing research to simplify the structure of the plates (i.e. introducing internal and external manifolding) and improve their performance in order to lower the costs.

To select the best material for the separator plates, a dual-atmosphere test under extreme conditions must be performed. The selected material must withstand the oxidizing and reducing condition under a given operating pressure and temperature. Similarly, a single-atmosphere test which includes passing high concentration oxidant or hydrogen over the selected separator plate must be satisfied.

Separator plates are usually manufactured from thin sheets of stainless steel. To protect the anode side of the bipolar plate from corrosion, coatings such as nickel or aluminum are used.

A wet-seal method is employed for the sealing of MCFCs. Coating the bipolar plate wet-seal area with aluminum helps to produce $LiAlO_2$ from the reaction of Al with Li_2CO_3. Sealing methods are further discussed in the next section.

3.2.5 Sealing

Sealing is a major challenge in high temperature fuel cells. However, due to the fact that the electrolyte of such fuel cells is impermeable to reactant gases, it could be utilized as the sealing of the fuel cell. Moreover, the electrolyte matrix of a MCFC has a plastic nature and could be used in the sealings. Sealing of the MCFC, also called wet-seal, is performed by utilizing the electrolyte to prevent gas from escaping through the edges of the cells. Using the electrolyte for the sealing has many advantages such as the compatibility of the electrolyte with other parts of the fuel cell, impermeability to the reactant gases and the ability to withstand thermal cycling.

3.2.6 Manifolding

Fuel cell manifolding is one of the most important aspects which influences all parameters related to the performance of the system. Manifolding can mainly be done in two different ways. External manifolding and interrnal manifolding. External manifolding is the simplest method which provides a good distribution of the reactant gases to the cells. Moreover, the pressure drop in the channels is kept to a minimum. The reactant gases are supplied at one end and the exhaust is removed from the opposite side of the stack. This leads to a symmetric and uniform distribution of the reactants in the fuel cell. Moreover, the active area of an externally manifolded fuel cell is much larger than the fuel cells with other types of manifoldings. Therefore, enhanced performance from an externally manifolded fuel cell is achieved. However, external manifolding suffers from gas leakage and carbonate ions migration because of the nature of the seals. In addition, as the reactants are fed to the anode and the cathode at right angles to one another (i.e. cross-flow), uneven temperature distribution occurs. Therefore, insulating gaskets to prevent gas leakage and thermal management to enhance the performance of externally manifolded fuel cells are necessary.

On the other hand, internal manifolding can be a feasible solution to all the limitations stated for an external manifolding. Gas is distributed through the ducts or channels (i.e. internal manifolds) within the bipolar plates. Therefore, by internal manifolding techniques manufacturing a wide variety of gas distribution geometries would be possible (e.g. co-flow, counter-flow, etc.).

Gas sealing for internal manifolding is obtained by using the electrolyte matrix as the sealant. The capacity of the fuel cell can be easily increased by stacking up more single cells and there will be no limitation with the internal manifolds unlike the external manifolding which requires different manifolds for different designs. However, the main disadvantage of internal manifolding is the complexity and high cost of manufacturing the patterned bipolar plates. An example of internal and external manifoldings is illustrated in Figure 4 below.

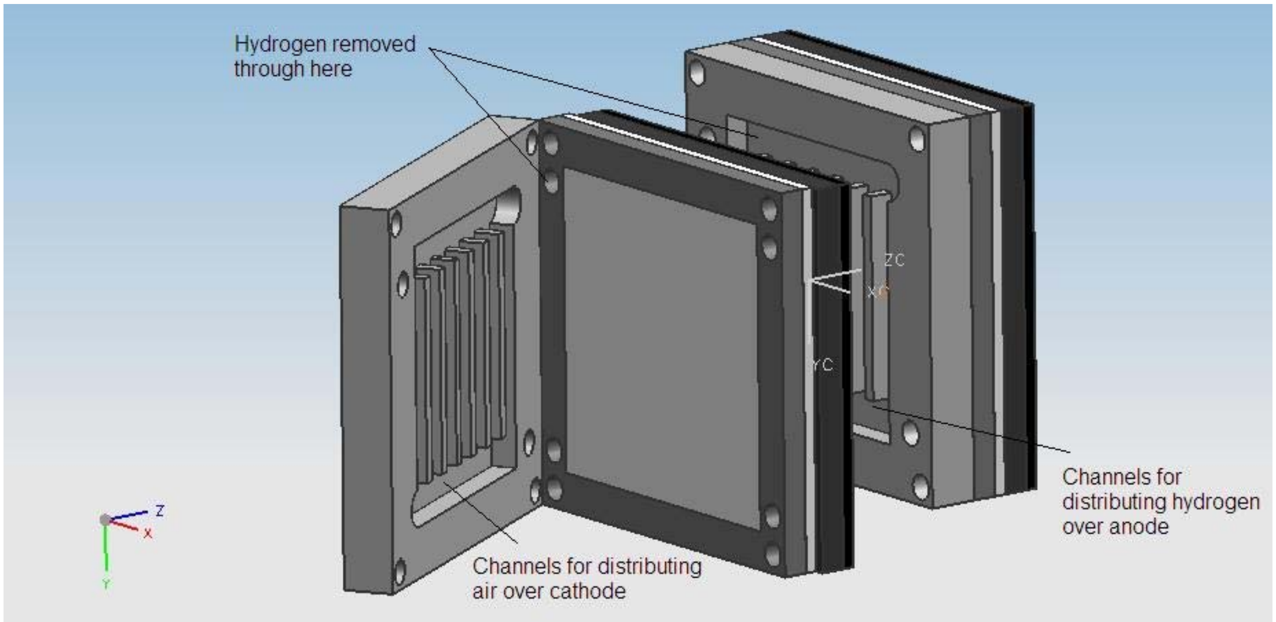

(a)

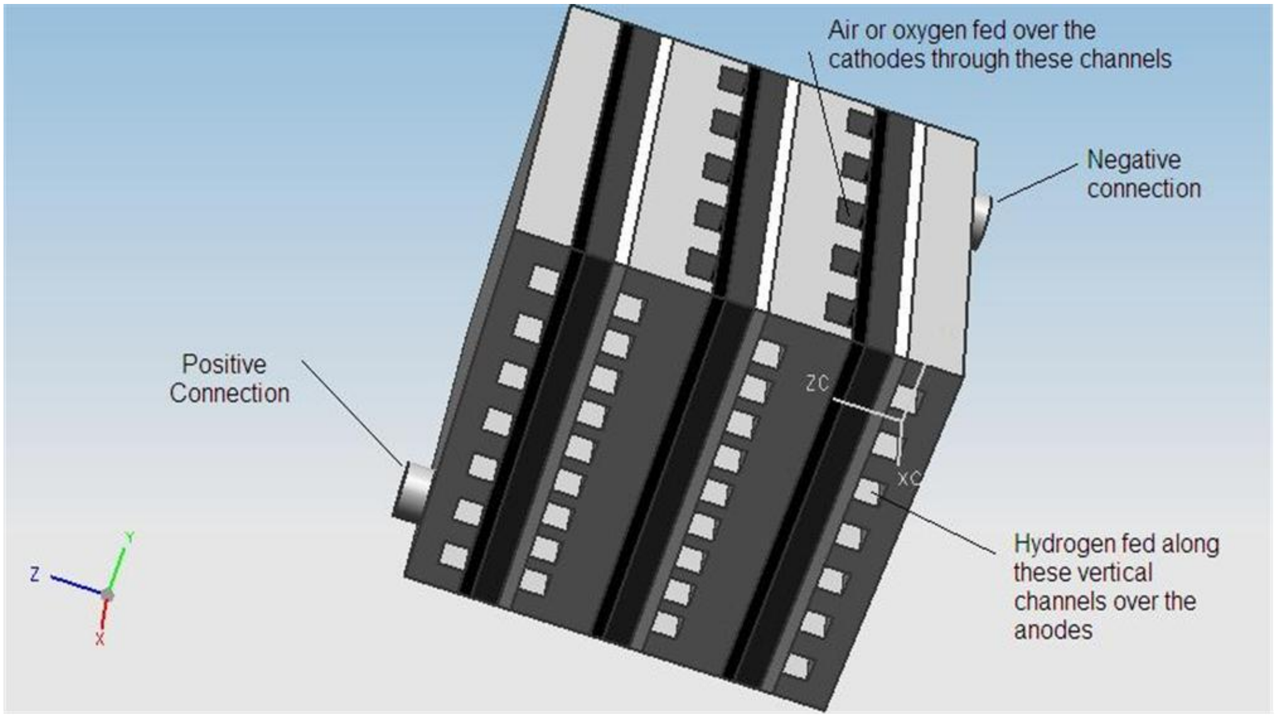

(b)

Figure 4: Schematics of an (a) internal and (b) external manifolding for MCFC.

Chapter 4: PERFORMANCE ANALYSIS ASPECTS

The performance of MCFCs is usually studied using the plot of voltage versus current density (polarization curve). The polarization graph depends on the fuel cell operating conditions such as reactant gases utilization and compositions. Assuming that the fuel cell is in thermodynamic equilibrium, the zero-current (i.e. open-circuit) voltage is identical to the reversible fuel cell potential. The Nernst equation 4.1 below, provides a relationship between the equilibrium cell potential (E_{eq}) and the standard cell potential (E^0) for the fuel cell reaction at thermodynamic equilibrium.

$$E_{eq}(T,P_i) = E^0(T,P) + \frac{RT}{zF} ln \left\{ \left[\frac{P_{H_2} P_{O_2}^{1/2}}{P_{H_2O}} \right] \left[\frac{P_{CO_2,c}}{P_{CO_2 a}} \right] \right\} \qquad (4.1)$$

where ‘a’ and ‘c’ denote anode and cathode, respectively. The value of $E_{eq}(T,P_i)$ is equal to the cell potential at temperature T and partial pressures P_i (in atm). $E^0(T,P)$ is the reversible cell voltage of a MCFC at P_i=1 atm and 650°C and can be calculated by [7].

$$E^0 = \frac{-\Delta \bar{g}_f}{zF} \qquad (4.2)$$

where ‘z’ is the number of electrons transferred for each molecule of fuel reacted in the fuel cell, ‘F’ is the Faraday constant and ‘$-\Delta \bar{g}_f$’ is the change in Gibbs free energy for the hydrogen reaction (i.e. $H_2 + \frac{1}{2} O_2 \rightarrow H_2O$).

Therefore, the cell voltage becomes

$$E^0 = \frac{197{,}000}{6 \times 96{,}485} = 1.02\ V \quad \text{(at 650°C and 1 atm)} \qquad (4.3)$$

As it can be seen from equation 4.1, the reversible cell potential is a function of the partial pressure of the reactants at both cathode and anode. Therefore, varying the concentration of the reactant gases at the inlet of the fuel cell alters the reversible cell voltage.

Moreover, the reversible potential also depends on the operating temperature. Effects of the operating pressure and temperature on the fuel cell performance are discussed in the following sections.

4.1 Effect of pressure

The effects of the operating pressure on the performance of the fuel cell are studied using the Nernst equation (i.e. Equation 4.1). If the cathode and the anode pressure are assumed to be constant and equal to the total pressure and the composition of the reactant gases remain the same, the change in the reversible cell voltage can be found as,

$$\Delta E_{eq,P} = E_{eq}(T,P_2) - E_{eq}(T,P_1) = \frac{RT}{4F} ln\left(\frac{P_2}{P_1}\right) \tag{4.4}$$

Therefore, with a typical MCFC operating temperature of 650^{o}C, a 46 mV increase of the reversible cell voltage is obtainable when the operating pressure increases 10 fold.

The main reasons for the increase of cell voltage are the enhanced reaction kinetics due to the increase in the reactant gases' partial pressures (concentrations). However, there are several disadvantages when running the MCFC at high operating pressures. Any small pressure difference between the anode and the cathode compartment of the fuel cell may result in an electrolyte matrix damage or crack. As a result, gas crossover may occur which deteriorates the performance of the fuel cell dramatically. Moreover, operating at elevated pressure may damage the sealing of the fuel cell. Hence, the fuel cell system must be enclosed within a pressure vessel. These vessels usually contain non-reactive gases such as nitrogen.

Higher operating pressures may also result in undesirable chemical reactions within the fuel cell. Carbon deposition due to the Boudouard reaction, and methane formation due to methanation reaction, are such examples.

$2CO \rightleftharpoons C + CO_2$ (Boudouard reaction) (4.5)

$CO + 3H_2 \rightleftharpoons CH_4 + H_2O$ (Methanation reaction) (4.6)

According to the Le Chatelier principle, increasing the operating pressure increases the formation of carbon and methane in the first and second reaction, respectively. The carbon formed could plug the pores of the anode and that results in reactant gas transport limitations. Methane formed has an unfavorable effect on the MCFC performance. Production of 1 mole of methane requires 3 moles of hydrogen and this can be seen as a wasteful use of fuel that could be used to generate power. These two problems could be avoided by adding water or increasing the partial pressure of the water in the reactant gas streams.

Increasing the operating pressure of the MCFC requires higher power for the compressor which introduces higher capital and operating costs. Therefore, it is not economical to pressurize MCFC systems with power outputs of 1 MW or less. Considering the practical constraints and the cost analysis of the system, pressures of above 5 bar may not be very beneficial for molten carbonate fuel cell systems [45].

4.2 Effect of temperature

Considering the concept of Gibbs free energy, any change in operating temperature affects the reversible potential of the fuel cell. The dependence of cell reversible and irreversible voltages on temperature is further discussed in the thermodynamic analysis chapter.

Moreover, chemical reactions which occur at the anode of the fuel cell are sensitive to the fuel cell temperature. These reactions are the Boudouard reaction, methanation reaction, water-gas shift reaction and methane decomposition reaction.

The methane decomposition and water-gas shift reactions are as follows:

$CH_4 \rightleftharpoons C + 2H_2$ (Methane decomposition reaction) (4.7)

$CO + H_2O \rightleftharpoons CO_2 + H_2$ (Water-Gas shift reaction) (4.8)

The water-gas shift reaction quickly approaches equilibrium at the operating temperature of an MCFC in the presence of the anode nickel catalysts. Therefore, carbon monoxide acts as an indirect source to produce hydrogen for the MCFC. Hence, the composition of the reactant gases and the percentage of completion of each chemical reaction depend on the fuel cell operating temperature.

The reversible cell potential is a weak function of temperature. However, the operating voltages are highly affected by the temperature. Increasing the fuel cell operating temperature results in a significant reduction of cathode polarization due to the enhanced reaction kinetics. Consequently, there will be a net increase in the actual cell potential.

Further increase of the cell temperature above 650^{o}C may result in undesirable electrolyte evaporation and material corrosion and, therefore, it should be avoided.

4.3 Effect of current density

Fuel cell effectiveness is computed by the power output of the fuel cell. The power output of an MCFC is a function of operating voltage and current density. Therefore, at first sight it might seem best to operate the MCFC at the maximum current density. However, increasing the current density results in an increase of the losses and irreversibilities. Fuel cell irreversibilities can be divided into three main groups.

1) Activation losses which occur at lower current densities; 2) Ohmic losses which are a linear function of current density and dominate at medium current densities; and 3) Concentration losses which dominate at high current densities.

Activation losses are mainly due to the low kinetic reaction rates near the three-phase zone. Therefore, it shows its effects at low current densities of the polarization curve. At intermediate current densities, Ohmic losses appear to be the dominant source of irreversibilities. Electrolyte resistance to the carbonate ions and of the bipolar plates and other metallic compartments are the main contributors to Ohmic losses. Concentration losses dominate when the fuel cell is operating at high current densities. Fuel and oxidant gases are depleted down the channels of the bipolar plates and across the electrodes. Increasing the current density may result in quicker depletion of the reactant gases which leaves low current densities at the exit of the fuel cell. Therefore, from the polarization curve, the steep decrease of the voltage at high current densities is the result of concentration losses.

4.4 Lifetime and performance

There are many factors that affect the lifetime and performance of a MCFC such as electrolyte loss, corrosion, dissolution of cells, increase in contact resistance, electrode creepage and sintering and electrolyte matrix shortening. Currently, 40,000 hours of operation is the desired goal for the lifetime of MCFC stacks. However, improvements and optimization of the fuel cell are essential to achieve such a high lifetime.

4.4.1 Electrolyte loss

Electrolyte loss is mainly due to the high operating temperature of the fuel cell and degradation of the fuel cell compartments over the operating time. Electrolyte loss may result in gas cross-over and reduction of the three-phase reaction zone. It mainly occurs by evaporation, electric potential-driven migration and corrosion processes.

4.4.2 Corrosion

A limiting factor for the MCFC life-time is the corrosion of metallic parts, especially for current collectors and separator plates. On the anode side of the cell, the operating conditions are more severe and the anode is in contact with high temperature molten carbonates that are partially impregnated into it. Also, the materials used at the anode side must be economically competitive, easy to form and shape, and most importantly they must be good electrical conductors.

An experiment on the corrosion of anodic parts was performed by Durante et al. [46]. To perform the corrosion test, they exposed the samples to Li/K molten carbonate at 650^{o}C and the anodic gas mixture of H_2/CO_2 (80/20), which was humidified at 500^{o}C, was passed through the assembly. In order to evaluate the composition of the oxide scale, its thickness, its compactness and internal corrosion, if present, the samples were examined to characterize the corrosion behavior by scanning electron microscope (SEM) equipped with energy dispersive X-ray spectrometer (EDS) and by optical microscope. Experimental results showed that the main degradation problems were related to the counter-diffusion of some metal elements (Cr, Fe, Mn) from base material into the nickel coating and of oxidant species (O_2, CO_2) from the external environment [47]. Also, carburization that affects the base material and leads to a brittleness in the material itself, was reported as a devastating factor affecting the behavior of trilayers (Ni/AISI310S/Ni assembly) in an anodic environment. Due to carburization, carbon diffuses through the Ni layer and enriches the base metal with a negative increment of hardness [47]. From the experiment performed after 3,000 h in a corrosion test, the trilayer shows an increment of electrical resistance. Formation of oxides through Ni grain layers is the main reason for the change in electrical resistance. Although there is only a small electrical resistance increase after 3,000h of operation, for a longer operating time further changes in resistance are expected which continue to reduce the efficiency of the cell.

Another investigation on corrosion has been carried out by Bergman et al. [48]. They used a laboratory MCFC cell with a specially designed cathode current collector in order to investigate the contact corrosion resistance between AISI 310 as current collector and two different cathode materials, NiO and $LiCoO_2$. In this experimental investigation, it was found that the contact resistance between the cathode and the current collector contributes to a large extent to the total cathode polarization. An iron-rich layer with a small amount of cobalt formed the corrosion layer between the $LiCoO_2$ cathode and the AISI 310 current collectors. However, the formed layer between the NiO cathode and the current collector was nickel-rich. Since the layer that formed at the interface of the $LiCoO_2$ cathode and AISI 310 current collector was a two-phase oxide, it had a lower conductivity compared to the NiO cathode.

Therefore, there is a need for further investigations in regards to the corrosion layers forming and the contact resistance between different parts of the cell compartments due to the lack of available results and study in this area.

4.4.3 Dissolution of NiO cathode

The cathode material, NiO, dissolves in the electrolyte and due to hydrogen diffusion into the matrix from the anode side and the presence of carbonate, metallic nickel precipitates in the pores of the matrix subsequently. The reactions to produce metallic nickel in the electrolyte are as follows:

Dissociation of NiO into the electrolyte

$$NiO + CO_2 \leftrightarrow Ni^{2+} + CO_3^{-2} \tag{4.9}$$

Producing metallic nickel from Ni^{2+}

$$Ni^{2+} + CO_3^{-2} + H_2 \leftrightarrow Ni + CO_2 + H_2O \tag{4.10}$$

The presence of Ni in the electrolyte results in performance reduction due to the short-circuiting across the electrolyte.

4.4.4 Electrolyte losses

The reaction between the electrolyte and the stack components because of the electrolyte loss results in lithiation of electrodes and the matrix fibers of Al_2O_3, and the corrosion of cell hardware. Evaporation of the electrolyte, especially K_2CO_3, would cause further electrolyte loss. This usually happens in the first 1,000h of the operation and is primarily dependent on the partial pressure of H_2O and CO_2, volume gas flow and electrolyte temperature and composition [49, 50].

4.4.5 Corrosion of bipolar plate

Depending on the type of separator plate used (internal manifolding or external manifolding), the corrosion rate of the plates differs. Using internal manifolding, the wet-seal area which is mainly covered by the electrolyte is in direct contact with other parts of the stack. Therefore, any severe corrosion in this area leads to short circuiting and direct reaction between the oxygen and hydrogen without any external electric charge gain. Sufficient coating of both sides of the separator plate using corrosion resistant materials helps to increase the performance and lifetime of the MCFC.

4.4.6 Electrolyte retention capacity

During the lifetime of the electrolyte, the matrix converts from α-$LiAlO_2$ to γ-$LiAlO_2$ which causes particle growth and increase of matrix pore size (e.g. [51, 52]). This results in a loss of capillary retention for electrolyte and, therefore, redistribution of electrolyte and finally cross-over of the reactants. It is suggested by Nishimura et al. [51] and Higaki et al. [52] to initially manufacture the matrix as γ-$LiAlO_2$ to reduce the corresponding problems.

4.4.7 Catalyst deactivation

In the case of internal reforming, deactivation of the catalyst occurs by sintering of the carrier material or of the nickel crystallites. Moreover, migration or evaporation and subsequent deposition of electrolyte can also deactivate the catalyst.

The reforming procedure and limitations are further discussed at the end of this chapter.

4.4.8 Matrix cracking

Matrix cracking causes the direct reaction of oxidant and fuel gas (i.e. cross-over) which introduces local overheating in the cell. Thermal cycling is the major cause of matrix cracking. Thermal cycling can occur during the cell operation, maintenance and failures in operation of the system.

4.4.9 High temperature creep of porous components

High temperature creep and sintering of the cathode and porous materials causes the thinning of the assembly leading to losses and reducing the performance of the MCFC [53, 54]. Using a flexible wet-seal area between the separator plates avoids the shrinkage and loss of electrical contact between cell components in internal manifolding stacks. In general, a flexible design facilitates the reduction of electric contact losses.

4.4.10 Contaminants and system aspects

The primary fuel for MCFCs is natural gas. However, in the near future gasified coal is expected to be another main fuel for MCFCs. Depending on the quality and location of the coal mined, the coal-derived fuels may contain a variety of contaminates. Contaminates such as sulfur (H_2S and SO_2) and halides (HCl) accelerate the corrosion of cell metallic compartments such as anodes. As a result, the performance of the fuel cell is severely affected. Therefore, appropriate fuel purification and removal of contaminants such as sulfur or chlorine compounds, is necessary to keep the degradation of the cell to its minimum. Table 1 and Table 2 show the coal-derived fuel gas contaminates, their possible negative effects and the maximum allowable limits for MCFCs respectively [44, 55].

Table 1: Typical coal-derived fuel gas contaminates and their negative effects on MCFCs.

Contaminates	Negative Effects
Sulfur compounds such as H_2S, CS_2, C_4H_4S, COS	Pores plugging, voltage loss and electrolyte sulfation
Halides such as HCl, HF, HBr	Increase the corrosion, performance degradation
Nitrogen compounds such as NH_3, HCN, N_2	NOx formation, reaction with electrolyte and performance degradation
Hydrocarbons such as C_6H_6, $C_{10}H_8$, $C_{14}H_{10}$	Carbon deposition
Trace metals such as Zink, Lead, Selenium, Arsenic	Poisoning Ni catalyst, precipitation/deposits on electrode

Table 2: Maximum allowable limits of contaminates in the fuel gas for MCFCs.

Contaminates	Maximum allowable limit
Sulfur compounds	< 1 ppm
Halides	< 10 ppm
NH_3	< 10000 ppm
Zink	< 20 ppm
Lead, Arsenic	< 1 ppm

4.5 Reforming

Reforming is a process in which natural gas is converted into hydrogen as the fuel for the fuel cell. The reforming process is an endothermic reaction and, therefore, the exhaust heat of the fuel cell could be utilized in providing the heat required for the reformation process. There are different approaches in utilizing the MCFC cathode exhaust heat as discussed below.

4.5.1 Direct Internal Reforming (DIR)

The fuel cell chemical reactions are exothermic and the resulting heat produced in the stack could be used for the reforming reaction directly. As a result, cooling of the fuel cell could be reduced as most of the heat produced by the fuel cell is used for the reforming reaction. The main reaction which occurs along the reformer catalysts is the methane reforming reaction.

$$CH_4 + H_2O \rightleftharpoons CO + 3H_2 \tag{4.11}$$

Therefore, utilizing the hydrogen which is the fuel for the MCFC moves the reaction towards completion. Utilizing a direct internal reforming system leads to a better hydrogen distribution in the fuel cell and, as a result, the temperature would be more evenly distributed.

The main problem with using direct internal reforming is the poisoning of the reformer catalysts. In order to have a sufficient rate of reforming, supported metal catalysts must be incorporated. Impurities of the fuel and creep of the liquid molten carbonate along the metallic cell components and transport in the gas phase in the form of alkali hydroxyl species could damage the catalysts and degrade the performance of the DIR- MCFC.

4.5.2 Indirect Internal Reforming (IIR)

Indirect internal reforming is the coupling of the reformer and the fuel cell stack in close but separate compartments. With this approach, the reformer benefits from the heat transfer from the fuel cell while it would be resistant to alkali/carbonate poisoning. Figure 5 is the schematic representation of direct and indirect internal reforming molten carbonate fuel cell.

4.5.3 External Reforming (ER)

External reforming takes place in a separate unit installed in the MCFC power plant. Cathode exhaust which posses a high energy content is burnt in a catalytic burner and the heat produced is supplied to the reformer for the endothermic methane reforming reaction to occur. Lower overall efficiency and higher capital costs are the main disadvantages of such systems. However, when there is a size limitation with the fuel cell stack, external reformers should be employed.

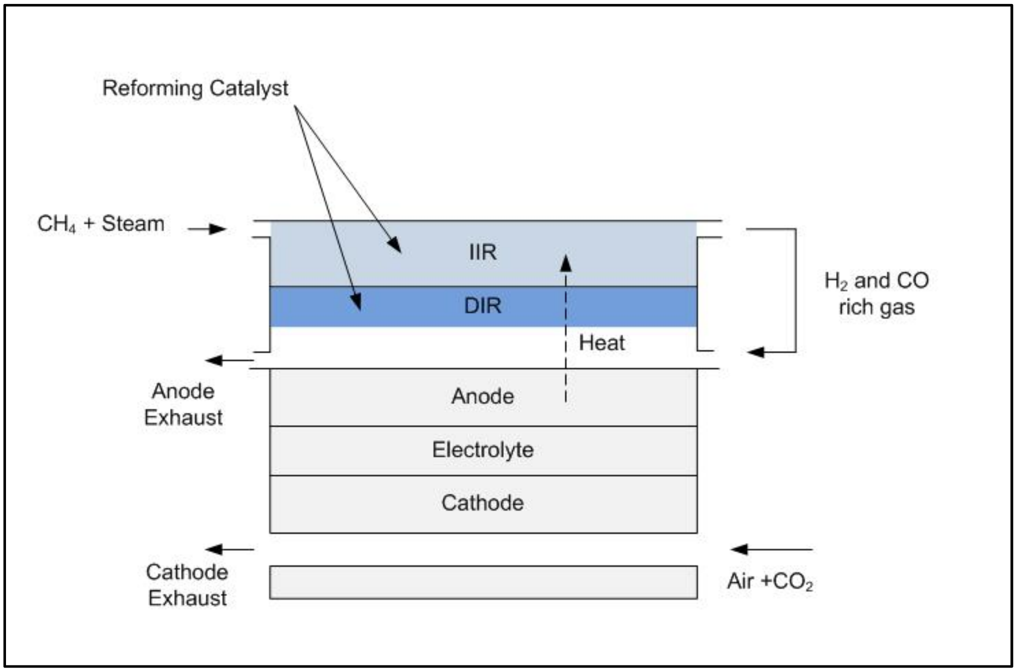

Figure 5: Schematic representation of direct and indirect internal reforming MCFC.

4.5.4 Advantages and disadvantages of internal and external reforming processes

Internal reforming in general has many advantages. The most important advantage is the lower cost of the MCFC system because there would not be any separate external reformer required. Moreover, the overall efficiency increases because the heat generated in the fuel cell could be directly utilized in the reforming reaction. Therefore, the power required for the air compression and recirculation is reduced. The methane conversion rate is quite high in the case of internal reforming because the produced hydrogen is directly utilized in the fuel cell electrochemical reaction. In contrast, an external reforming system is separated both thermally and physically from the fuel cell and, therefore, no instantaneous heat or mass transfer would be possible.

Another important advantage of internal reforming is that there would be less steam required for the reforming reaction. Steam is supplied from the product of the anode chemical reaction of the MCFC.

4.5 Advantages and disadvantages of MCFCs

Notwithstanding the general advantages of fuel cells such as essentially zero emissions and high efficiencies, Table 1 summarizes the advantages and disadvantage of MCFC systems.

Table 3: Advantages and disadvantages of MCFC systems

Advantages	Disadvantages
High operating pressure which results in lower irreversbilities	High costs
High operating temperature which results in improved reaction kinetics and lower irreversibilities	Not suitable for portable applications
High efficiency	Sealing
Suitable for use as combined cycle	Cell component degradation at high operating temperature
Ability to work with many hydrocarbons such as natural gas	Corrosive electrolyte results in the anode and cathode performance degradation

Chapter 5: THERMODYNAMIC ANALYSIS

This chapter deals with the thermodynamic analysis of MCFC hybrid systems. Firstly, a brief description and equations related to the current density and voltage are given. Moreover, assumptions made for the analysis are stated. Finally, efficiency with two different approaches is defined and the corresponding results are discussed.

5.1 Current, current density, cell potential and irreversibilities

The MCFC fuel cell current can be determined based on the molar amount of oxygen or carbon monoxide utilized in the fuel cell as follows,

Molar O_2 usage = I/ 2F (5.1)

Molar CO usage = I / 2F (5.2)

However, it is more popular to divide the fuel cell current by the fuel cell surface area and refer to it as the current density instead. Using the definition of the current density and electrical power we have,

Stack power = cell voltage × i × active surface area× number of cells (5.3)

where 'i' is the current density (current density = I / A). (5.4)

The cell voltage used in the definition of the stack power is the output voltage of the fuel cell. It could be computed using:

$$V_{cell} = E_{eq} - i(R_{ohmic} + \eta_{anode} + \eta_{cathode}) \ , \tag{5.5}$$

where E_{eq} is the equilibrium cell potential defined previously; R_{ohmic} is the Ohmic cell resistance which could be calculated by using the experimental correlation from e.g. [27] as,

$$R_{ohmic} = 0.5 \times 10^{-4} \times exp\left[3016\left(\frac{1}{T_{FC}} - \frac{1}{923}\right)\right] \tag{5.6}$$

η_{anode}: Re-scaled anodic overpotential which could be estimated by using the following empirical equation [27]:

$$\eta_{anode} = 2.27 \times 10^{-9} \times exp\left(\frac{6435}{T_{FC}}\right) P_{H_2}^{-0.42}. P_{CO_2}^{-0.17}. P_{H_2O}^{-1.0} \tag{5.7}$$

$\eta_{cathode}$: Re-scaled cathodic overpotential which could be estimated by using the following empirical equation [27]:

$$\eta_{cathode} = 7.505 \times 10^{-10} \times exp\left(\frac{9298}{T_{FC}}\right) P_{O_2}^{-0.43}. P_{CO_2}^{-0.09} \tag{5.8}$$

where 'P_i' is the partial pressure of species 'i' at the inlet and 'FC' stands for fuel cell. These equations are only valid for operating temperatures of 600-700°C (e.g. [56]).

Equation 5.5 simply rolls all complex dynamics of the MCFC unit cell and stack level into one effective expression, given by a fit to experimental data in the form of polarization curves. Moreover, both the concentration and activation losses are being incorporated into equation 5.7 and 5.8.

5.2 State equations

In order to be able to do the performance analysis of the hybrid system, state properties such as enthalpy, entropy and exergy of each gas flow stream are defined in this section.

The molar enthalpy and entropy can be found as follows (e.g. [57-59]):

$$\bar{h} = RT(\beta_1 + \frac{\beta_2}{2}T + \frac{\beta_3}{2}T^2 + \frac{\beta_4}{2}T^3 + \frac{\beta_5}{2}T^4 + \frac{\beta_6}{T}) \tag{5.9}$$

$$\bar{s} = R(\beta_1 \ln(T) + \beta_2 T + \frac{\beta_3}{2}T^2 + \frac{\beta_4}{3}T^3 + \frac{\beta_5}{4}T^4 + \beta_7) \tag{5.10}$$

where β_i is taken from JANAF tables [60] .

The molar exergy term is the sum of physical, thermal and chemical exergetic terms as follows:

$$\bar{\Psi}_i = \left(\bar{h}_i(T) - \bar{h}_i(T_0)\right) - T_0\left(\bar{s}_i(T) - \bar{s}_i(T_0)\right) + RT_0 \ln(X_i) + \bar{\Psi}_i^{chemical} \qquad (5.11)$$

where X_i is the mole fraction of species 'i' and $\bar{\Psi}_i^{chemical}$ is the chemical exergy.

There are several definition and measurements to obtain the standard chemical exergy of elements, organic and inorganic substances (e.g. [10, 61, 62]).

However, the chemical exergy values used in this thesis are assumed to be constant and taken from the exergoecology portal [63] and Morris et al. [64] (Table 4):

Table 4: Chemical exergy of several gaseous species.

Component, i	**N_2**	**O_2**	**H_2O**	**CO_2**	**CH_4**
Standard chemical exergy $ex_{ch,i}$ (kJ/kmol)	639	3,951	8,636	14,176	82,4348

5.3 General balance equations

A general balance equation for any quantity in a system can be written as [65]

Input + Generation – Output- Consumption = Accumulation (5.12)

Therefore, general mass, energy, entropy and exergy balance equations may be written by (e.g. [65, 66])

Mass inlet – Mass output = Mass accumulation (5.13)

Energy inlet – Energy outlet = Energy accumulation (5.14)

Entropy input + Entropy generation – Entropy output = Entropy accumulation (5.15)

Exergy input – Exergy output – Exergy destruction = Exergy accumulation (5.16) where the main contributors to the exergy destruction are the chemical reaction, mixing, heat transfer, friction and phase change.

5.4 Heat Recovery Ratio (HRR)

Heat recovery is one of the most efficient techniques used to increase the efficiency of hybrid systems by using the waste heat which is exhausted to the environment. There are many studies available in the literature where the heat recovery process is used as one of the main attributes in enhancing the performance of industrial systems (e.g. [67-69]). The heat recovery ratio can be defined, based on the electrical energy output of the hybrid system, as

$$Heat\ Recovery\ Ratio\ (HRR) = \frac{The\ amount\ of\ heat\ recovered\ from\ the\ system}{Total\ electrical\ energy\ output} \tag{5.17}$$

Moreover, the heat recovery ratio can be defined in a similar way, based on the electrical energy input to the hybrid system, as

$$Heat\ Recovery\ Ratio\ (HRR) = \frac{The\ amount\ of\ heat\ recovered\ from\ the\ system}{Total\ electrical\ energy\ input} \tag{5.18}$$

5.5 General efficiency equations

General energy and exergy efficiencies for a steady-state process can be defined as follows [65]:

$$\eta_{energy} = \frac{Energy\ in\ product\ output}{Energy\ in\ inputs} = 1 - \frac{Energy\ loss}{Energy\ in\ inputs} \tag{5.19}$$

$$\eta_{exergy} = \frac{Exergy\ in\ product\ output}{Exergy\ in\ inputs} = \frac{Exergy\ loss\ plus\ consumption}{Exergy\ in\ inputs} \tag{5.20}$$

Exergy-based efficiencies for steady-state devices are defined as follows [65]:

$$Rational\ efficiency = \frac{Total\ exergy\ output}{Total\ exergy\ input} = 1 - \frac{Exergy\ consumption}{Total\ exergy\ input} \tag{5.21}$$

$$Task\ efficiency = \frac{Theoretical\ minimum\ exergy\ input\ required}{Actual\ exergy\ input} \tag{5.22}$$

The bottoming cycle efficiencies could be defined as:

$$\eta_{energy} = \frac{Turbine/turboexpander\ work\ output - compressor\ work\ required}{Energy\ in\ inputs - Fuel\ cell\ work\ output} \tag{5.23}$$ *

$$\eta_{exergy} = \frac{Turbine/turboexpander\ work\ output - compressor\ work\ required}{Exergy\ in\ inputs - Fuel\ cell\ work\ output} \tag{5.24}$$

The subsystem energy and exergy efficiencies are defined using:

$$\eta_{energy,subsystem} = \frac{Turbin/turboexpander\ work\ output}{Energy\ in\ inputs} \tag{5.25}$$

$$\eta_{exergy} = \frac{Turbin/turboexpander\ work\ output}{Exergy\ in\ inputs} \tag{5.26}$$

*Note: Turbine, turboexpander and compressor correspond to the components of the hybrid systems studied in the next chapter.

Chapter 6: CASE STUDIES

6.1 Case study 1: Thermodynamic analysis of a MCFC combined system

The first study performed here is an exergy and energy analysis of a non-internal reforming pressurized MCFC with a bottoming-cycle turbocompressor of the type proposed in the 1990s by MC-Power (Burr Ridge, IL, out of business since 2000) and Ansaldo (Genoa, Italy). Full thermodynamic analysis conducted here includes mass, energy and exergy balance equations, overall and bottoming cycle energy and exergy efficiencies and exergy destruction calculations. Moreover, a sensitivity study to investigate the variation of system operating conditions on the overall performance of the MCFC and the system is performed.

6.1.1 System description

Natural gas after filtration and desulphurization is mixed with steam which is preheated from the stack exhaust gases. The mixture is then heated further in a regenerative heat exchanger and fed to the reformer. After the reforming reaction takes place, the exit gas is passed through the regenerative heat exchanger again and finally fed to the anode of the MCFC. A fraction of hydrogen input, and also some residual $CH_{4,}$ pass the anode unreacted. Therefore, following the electrochemical reaction in the stack, the exhaust mixed with a fraction of cathode exhaust is burnt in the catalytic burner in order to produce the heat necessary for the endothermic reactions taking place in the reformer. The heat produced in the catalytic burner is directly transferred to the reformer and it is assumed that there is no heat transfer with the surroundings in this study. The catalytic burner exhaust, which is a hot mixture rich in CO_2, is mixed with fresh air coming from the compressor and fed to the cathode.

Figure 6 illustrates the schematic of the hybrid system studied in this section. Moreover, temperature and pressure values of all the streams are indicated in the graph.

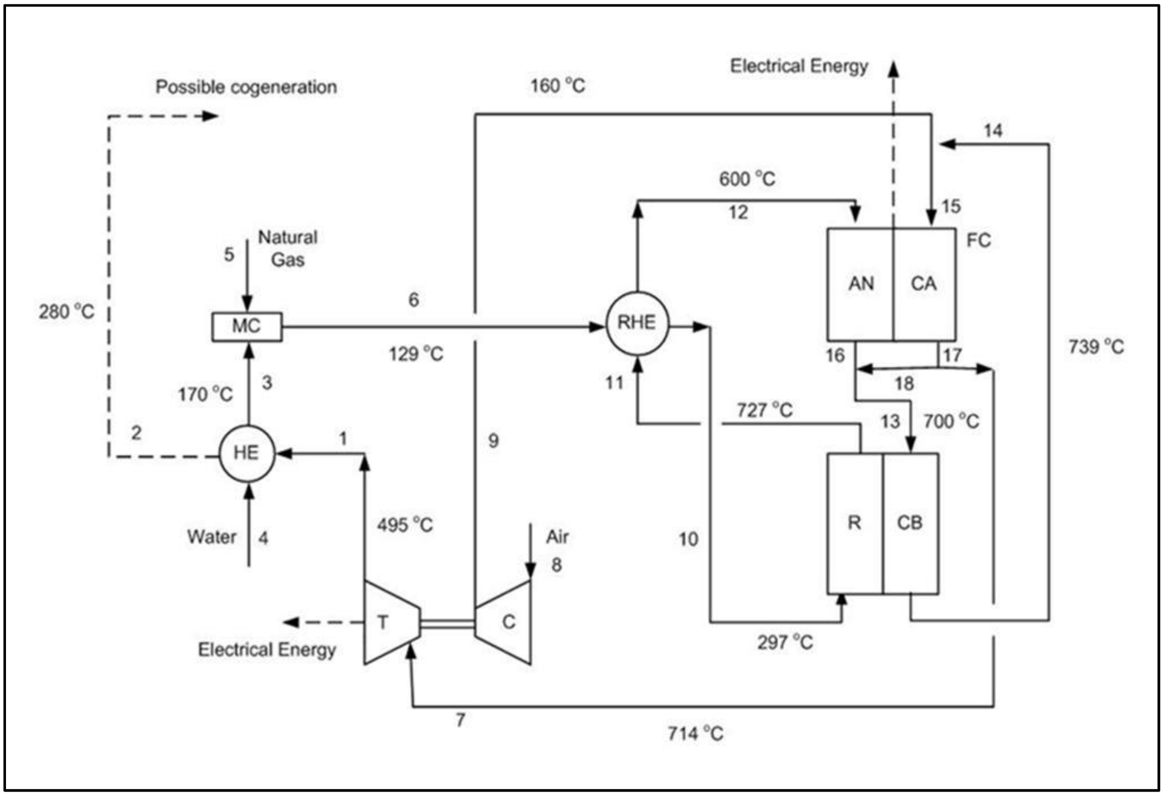

Figure 6 : Schematic of the MCFC system for the first case study (HE: Heat Exchanger, RHE: Regenerative Heat Exchanger, MC: Mixing Chamber, CB: Catalytic Burner, R: Reformer, T: Turbine, C: Compressor, CA: Cathode, AN: Anode).

6.1.2 Assumptions

Similar to all other types of fuel cells, the operating principle of MCFCs is basically the indirect combination of hydrogen and oxygen to produce water, employing an electrolyte, thereby producing electrical energy and heat. The assumptions made in this analysis are as follows:

- Steady state operation for all components.
- All units are based on the SI unit system, e.g., kPa for pressure, K for temperature and kJ/kg for enthalpy.
- All stream gases are ideal gases and, therefore, ideal gas properties using EES (Engineering Equation Solver) software [70] are employed.
- The hydrogen utilization factor is taken to be 70 % in this study.
- 85 % of methane is reformed in the reformer and the rest is simply passing through the fuel cell without any chemical reaction but burnt completely in the catalytic burner.
- The heat exchanger, pumps, compressor and turbine are adiabatic and, hence, no heat transfer occurs between them and the surroundings.
- All kinetic and potential exergetic terms are negligible.
- The chemical exergetic term does not change in the turbine, pumps, compressor or the heat exchanger.
- The outlet of the cathode, after increasing the temperature of the inlet water, is discharged to the environment. (It is possible to use this high temperature mixture in a cogeneration system and achieve higher total efficiencies.)

- The ambient temperature and pressure are constant (T_0 and P_0) and would obviously change the system exergetic efficiency if they are subjected to any change.
- The total heat required for the reforming reactions in the reformer (the reforming reaction is endothermic) is supplied from the catalytic burner and no heat is lost from these systems.
- Some fraction of heat generated by the stack is lost due to convective cooling and radiation, the rest exits with the cathode exhaust.
- The combination of a compressor and turbine as a turbocharger is used in this system. Therefore, a fraction of power produced by the turbine is used in the compressor and the rest is a useful power output.
- The compressor increases the inlet air pressure from 1 atm to 4 atm.
- Molar flow rates for streams where any chemical reaction take place can be used in order to find the energy balance equations.
- Air is an ideal gas with a composition of 21 % oxygen and 79 % nitrogen.
- Metal dusting reactions which result in a deteriorating performance of the MCFC, are neglected.
- Isentropic operation is assumed for the compressor and the turbine.
- The inlet mass flow rate of natural gas, water and air are taken from De Simon et al. [3] which are 74.5 kg/h, 252 kg/h and 2250 kg/h respectively.

6.1.3 Analysis

Starting with mass, energy and exergy balances for each component and the whole system, the exergy losses and overall efficiencies of the hybrid system are found (the technique used to write the mass, energy and exergy balance equations are utilized from Dincer et al. [65] and Moran et al. [71]).

Heat exchanger (HE):

Water input at (4) is heated to 170°C through the heat exchanger. The burner exhaust after exchanging heat with water can be used for cogeneration purposes.

The mass balance equation for the turbine exhaust passing through the HE is:

$$\sum_i \dot{n}_{i,1} = \sum_i \dot{n}_{i,2} \tag{6.1}$$

$$\dot{m}_1 = \dot{m}_2 \tag{6.2}$$

where 'i' is the species entering and leaving the heat exchanger, '$\dot{n}_i$' and '$\dot{m}_i$' denote molar and mass flow rates, respectively.

No reaction takes place in this heat exchanger. Therefore, the water composition leaves the heat exchanger unchanged and the mass flow rate remains the same.

$$\dot{n}_3 = \dot{n}_4 \tag{6.3}$$

$$\dot{m}_3 = \dot{m}_4 \tag{6.4}$$

The energy balance equation is

$$\dot{n}_3\bar{h}_3 + \sum_{i=1}^{N} \dot{n}_{i,2}\bar{h}_{i,2} = \dot{n}_4\bar{h}_4 + \sum_{i=1}^{N} \dot{n}_{i,1}\bar{h}_{i,1} \tag{6.5}$$

where $\bar{h}_i$ is the molar enthalpy.

The exergy balance equation reads

$$\dot{n}_4\overline{\Psi}_4 + \sum_{i=1}^{N} \dot{n}_{i,1}\overline{\Psi}_{i,1} - \dot{n}_3\overline{\Psi}_3 - \sum_{i=1}^{N} \dot{n}_{i,2}\overline{\Psi}_{i,2} - \dot{E}x_{dest,HE} = 0 \tag{6.6a}$$

$$\dot{E}x_{dest,HE} = \dot{n}_4\overline{\Psi}_4 + \sum_{i=1}^{N} \dot{n}_{i,1}\overline{\Psi}_{i,1} - \dot{n}_3\overline{\Psi}_3 - \sum_{i=1}^{N} \dot{n}_{i,2}\overline{\Psi}_{i,2} \tag{6.6b}$$

where $\dot{E}x_{dest,HE}$ is the exergy destruction; $\overline{\Psi}_i$ is the molar flow availability (i.e. exergy).

Mixing chamber (MC):

Natural gas (5) and water (3) are mixed together in the mixing chamber and the output (6) is directed towards the regenerative heat exchanger.

The mass balance equation is:

$$\dot{m}_3 + \dot{m}_5 = \dot{m}_6 \tag{6.7}$$

The energy balance equation is:

$$\dot{n}_3\bar{h}_3 + \dot{n}_5\bar{h}_5 = \dot{n}_6\bar{h}_6 \tag{6.8}$$

The exergy balance equation is:

$$\dot{n}_3\bar{\Psi}_3 + \dot{n}_5\bar{\Psi}_5 - \dot{n}_6\bar{\Psi}_6 - \dot{E}x_{dest,MC} = 0 \tag{6.9a}$$

$$\dot{E}x_{dest,MC} = \dot{n}_3\bar{\Psi}_3 + \dot{n}_5\bar{\Psi}_5 - \dot{n}_6\bar{\Psi}_6 \tag{6.9b}$$

Turbine (T):

Hot depleted cathode gas (7) enters the turbine and leaves at (1) to produce power necessary to run the compressor as well as the electrical power output.

The mass balance equations are:

$$\sum_i \dot{n}_{i,1} = \sum_i \dot{n}_{i,7} \tag{6.10}$$

$$\dot{m}_1 = \dot{m}_7 \tag{6.11}$$

The energy balance equation reads

$$\sum_{i=1}^{N} \dot{n}_{i,7}\bar{h}_{i,7} - \sum_{i=1}^{N} \dot{n}_{i,1}\bar{h}_{i,1} - \dot{W}_{s,net} = 0 \tag{6.12}$$

where $\dot{W}_{s,net}$ is the net electrical power output from the turbine. A fraction of total power produced in the turbine is used in the compressor to compress air.

The exergy balance equation becomes

$$\sum_{i=1}^{N} \dot{n}_{i,7}\bar{\Psi}_{i,7} - \sum_{i=1}^{N} \dot{n}_{i,1}\bar{\Psi}_{i,1} - \dot{W}_{s,net} - \dot{E}x_{dest,T} = 0 \tag{6.13a}$$

$$\dot{E}x_{dest,T} = \sum_{i=1}^{N} \dot{n}_{i,7}\overline{\Psi}_{i,7} - \sum_{i=1}^{N} \dot{n}_{i,1}\overline{\Psi}_{i,1} - \dot{W}_{s,net} \tag{6.13b}$$

Compressor (C):

Air from the environment (8) enters the compressor and high pressure air leaves at (9). Power to run the compressor is supplied by the turbine.

The mass balance equation is:

$$\dot{n}_8 = \dot{n}_9 \tag{6.14}$$

$$\dot{m}_8 = \dot{m}_9 \tag{6.15}$$

The energy balance equation takes the form

$$\dot{n}_8\bar{h}_8 - \dot{n}_9\bar{h}_9 + \dot{W}_x = 0 \tag{6.16}$$

where $\dot{W}_x$ is the fraction of turbine electrical energy used in the compressor to compress the inlet air.

The exergy balance equation reads

$$\dot{n}_8\overline{\Psi}_8 - \dot{n}_9\overline{\Psi}_9 + \dot{W}_x - \dot{E}x_{dest,C} = 0 \tag{6.17a}$$

$$\dot{E}x_{dest,C} = \dot{n}_8\overline{\Psi}_8 - \dot{n}_9\overline{\Psi}_9 + \dot{W}_x \tag{6.17b}$$

Regenerative heat exchanger (RHE):

The mixture of methane and water (6) is passed through the regenerative heat exchanger and leaves at (10). It is heated by the excess heat from the reformer stream (11 to 12).

The mass balance equations are

$$\sum_i \dot{n}_{i,6} = \sum_i \dot{n}_{i,10} \tag{6.18}$$

$$\sum_i \dot{n}_{i,11} = \sum_i \dot{n}_{i,12} \tag{6.19}$$

$$\dot{m}_6 = \dot{m}_{10} \tag{6.20}$$

$$\dot{m}_{11} = \dot{m}_{12} \tag{6.21}$$

The energy balance equation reads

$$\sum_{i=1}^{N} \dot{n}_{i,6}\bar{h}_{i,6} + \sum_{i=1}^{N} \dot{n}_{i,11}\bar{h}_{i,11} - \sum_{i=1}^{N} \dot{n}_{i,10}\bar{h}_{i,10} - \sum_{i=1}^{N} \dot{n}_{i,12}\bar{h}_{i,12} = 0 \tag{6.22}$$

The exergy balance equation is

$$\sum_{i=1}^{N} \dot{n}_{i,6}\bar{\Psi}_{i,6} + \sum_{i=1}^{N} \dot{n}_{i,11}\bar{\Psi}_{i,11} - \sum_{i=1}^{N} \dot{n}_{i,10}\bar{\Psi}_{i,10} - \sum_{i=1}^{N} \dot{n}_{i,12}\bar{\Psi}_{i,12} - \dot{E}x_{dest,RHE} = 0$$

(6.23a)

$$\sum_{i=1}^{N} \dot{E}x_{dest,RHE} = \sum_{i=1}^{N} \dot{n}_{i,6}\bar{\Psi}_{i,6} + \sum_{i=1}^{N} \dot{n}_{i,11}\bar{\Psi}_{i,11} - \sum_{i=1}^{N} \dot{n}_{i,10}\bar{\Psi}_{i,10} - \sum_{i=1}^{N} \dot{n}_{i,12}\bar{\Psi}_{i,12}$$

(6.23a)

Reformer (R):

The mixture of methane and water (10) enters the reformer and after the methane reforming reaction occurs, it leaves at (11).

The mass balance equations are

$$\sum_i \dot{n}_{i,10} = \sum_i \dot{n}_{i,11} \tag{6.24}$$

$$\dot{m}_{10} = \dot{m}_{11} \tag{6.25}$$

The energy balance equation reads

$$-\sum_{i=1}^{N} \dot{n}_{i,11}\bar{h}_{i,11} + \sum_{i=1}^{N} \dot{n}_{i,10}\bar{h}_{i,10} + \dot{Q}_R = 0 \tag{6.26}$$

where $\dot{Q}_R$ is the heat transferred from the catalytic burner (CB) for the endothermic reaction taking place inside the reformer.

The exergy balance equation is given by

$$-\sum_{i=1}^{N} \dot{n}_{i,11}\bar{\Psi}_{i,11} + \sum_{i=1}^{N} \dot{n}_{i,10}\bar{\Psi}_{i,10} - (1 - \frac{T_0}{T_{RF}})\dot{Q}_R - \dot{E}x_{dest,R} = 0 \tag{6.27a}$$

$$\dot{E}x_{dest,R} = -\sum_{i=1}^{N} \dot{n}_{i,11}\bar{\Psi}_{i,11} + \sum_{i=1}^{N} \dot{n}_{i,10}\bar{\Psi}_{i,10} - (1 - \frac{T_0}{T_{RF}})\dot{Q}_R \tag{6.27b}$$

where T_{RF} is the average reformer body temperature.

Catalytic burner (CB):

The exit gas mixture from the MCFC (13) enters the catalytic burner and in order to produce CO_2 for the cathode (14), it is burnt with excess O_2.

The mass balance equations are

$$\sum_i \dot{n}_{i,13} = \sum_i \dot{n}_{i,14} \tag{6.28}$$

$$\dot{m}_{13} = \dot{m}_{14} \tag{6.29}$$

The energy balance equation reads

$$-\sum_{i=1}^{N} \dot{n}_{i,14}\bar{h}_{i,14} + \sum_{i=1}^{N} \dot{n}_{i,13}\bar{h}_{i,13} + \dot{Q}_{CB} = 0 \tag{6.30}$$

The exergy balance equation is given by

$$-\sum_{i=1}^{N} \dot{n}_{i,14}\bar{\Psi}_{i,14} + \sum_{i=1}^{N} \dot{n}_{i,13}\bar{\Psi}_{i,13} - (1 - \frac{T_0}{T_{CB}})\dot{Q}_{CB} - \dot{E}x_{dest,CB} = 0 \tag{6.31a}$$

$$\dot{E}x_{dest,CB} = -\sum_{i=1}^{N} \dot{n}_{i,14}\bar{\Psi}_{i,14} + \sum_{i=1}^{N} \dot{n}_{i,13}\bar{\Psi}_{i,13} - (1 - \frac{T_0}{T_{CB}})\dot{Q}_{CB} \tag{6.31b}$$

where $\dot{Q}_{CB}$ is the heat lost from the catalytic burner which is provided to the reformer; T_{CB} is the average body temperature of the catalytic burner.

MCFC (FC):

The molten carbonate fuel cell is the main component of the combined system under consideration. Its main components are the anode, cathode and the electrolyte. However, we treat the MCFC as one unit, consisting of anode and cathode, without resolving the unit cell and stack level dynamics (see Eqs. (6.34)-(6.35) below).

The mass balance equations are

$$\dot{m}_{12} = \dot{m}_{16} \tag{6.32}$$

$$\dot{m}_{15} = \dot{m}_{17} \tag{6.33}$$

The energy balance equation reads

$$\sum_{i=1}^{N} \dot{n}_{i,15}\bar{h}_{i,15} - \sum_{i=1}^{N} \dot{n}_{i,17}\bar{h}_{i,17} + \sum_{i=1}^{N} \dot{n}_{i,12}\bar{h}_{i,12} - \sum_{i=1}^{N} \dot{n}_{i,16}\bar{h}_{i,16} - \dot{Q}_{FC} - \dot{W}_{FC} = 0 \tag{6.34}$$

The exergy balance equation becomes

$$\sum_{i=1}^{N} \dot{n}_{i,15}\bar{\Psi}_{i,15} - \sum_{i=1}^{N} \dot{n}_{i,17}\bar{\Psi}_{i,17} + \sum_{i=1}^{N} \dot{n}_{i,12}\bar{\Psi}_{i,12} - \sum_{i=1}^{N} \dot{n}_{i,16}\bar{\Psi}_{i,16} - \left(1 - \frac{T_0}{T_{FC}}\right) r\dot{Q}_{FC} - \dot{W}_{FC} - \dot{E}x_{dest,FC} = 0 \tag{6.35a}$$

$$\dot{E}x_{dest,FC} = \sum_{i=1}^{N} \dot{n}_{i,15}\bar{\Psi}_{i,15} - \sum_{i=1}^{N} \dot{n}_{i,17}\bar{\Psi}_{i,17} + \sum_{i=1}^{N} \dot{n}_{i,12}\bar{\Psi}_{i,12} - \sum_{i=1}^{N} \dot{n}_{i,16}\bar{\Psi}_{i,16} - \left(1 - \frac{T_0}{T_{FC}}\right) r\dot{Q}_{FC} - \dot{W}_{FC} \tag{6.35b}$$

where T_{FC} is the average bulk temperature of the fuel cell; $\dot{W}_{FC}$ is the electrical energy output from the MCFC; 'r' is the percentage of heat transferred through radiation or convection by the cell walls.

6.1.4 Miscellaneous equations

6.1.4.1 Utilization equations

The hydrogen, CO and oxidant utilization factors are defined using the corresponding equation from ref [72] as follows:

$$U_{H_2} = \frac{\dot{n}_{H_2,11} - \dot{n}_{H_2,16}}{\dot{n}_{H_2,11}} \tag{6.36}$$

$$U_{CO} = \frac{\dot{n}_{CO,11} - \dot{n}_{CO,16}}{\dot{n}_{CO,11}} \tag{6.37}$$

$$U_{CO_2} = \frac{\dot{n}_{CO_2,15} - \dot{n}_{CO_2,17}}{\dot{n}_{CO_2,15}} \tag{6.38}$$

Therefore, considering the water produced in the fuel cell we have

$$\dot{n}_{H_2O,16} = \dot{n}_{H_2O,11} + \dot{n}_{H_2,11}U_{H_2} \tag{6.39}$$

Nitrogen is an inert gas and passes the cathode without any reaction. Therefore, we have

$$\dot{n}_{N_2,15} = \dot{n}_{N_2,17} \tag{6.40}$$

6.1.4.2 Efficiency equations

Calculation of the overall energy and exergy efficiencies of the hybrid system follows:

$$\eta_{energy} = \frac{\dot{W}_{FC}+\dot{W}_S-\dot{W}_x}{\dot{n}_{fuel}\times LHV} \tag{6.41a}$$

If the heat content of stream (2) is utilized for a cogeneration purpose, the overall energy efficiency becomes

$$\eta_{energy} = \frac{\dot{W}_{FC}+\dot{W}_S-\dot{W}_x+\dot{Q}_2}{\dot{n}_{fuel}\times LHV} \tag{6.41b}$$

$$\eta_{exergy} = \frac{\dot{W}_{FC}+\dot{W}_S-\dot{W}_x}{\sum_i (\dot{n}_i\times ex_i)} = 1 - \frac{\sum \dot{Ex}_{dest}}{\sum_i (\dot{n}_i\times ex_i)} \tag{6.42}$$

where ‘i’ denotes the fuel, air and water at inlet; LHV is the lower heating value of fuel taken from [73]; $\sum \dot{Ex}_{dest}$ is the total exergy destruction in the compressor, turbine, heat exchanger, mixing chamber, fuel cell, reformer and catalytic burner. Moreover, as the cathode exhaust after the water heating is released to the environment, the exergy content of stream 2 could be included as the overall exergy destruction.

The bottoming cycle energy and exergy efficiency could be defined according to:

$$\eta_{energy} = \frac{\dot{W}_S-\dot{W}_x}{\dot{n}_{fuel}\times LHV-\dot{W}_{FC}} \tag{6.43}$$

$$\eta_{exergy} = \frac{\dot{W}_S-\dot{W}_x}{\sum_i (\dot{n}_{fuel}\times ex_{fuel})-\dot{W}_{FC}} \tag{6.44}$$

Efficiency is defined as a static efficiency in equations 5.54 and 5.55. This means that the total fuel supplied to the fuel cell is assumed to be constant. Therefore, by increasing the current density, the efficiency is expected to have the same trend as the fuel cell power output. However, efficiency could also be defined differently with a dynamic expression to take into account the variation of fuel required for different power outputs. The dynamic efficiency expression is used for the analysis of the Enbridge MCFC system.

6.2 Case study 2: Thermodynamic analysis of an Enbridge Inc. MCFC system

In this section, an exergy and energy analysis of a non-internal reforming pressurized MCFC with a bottoming-cycle turboexpander is performed. This system is similar to the MCFC combined system built for Enbridge Inc. in Toronto and, by using the limited data available, a thermodynamic analysis is performed. Mass, energy and exergy balance equations are written here similar to the system studied before, and exergy and energy efficiencies are calculated. In addition, a comparative study is performed to investigate the effects of varying the system operating conditions on the overall performance and efficiency.

6.2.1 System description

High pressure natural gas (350 psi, 24 atm) is passed through a turboexpander to produce 1 MW of electricity towards the grid. Due to the expansion of the gas, pressure drops dramatically and, as a result, the temperature of the gas decreases. If the gas entering the turboexpander is not preheated, it would lead to pipeline freezing after the expansion. For this reason, it is preheated by utilizing the cathode exhaust heat. After the expansion, a fraction of gas is directed towards the mixing chamber for use in the MCFC system. The remaining gas is supplied to households in the low pressure pipes.

The schematic Enbridge MCFC system is given in Figure 7.

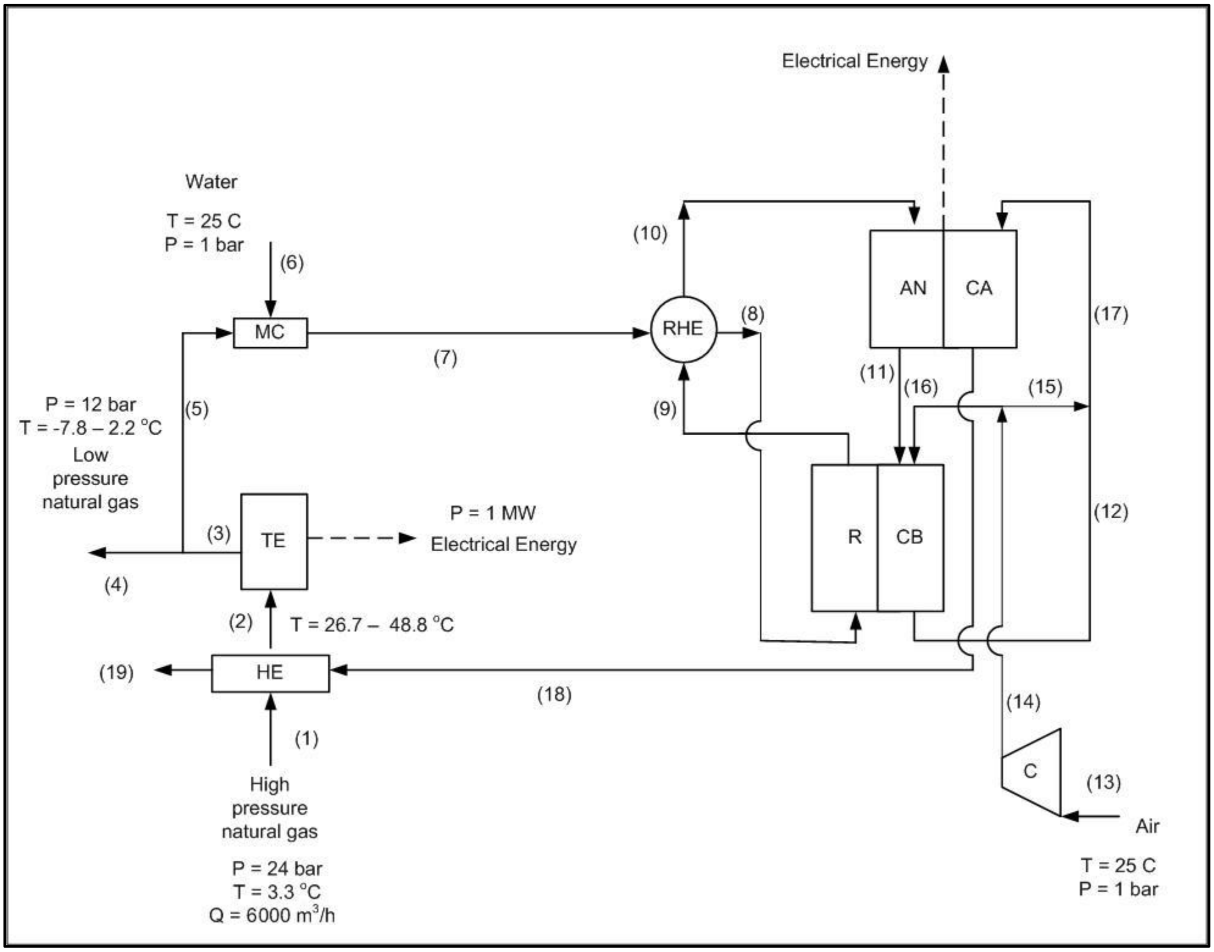

Figure 7 : Schematic of the MCFC system for the second case study (HE: Heat Exchanger, RHE: Regenerative Heat Exchanger, MC: Mixing Chamber, CB: Catalytic Burner, R: Reformer, TE: TurboExpander, C: Compressor, CA: Cathode, AN: Anode).

6.2.2 Assumptions

The main assumptions used for the Enbridge MCFC system analysis are taken from the first case study. However, there are several specific assumptions made for the Enbridge system as follows:

- The turboexpander has a maximum power output of 1 MW.
- The cathode exhaust is directly used to increase the temperature of the input gas to the system.
- The MCFC stack consists of 300 single fuel cells and it can provide a power output as high as 1.2 MW.
- Reformer and catalytic burner chemical reactions are assumed to reach completion.
- The high pressure (i.e. 350 psi) natural gas volume flow rate is assumed to be 6,000 m^3/h.
- The turboexpander operates adiabatically. Therefore, there is not any heat interaction between the device and the environment and the corresponding terms in the energy and exergy equations are assumed to be zero.
- The temperature and pressure of each stream are given as follows:

6.2.3 Analysis

This section deals with the analysis of the Enbridge MCFC hybrid system. Similar procedures and equations as in the first case study are used for this system. However, the bottoming cycle equations differ from the first study and they are explained here.

Table 5: Temperature and pressure of each stream of the Enbridge hybrid MCFC system.

Temperature [K]		Pressure [bar]	
T1	276.5	**P1**	24
T2	297.81	**P2**	24
T3	275.61	**P3**	12
T4	269.3	**P4**	12
T5	269.3	**P5**	12
T6	298.15	**P6**	12
T7	288.2	**P7**	12
T8	500	**P8**	12
T9	700	**P9**	12
T10	625	**P10**	12
T11	923.15	**P11**	12
T12	1273.15	**P12**	12
T13	298.15	**P13**	1
T14	673.15	**P14**	12
T15	673.15	**P15**	12
T16	673.15	**P16**	12
T17	1023.15	**P17**	12
T18	923.15	**P18**	12
T19	773.15	**P19**	12

6.2.3.1 Balance Equations

<u>Heat exchanger (HE):</u>

High pressure natural gas input at (1) is heated to 26.7^{o}C–48.8^{o}C through the heat exchanger. The MCFC cathode exhaust, after exchanging heat with natural gas, can be used for cogeneration purposes (19).

The mass balance equation for the MCFC exhaust passing through the HE is

$$\sum_i \dot{n}_{i,18} = \sum_i \dot{n}_{i,19} \tag{6.45}$$

$$\dot{m}_{18} = \dot{m}_{19} \tag{6.46}$$

where ‘i’ is the species entering and leaving the heat exchanger, ‘$\dot{n}_i$’ and ‘$\dot{m}_i$’ denote molar and mass flow rates, respectively.

No chemical reaction takes place in the heat exchanger. Therefore, natural gas leaves the heat exchanger unchanged and its mass flow rate remains the same.

$$\dot{n}_1 = \dot{n}_2 \tag{6.47}$$

$$\dot{m}_1 = \dot{m}_2 \tag{6.48}$$

The energy balance equation is

$$\dot{n}_1\bar{h}_1 + \sum_{i=1}^{N} \dot{n}_{i,18}\bar{h}_{i,18} = \dot{n}_2\bar{h}_2 + \sum_{i=1}^{N} \dot{n}_{i,19}\bar{h}_{i,19} \tag{6.49}$$

The exergy balance equation reads

$$\dot{n}_1\bar{\Psi}_1 + \sum_{i=1}^{N} \dot{n}_{i,18}\bar{\Psi}_{i,18} - \dot{n}_2\bar{\Psi}_2 - \sum_{i=1}^{N} \dot{n}_{i,19}\bar{\Psi}_{i,19} - \dot{E}x_{dest,HE} = 0 \tag{6.50a}$$

$$\dot{E}x_{dest,HE} = \dot{n}_1\bar{\Psi}_1 + \sum_{i=1}^{N} \dot{n}_{i,18}\bar{\Psi}_{i,18} - \dot{n}_2\bar{\Psi}_2 - \sum_{i=1}^{N} \dot{n}_{i,19}\bar{\Psi}_{i,19} \tag{6.50b}$$

Turboexpander (TE):

High pressure natural gas passes through the turboexpander and its pressure and temperature drops. The gas expansion results in 1 MW power output according to the Enbridge data provided. The mass, energy and exergy balance equations of the turboexpander are:

Mass balance:

$$\dot{n}_2 = \dot{n}_3 \tag{6.51}$$

$$\dot{n}_3 = \dot{n}_4 + \dot{n}_5 \tag{6.52}$$

$$\dot{m}_2 = \dot{m}_3 \tag{6.53}$$

$$\dot{m}_3 = \dot{m}_4 + \dot{m}_5 \tag{6.54}$$

The energy balance equation reads

$$\sum_{i=1}^{N} \dot{n}_{i,2}\bar{h}_{i,2} - \sum_{i=1}^{N} \dot{n}_{i,3}\bar{h}_{i,3} - \dot{W}_{TE} = 0 \tag{6.55}$$

where $\dot{W}_{TE}$ is the electrical power output of the turboexpander.

The exergy balance equation becomes

$$\sum_{i=1}^{N} \dot{n}_{i,2}\overline{\Psi}_{i,2} - \sum_{i=1}^{N} \dot{n}_{i,3}\overline{\Psi}_{i,3} - \dot{W}_{TE} - \dot{Ex}_{dest,TE} = 0 \tag{6.56a}$$

$$\dot{Ex}_{dest,TE} = \sum_{i=1}^{N} \dot{n}_{i,2}\overline{\Psi}_{i,2} - \sum_{i=1}^{N} \dot{n}_{i,3}\overline{\Psi}_{i,3} - \dot{W}_{TE} \tag{6.56b}$$

where subscript “TE” stands for turboexpander.

6.2.3.2 Heat recovery ratio

Heat recovery ratio for the Enbridge hybrid system is defined as follows:

$$\text{Heat Recovery Ratio (HRR)} = \frac{\text{Heat recovered}}{\text{Power output}} = \frac{\dot{n}_{\text{gas inlet}}\overline{C}_{p}(T_2 - T_1)}{\dot{W}_{TE}} \tag{6.57}$$

6.2.3.2 Efficiency definition

The expressions used to define the efficiency of the hybrid system in this section differ from the first case study. Efficiencies defined for the Enbridge hybrid system are the dynamic efficiencies. Therefore, the current density and the total fuel molar flow rate are interrelated. As a result, the denominator in the efficiency definition (i.e. required molar flow rate) is a function of the numerator (i.e. power output) which itself relates to the current density. Hence,

$$\eta_{energy} = \frac{\dot{W}_{FC} + \dot{W}_{TE} - \dot{W}_{x}}{\dot{n}_{fuel,required} \times LHV} \tag{6.58}$$

$$\eta_{exergy} = \frac{\dot{W}_{FC} + \dot{W}_{TE} - \dot{W}_{x}}{\sum_{i} (\dot{n}_{i} \times ex_{i})} = 1 - \frac{\sum \dot{Ex}_{dest}}{\sum_{i} (\dot{n}_{i} \times ex_{i})} \tag{6.59}$$

where $\dot{n}_{fuel,required}$ is the required molar fuel flow rate and it is a function of fuel cell current density.

The subsystem energy and exergy efficiencies could be defined using:

$$\eta_{energy,subsystem} = \frac{\dot{W}_{TE}}{\dot{n}_{fuel,required} \times LHV} \tag{6.60}$$

$$\eta_{exergy} = \frac{\dot{W}_{TE}}{\sum_{i} (\dot{n}_{i} \times ex_{i})} \tag{6.61}$$

Chapter 7: PERFORMANCE OPTIMIZATION

This chapter deals with the optimization of a MCFC. The fuel cell power output is constructed as a function of the main operating parameters of the MCFC (i.e. operating pressure, temperature and current density). There are specific constraints defined on fuel cell parameters which help the convergence of the optimization process.

7.1 Derivation of the objective function

In any optimization process, an objective function (i.e. cost function) and several constraints must be defined. However, in some cases there is not any limit on the constraints and the problem turns into an unconstraint optimization problem. Based on the type of the objective function, an optimization process could be divided into linear, quadratic, nonlinear optimization, etc. The optimization of MCFC power output described here is a nonlinear optimization problem and the MATLAB optimization toolbox is utilized for the computations.

The general format of any optimization problem is as follows:

Minimize f(x), subject to several constraints, where ‘x’ is the n×1 column vector of variables that minimizes f(x) at $f^*(x^*)$.

The studied objective function for the optimization process is the fuel cell power output which is a function of operating voltage, current density and number in cells of the stack.

$$\dot{W}_{FC} = V \times I \times n \tag{7.1}$$

where ‘V’, ‘I’ and ‘n’ are the fuel cell voltage, current and number of cells of a fuel cell stack, respectively.

'I' is the current of the fuel cell in Amperes. It is the product of the current density (A/m^2) and the fuel cell active area. However, as the optimization process proposed here does not focus on optimization of the fuel cell surface area, the MCFC current is used in all the computations. The current is assumed to be an independent property and any changes in current would affect the voltage and power of the fuel cell subsequently.

The number 'n' of single cells in a stack is assumed to be constant and equal to 100.

'V', the fuel cell voltage, is a dependent function of many variables such as the partial pressures of the streams, current density, etc.

In order to study the impact of the variation of fuel cell operating pressure on the power output, the pressure is assumed to be a product of a new variable, 'r', and the ambient pressure (i.e. $P = r \times P_{atm}$). Therefore, the optimization process could be employed to find the optimum value of 'r' in any given optimization search domain.

Overall, the chemical reaction $H_2 + 0.5O_2 \rightarrow H_2O$ takes place in the fuel cell. Therefore, the Gibbs free energy of formation of water could be computed using:

$$G = H - T \times S \rightarrow \bar{g}_f = \bar{h}_f - T\bar{s} \tag{7.2}$$

Hence, assuming that the fuel cell operates at a constant temperature, it reads:

$$\Delta\bar{g}_f = \Delta\bar{h}_f - T\Delta\bar{s} \tag{7.3}$$

where

$$\Delta\bar{h}_f = \left(\bar{h}_f\right)_{H_2O} - \left(\bar{h}_f\right)_{H_2} - 0.5\left(\bar{h}_f\right)_{O_2} \tag{7.4}$$

$$\Delta\bar{s}_f = \left(\bar{s}_f\right)_{H_2O} - \left(\bar{s}_f\right)_{H_2} - 0.5\left(\bar{s}_f\right)_{O_2} \tag{7.5}$$

In order to calculate the molar enthalpy and entropy we have:

$$\bar{h}_T = \bar{h}_{298.15} + \int_{298.15}^{T} \bar{C}_p dT \tag{7.6}$$

$$\bar{s}_T = \bar{s}_{298.15} + \int_{298.15}^{T} \frac{1}{T} \bar{C}_p dT \tag{7.7}$$

Using the equations below, the molar heat capacity of steam, hydrogen and oxygen can be evaluated.

For steam:

$$\bar{C}_p = 143.05 - 58.040T^{0.25} + 8.2751T^{0.5} - 0.036989T \tag{7.8}$$

For H_2:

$$\bar{C}_p = 56.505 - 22222.6T^{-0.75} + 116500T^{-1} - 560700T^{-1.5} \tag{7.9}$$

For O_2:

$$\bar{C}_p = 37.432 - 2.0102\times10^{-5}T^{1.5} - 178570T^{-1.5} - 2368800T^{-2} \tag{7.10}$$

Table 6 below shows the standard molar enthalpy and entropy of a hydrogen fuel cell at 298.15 K and standard pressure [74].

Table 6: Standard molar enthalpy and entropy of a hydrogen fuel cell at STP.

Species	$\bar{h}_f$ [kJ/kmol]	$\bar{s}_f$ [kJ/kmol K]
H_2O (liquid)	-285838	70.05
H_2O (steam)	-241827	188.83
H_2	0	130.59
O_2	0	205.14

The partial pressure of each species used in computing the overpotential is as follows:

$$P_{H_2} = P_{total} \times (\dot{n}_{H_2,12}/\dot{n}_{total,12}) \tag{7.11}$$

$$P_{CO_2,c} = P_{total} \times (\dot{n}_{CO_2,15}/\dot{n}_{total,15}) \tag{7.12}$$

$$P_{CO_2,a} = P_{total} \times (\dot{n}_{CO_2,12}/\dot{n}_{total,12}) \tag{7.13}$$

$$P_{O_2} = P_{total} \times (\dot{n}_{O_2,15}/\dot{n}_{total,15}) \tag{7.14}$$

$$P_{H_2O} = P_{total} \times (\dot{n}_{H_2O,12}/\dot{n}_{total,12}) \tag{7.15}$$

where

$P_{total} = r \times P_{atm}$ (i.e. r × atmospheric pressure [bar]) (7.16)

7.2 Defining the constraints

The variables selected as constraints are the fuel cell temperature, current density and ‘r’. MCFCs usually operate at 650°C. However, a variation of fuel cell temperature in the range of $600 < T_{FC} < 700$ [°C] is chosen for this study. Higher or lower temperatures than this limit would not be feasible due to resulting higher overpotentials at lower temperature and manufacturing difficulties at higher temperatures.

The current density range varies from 0.2 A/cm^2 to 0.8 A/cm^2. Current densities lower and higher than the limits selected may not be suitable or feasible for a MCFC. Therefore, the maximum power output should ideally have a current density within the range specified. The active area of each cell is assumed to be 1 m^2 and, therefore, the current has a range of 2000 to 8000 A.

The stack operating pressure is limited by the impediments related to the sealing and manufacturing difficulties of the MCFC. Therefore, ‘r’ is constrained by $1< r <10$

(i.e. $1\text{atm} < P_{total} < 10\text{atm}$).

Therefore, the optimization problem can be stated as following:

Minimize $f(I, T_{FC}, r) = -\dot{W}_{FC} = -V \times I \times n$ (7.17)

where

$$V = E_{eq} - i \times (\eta_{act} + \eta_{conc} + \eta_{ohm}) \qquad (i = I / \text{Active cell area}) \qquad (7.18)$$

$$E_{eq}(T, P_i) = E^0(T, P) + \frac{RT}{nF} ln\left\{\left[\frac{P_{H_2}P_{O_2}^{1/2}}{P_{H_2O}}\right]\left[\frac{P_{CO_2,c}}{P_{CO_2a}}\right]\right\} \qquad (7.19)$$

$$P_{H_2} = P_{total} \times \left(\dot{n}_{H_2,12}/\dot{n}_{total,12}\right) \qquad (7.20)$$

$$P_{CO_2,c} = P_{total} \times \left(\dot{n}_{CO_2,15}/\dot{n}_{total,15}\right) \tag{7.21}$$

$$P_{CO_2,a} = P_{total} \times \left(\dot{n}_{CO_2,12}/\dot{n}_{total,12}\right) \tag{7.22}$$

$$P_{O_2} = P_{total} \times \left(\dot{n}_{O_2,15}/\dot{n}_{total,15}\right) \tag{7.23}$$

$$P_{H_2O} = P_{total} \times \left(\dot{n}_{H_2O,12}/\dot{n}_{total,12}\right) \tag{7.24}$$

$$\bar{g}_f = \bar{h}_f - T\bar{s} \tag{7.25}$$

$$\Delta\bar{h}_f = \left(\bar{h}_f\right)_{H_2O} - \left(\bar{h}_f\right)_{H_2} - 0.5\left(\bar{h}_f\right)_{O_2} \tag{7.26}$$

$$\Delta\bar{s}_f = \left(\bar{s}_f\right)_{H_2O} - \left(\bar{s}_f\right)_{H_2} - 0.5\left(\bar{s}_f\right)_{O_2} \tag{7.27}$$

$$\bar{h}_{H_2O} = 143.05 \times T_{FC} - 46.432 \times {T_{FC}}^{1.25} + 5.517 \times {T_{FC}}^{1.5} - 0.018 \times {T_{FC}}^{2} - 253754.1197 \tag{7.28}$$

$$\bar{s}_{H_2O} = 143.05 \times \ln\left(T_{FC}\right) - 232.16 \times {T_{FC}}^{0.25} + 16.55 \times {T_{FC}}^{0.5} - 0.036989 \times {T_{FC}}^{0.5} + 63.76 \tag{7.29}$$

$$\bar{h}_{H_2} = 56.505 \times T_{FC} - 88890.4 \times {T_{FC}}^{0.25} + 116500 \times \ln(T_{FC}) + 1121400 \times {T_{FC}}^{-0.5} - 376189.944 \tag{7.30}$$

$$\bar{s}_{H_2} = 56.505 \times T_{FC} + 29630.13 \times {T_{FC}}^{-0.75} - 116500 \times {\mathrm{T_{FC}}}^{-1} + 373800 \times {T_{FC}}^{-1.5} - 286.178 \tag{7.31}$$

$$\bar{h}_{O_2} = 37.432 \times T_{FC} + 0.804 \times {T_{FC}}^{-5} + 357140 \times {\mathrm{T_{FC}}}^{-0.5} - 2368800 \times {T_{FC}}^{-1} - 23911.05729 \tag{7.32}$$

$$\bar{s}_{O_2} = 37.432 \times \ln\left(T_{FC}\right) + 1.34 \times 10^{-5} \times {T_{FC}}^{1.5} + 119046.67 \times {\mathrm{T_{FC}}}^{-1.5} - 1184400 \times {T_{FC}}^{-2} - 18.0017 \tag{7.33}$$

$$R_{ohmic} = 0.5 \times 10^{-4} \times exp\left[3016\left(\frac{1}{T_{FC}} - \frac{1}{923}\right)\right] \tag{7.34}$$

$$\eta_{anode} = 2.27 \times 10^{-9} \times exp\left(\frac{6435}{T_{FC}}\right) P_{H_2}^{-0.42} . P_{CO_2}^{-0.17} . P_{H_2O}^{-1.0} \tag{7.35}$$

$$\eta_{anode} = 7.505 \times 10^{-10} \times exp\left(\frac{9298}{T_{FC}}\right) P_{O_2}^{-0.43} . P_{CO_2}^{-0.09} \tag{7.36}$$

With the following constraints:

$600 < T_{FC} < 700$ [°C] (7.37)

$0.2 < i < 0.8$ [A/cm^2] (7.38)

$1 < r < 10$ (7.39)

7.3 Solution Methodology

The constraints of this optimization problem are considered as linear bounds and the optimization toolbox is used to tackle this analysis. The solver used for this study is the 'fmincon' for constrained nonlinear optimization and a medium scale algorithmic is used. Sequential quadratic programming is the method used in the fmincon function and the algorithm of the nonlinear optimization used for this analysis is described next [75, 76]:

The Sequential Quadratic Programming algorithm for nonlinear minimization is chosen with inequality constraints:

1) Input an initial point $\{x_0, \mu_0\}$ with $c_j(x_0) \geq 0$ (j=1, 2, ….q) and $\mu_0 \geq 0$

Set k = 0 and tolerance 'ε'.

2) Evaluate Y_k , A_k , g_k and c_k using equations below:

$$\nabla_x^2 L(x_x, \mu_x) = \nabla_x^2 f(x_k) - \sum_{j=1}^{q} (\mu_k)_j \nabla_x^2 \mathrm{c_j}(\mathrm{x_k}) = Y_k \tag{7.40}$$

$$g_k = \nabla_x \mathrm{f}(\mathrm{x_k}) \tag{7.41}$$

$$A_k = \begin{bmatrix} \nabla^T \mathrm{c}_1(\mathrm{x_k}) \\ . \\ . \\ \nabla^T \mathrm{c}_1(\mathrm{x_k}) \end{bmatrix} \tag{7.42}$$

$$c_k = \left[c_1(x_k) \ldots c_q(x_k)\right]^T \tag{7.43}$$

3) Solve the Quadratic Programming problem and compute Lagrange multiplier μ_{k+1}.

Minimize : $\frac{1}{2}\delta^T Y_K \delta + \delta^T g_k$

Subject to: $A_k \delta \geq -c_k$

$$\hat{\mu}_{k+1} = (A_{ak} A_{ak}^T)^{-1} A_{ak} (Y_k \delta_x + g_k) \tag{7.44}$$

4) Set $x_{x+1} = x_1 + \delta_x$. If $\|\delta_x\| \leq \varepsilon$, output $x^* = x_{k+1}$ and stop. Otherwise, set k = k + 1, and repeat from step 2.

The algorithm is assigned a feasible start point (i.e. $\{x_0, \mu_0\}$) that satisfies $c_j(x_0) \geq 0$ (j=1, 2, ….q) and $\mu_0 \geq 0$, and initializes the tolerance and 'k' for the start. The values of Y_k , A_k , g_k and c_k are found using the equations provided. 'Y_k' is the second derivative of the Lagrangian equation. It relates the second derivative of both the objective function and constraints. 'g_k' is the gradient of the objective function at x_k (k^{th}) iteration. Gradient of the objective function is the most important variable that identifies the search direction towards the minimizer. 'A_k' and 'C_k' are used to obtain the required variables for the quadratic programming step (i.e. step 3)

In the next section, quadratic programming must be performed. This stage is located in a loop and performs the quadratic programming sequentially. It also finds the Lagrange multipliers by using the variables found in the previous stages. The algorithm finally checks if convergence is achieved (i.e. $\|\delta_x\| \leq \varepsilon$) and, if this condition is not satisfied, the loop may start from the beginning. The algorithm stops when the value of $\|\delta_x\|$ is less than or equal to the tolerance defined at the beginning of the program.

In cases where it is difficult to supply the gradient of the objective function and the constraints to the solver, the approximation solver in the toolbox could be used. The gradient and Hessian of the objective function are approximated using the toolbox for this study.

For ease of implementing the codes, the three variables of pressure coefficient (r), current (I), and operating fuel cell temperature (T_{FC}) are substituted by x(1), x(2) and x(3) respectively. Therefore, the search point $x = [r \;\; I \; T_{FC}]^T$ could be replaced with a new format of $x = [x(1)\; x(2)\; x(3)]^T$ for this analysis.

Considering the constraints introduced above, the lower and upper bounds could be defined according to:

- Lower bound: $[1\ 2000\ 873.15]^T$ and
- Upper bound: $[10\ 8000\ 973.15]^T$.

7.4 Assumptions

There are several assumptions that need to be made in order to conduct the optimization process.

- The Gradient and Hessian of the objective function and the constraints are approximated by the MATLAB optimization software.
- Total fuel flow rates of 10,000, 20,000 and 30,000 mol/h and oxidant flow rates of 30,000, 40,000 and 50,000 mol/h are selected for the analysis.
- The reformer operating pressure and temperature are assumed to be 760°C and 3 atm, respectively.
- The oxidant consists of nitrogen, oxygen and carbon dioxide (60 % dry air, 30 % oxygen).
- The fuel consists of methane, water, hydrogen, carbon monoxide and carbon dioxide.

- Mole fractions of the reactants are the reformer exit stream mole fractions and are calculated from the reformer temperature and pressure, using the StanJan online software [77].

Chapter 8: COST ANALYSIS

A simplified and novel approach for the cost analysis of the Enbridge MCFC hybrid system is explained here.

The Enbridge MCFC hybrid system is to provide low pressure gas as well as 2.2 MW of electricity to customers. Therefore, the fluctuations in electricity and gas prices would affect the payback period of the hybrid system. Figure 8 demonstrates the old-fashioned, current and future Enbridge system schematics.

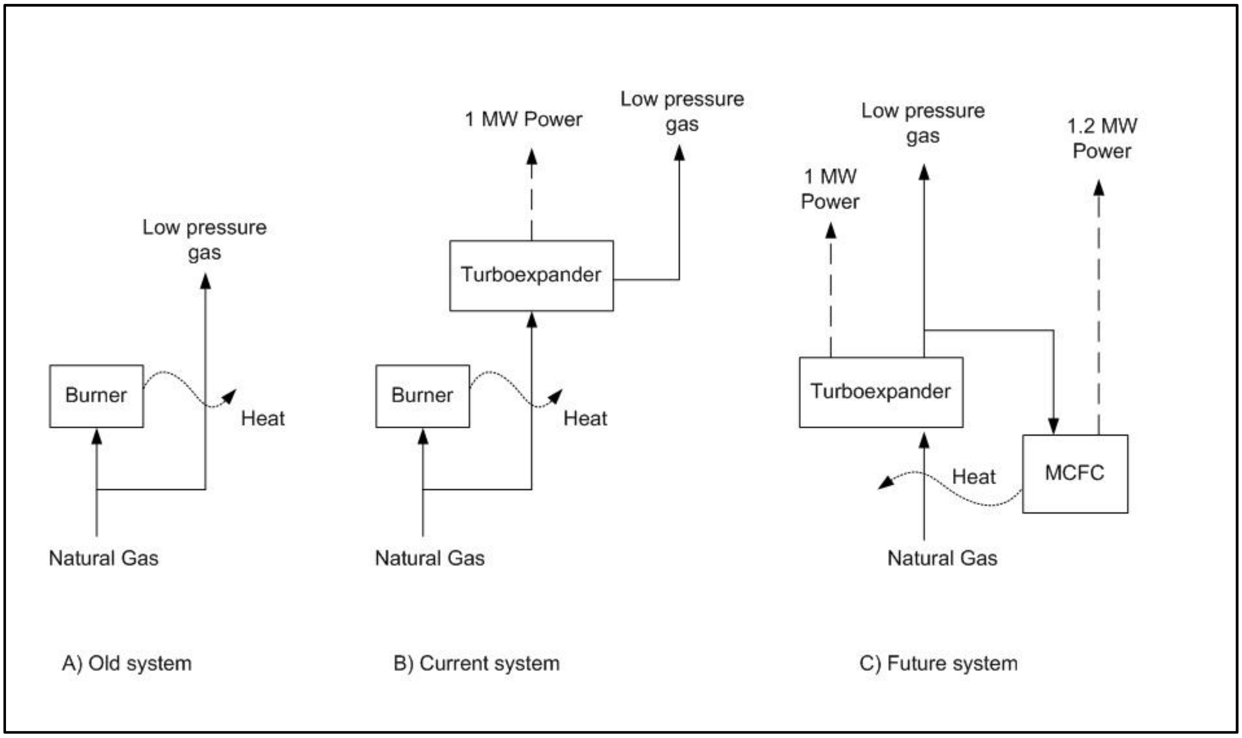

Figure 8: Schematics of old-type, current and future Enbridge Inc. system.

The main assumptions made for the cost analysis are tabulated in Table 7.

Table 7: Main assumptions made for the cost analysis of the Enbridge system.

Operational hours per day	24	**Carbon offset cost**	$20 / ton
Price of kWh sold(c) (base case)	$0.06	**Previous daily carbon dioxide produced(b)**	2851.2 kg
Total kW power output	2,200		
Wholesale cost of 1 MMbtu gas(d) (base case)	$8	**Overhead(a)**	20 % of the first year revenue
Direct labor	10 % of the first year revenue	**Capital cost**	$8,000,000
Sold natural gas price(e)	$0.4 / m^3		

(a) Consists of indirect labor and materials.

(b) This figure is computed by assuming that natural gas is directly burnt to heat up the inlet gas that enters the valve or turboexpander.

©Since the revenue generated from gas and electricity sales from the previous system are sunk costs and have already been taken into consideration, for the purpose of this study only costs and revenue generated as a direct impact from the addition of the MCFC system are considered in calculations.

(d) Ref. [78].

(e) Ref. [79].

The operating costs of the Enbridge system consist of overheads, direct material and direct labor. An annual 4 % (i.e. assumed to be the same as the inflation rate) increase in direct labor and overheads costs is assumed for this study. This is because of the increase in costs of training, insurance, pension, etc. corresponding to the direct and indirect labor work. The direct material (natural gas and electricity) cost is assumed to increase by the inflation rate (assumed to be 4 % from ref. [80]). In order to investigate the effects of varied electricity costs on the overall cost analysis, three different case studies are performed. A 6 cent/kWh (current price in Ontario [81]), 11 cent/kWh (cost of electricity generated from wind in Ontario) and 22 cent/kWh (electricity cost in Germany [82]) are selected to cover a wide range of variation in the electricity cost. However, the natural gas price is assumed to only increase by the inflation rate because of its very volatile price variations and for lack of better models.

Therefore, the main assumptions made for the cost analysis of the Enbridge system are as follows:

1) The MCFC unit needs to be replaced after 40,000 hours (optimistic figure) of operation. However, the costs related to the new system is not included in the cost analysis. It is assumed that the efficiency and performance improvements of the Enbridge system during the next 30 years offset the cost of the new MCFC system in every 40,000 hours of operational time.
2) The system is assumed to be reasonably automated in order to keep the labor work as low as possible.
3) Carbon offset is an important issue and it is included as a potential saving for the Enbridge system. The amount of carbon dioxide produced in the "future" system is comparable to the amount produced in the conventional system (natural gas direct burning). Moreover, considering the future costs of carbon offset and the tendency of most governments in turning towards green energy, the potential savings of the Enbridge system increases dramatically during its operational time. Tax credit is also included in the potential savings calculations.

Chapter 9: RESULTS AND DISCUSSION

This chapter deals with the main results and numerical findings. Firstly, general results obtained from an analysis of the performance of a MCFC are presented. It is followed by the results related to the first case study. Subsequently, the results from the performance analysis of the Enbridge MCFC hybrid system are discussed. Finally, the optimization process and the cost analysis are discussed in the last two sections of this chapter.

9.1 General results

This section involves the results obtained from the performance analysis of a reformer and a MCFC. The products of the chemical reactions that occur in the external reformer are assumed to be directly supplied to the fuel cell. Therefore, the results presented here are obtained from the analysis of the combined reformer-fuel cell system.

9.1.1 Reformer

The reformer operating temperature and pressure are the main two factors that affect the degree of completion of the reforming chemical reactions. StanJan [77] is used in computation of the equilibrium mole fractions. The reforming reaction that takes place in the reformer is as follows: $CH_4 + H_2O \rightleftharpoons CO + 3H_2$

Figure 9 and Figure 10 and Figure 11 are essentially reflecting the Le Chatelier's principle. Figure 9 illustrates the effect of changing the operating temperature on the equilibrium mole fraction of the species at constant pressure and steam/carbon ratio.

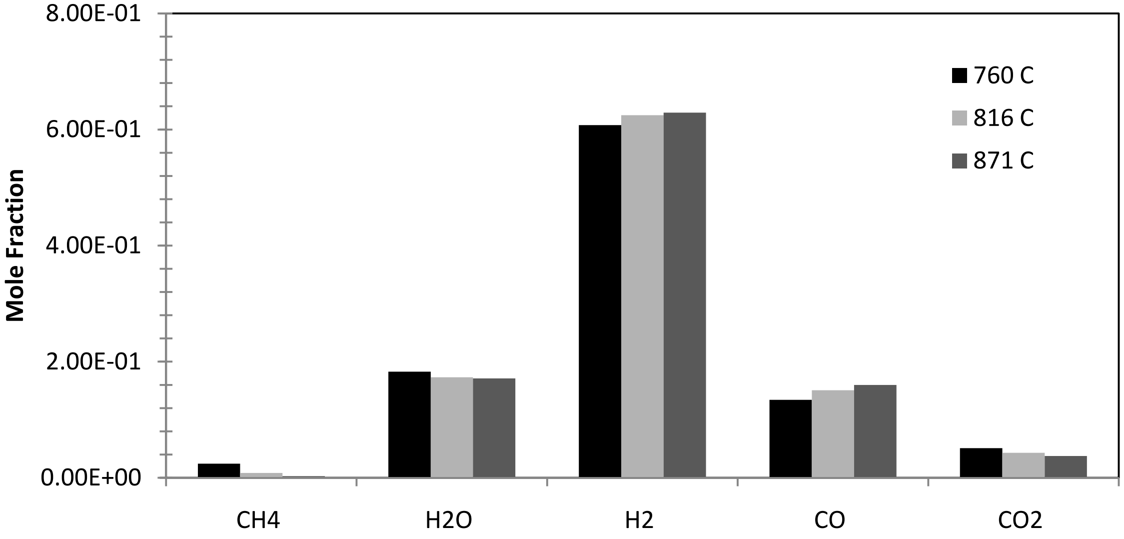

Figure 9: Effects of the variation of the operating temperature on the equilibrium mole pressures at constant pressure and steam/carbon ratio (P = 3 atm, S/C = 2).

Effects of changing the reformer operating pressure on the equilibrium mole fractions at constant temperature and steam/carbon ratio are shown in Figure 10.

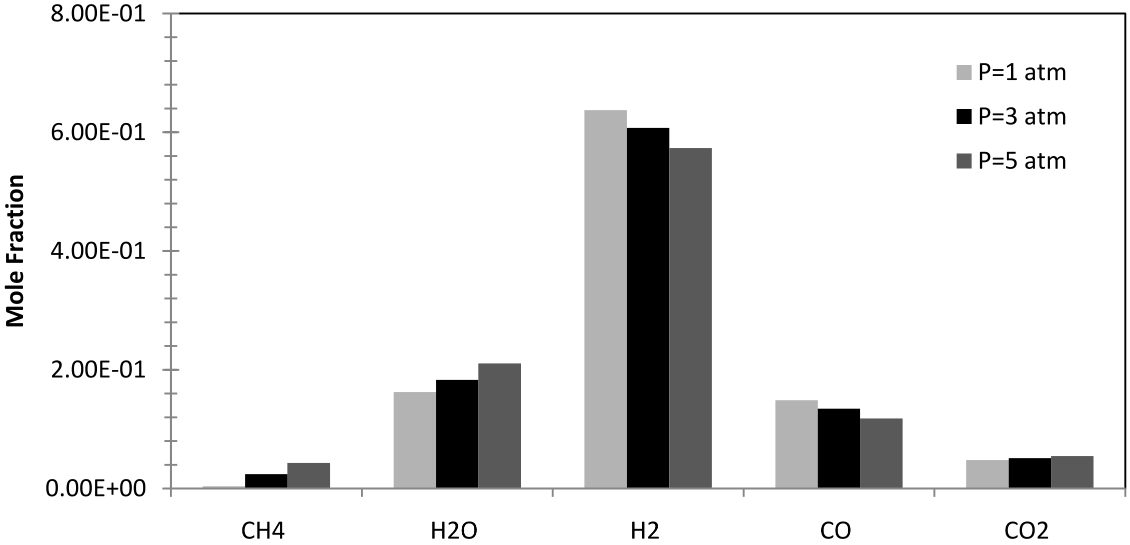

Figure 10: Effects of the variation of the operating pressure on the equilibrium mole pressures at constant temperature and steam/carbon ratio (T = 760^{o}C, S/C = 2).

Figure 11 demonstrates the variation of equilibrium mole fractions by varying the steam/carbon ratio at constant temperature and pressure.

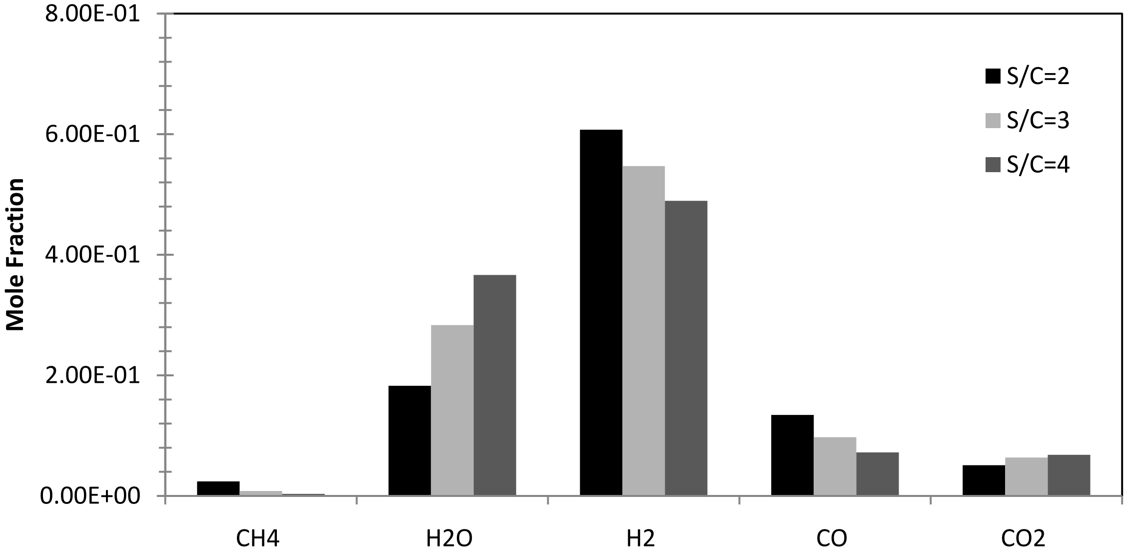

Figure 11: Variation of equilibrium mole fractions by varying the steam/carbon ratio at constant temperature and pressure (T = 760°C, P = 3 atm).

The reformer must be adjusted and optimized in order to cope with the fuel cell operation. Therefore, it is crucial to ensure that the reforming products match with the fuel requirements of the fuel cell.

As it can be seen from the graphs presented above, lowering the reformer operating pressure and steam/carbon ratio increases the amount of the hydrogen produced which is the main fuel for the MCFC. Increasing the temperature, however, enhances the performance of the reformer. Varying the steam/carbon ratio shows the most noticeable effect on the performance of the reformer. In contrast, temperature or pressure variations do not affect the exit stream composition significantly.

9.1.2 Molten carbonate fuel cell stack

In this section, using the equations provided for the MCFC, the performance of a molten carbonate fuel cell stack is investigated. Effects of fuel, oxidant and current density variation on the performance and efficiency of the system are examined. For the base case study, 20,000 mol/h of fuel and 40,000 mol/h of oxidant are provided for the fuel cell. The fuel required for the MCFC is prepared from the reformation of natural gas and steam at 760°C and 3 atm, and the oxidant has a composition of 70 % dry air / 30 % carbon dioxide.

Figure 12 below, is the plot of voltage vs. current density at different oxidant flow rates. The fuel cell voltage drops as the current density increases in an almost linear fashion. This is due to the increase of the irreversibilities and transport limits at high current densities. Varying the oxidant flow rate does not have a significant effect on the fuel cell voltage.

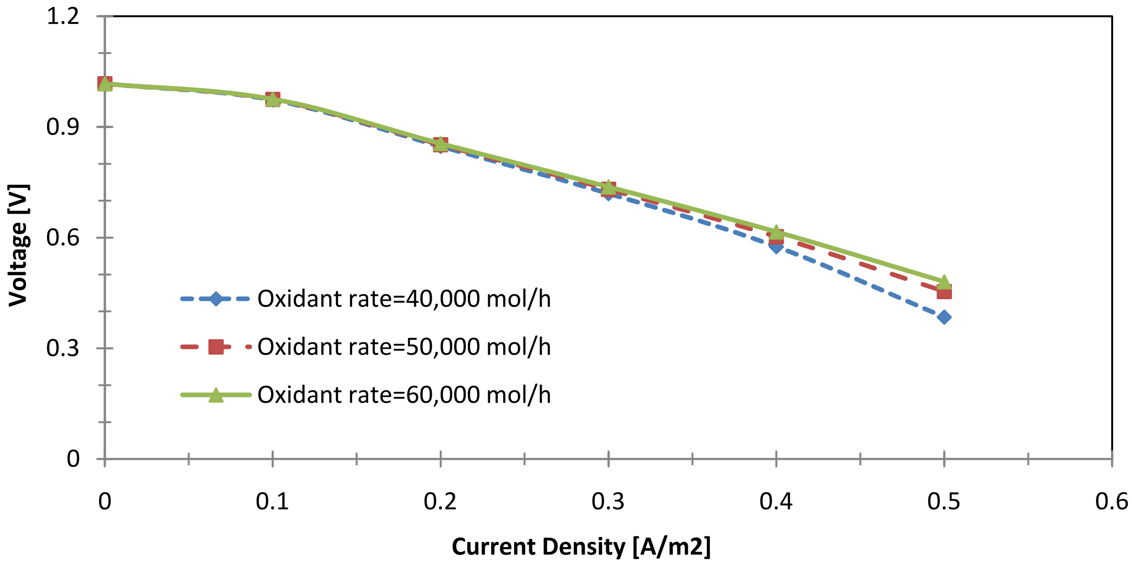

Figure 12: Plot of voltage vs. current density at different oxidant flow rates and constant fuel flow rate (= 20,000 mol/h).

The variation of the fuel cell voltage versus the current density at different fuel flow rates is exhibited in Figure 13.

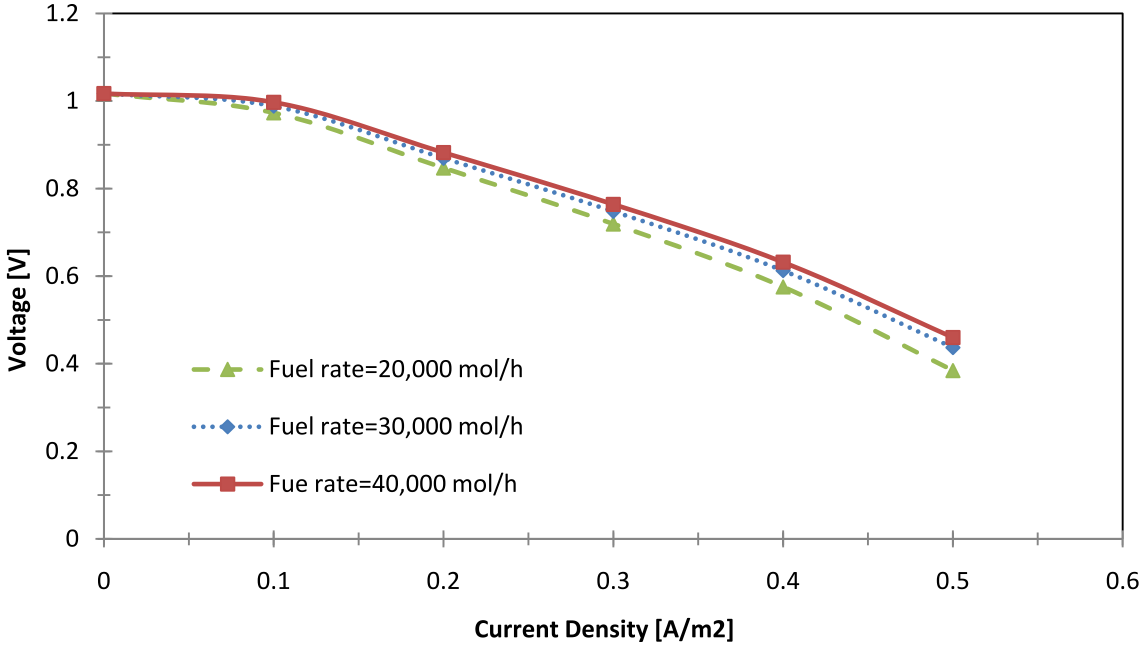

Figure 13: Plot of voltage versus current density at different fuel flow rates and constant oxidant flow rate (= 40,000 mol/h).

The variation of the fuel flow rate has a slight effect on the performance of the fuel cell. However, at lower fuel flow rates the fuel stream gets depleted of hydrogen and, as a result, the voltage drops quickly towards zero at high current densities.

Figure 14 and Figure 15 illustrate the variation of fuel cell power output with varying current density for different fuel and oxidant flow rates, respectively.

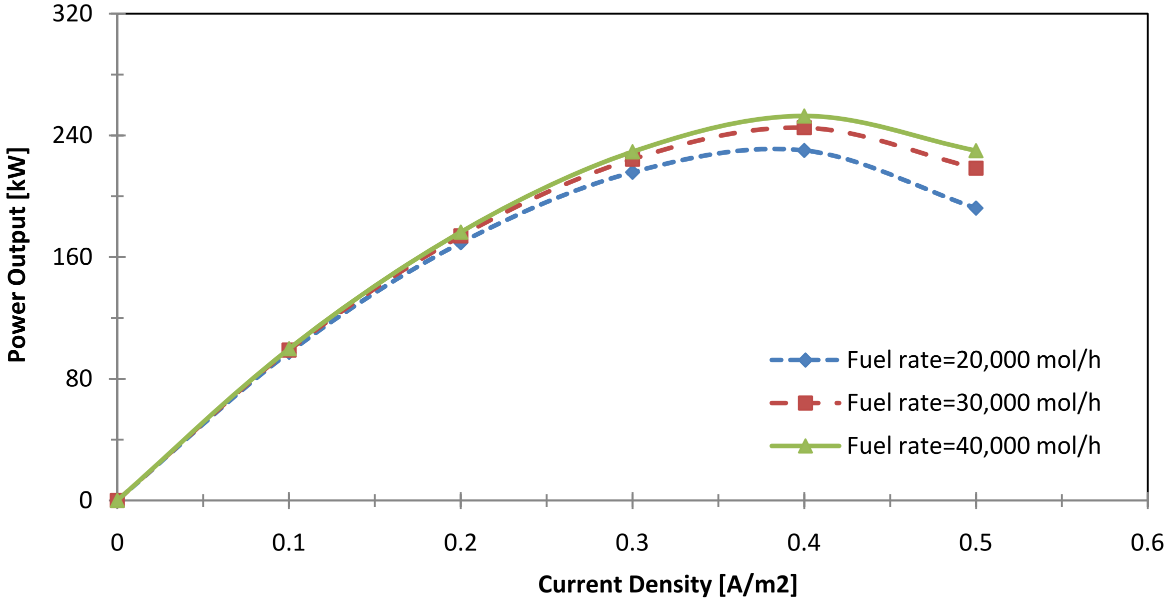

Figure 14: Plot of fuel cell power output versus current density for different fuel flow rates at constant oxidant flow rate (= 40,000 mol/h).

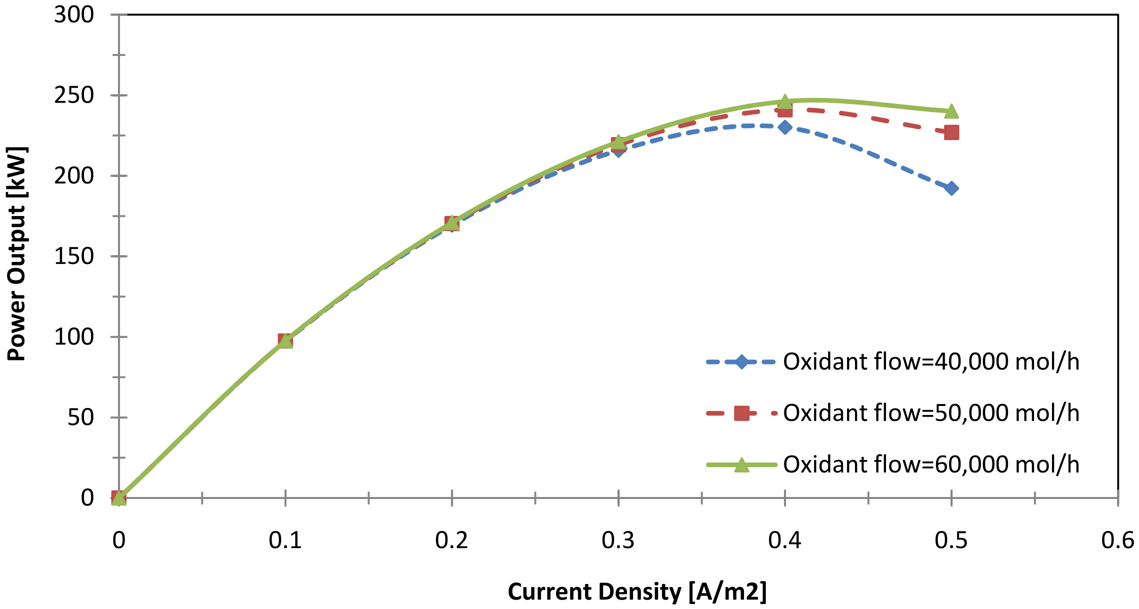

Figure 15: Plot of fuel cell power output versus current density for different oxidant flow rates at constant fuel flow rate (= 20,000 mol/h).

As it can be seen in these figures, the power output of the MCFC increases with the initial increase in current density. After reaching its peak, it decreases at higher current densities when irreversibilities dominate. This pattern can also be seen in the plot of the static efficiency.

Using the definition of the static efficiency (i.e. equations 6.41 & 6.42) and the results obtained from the calculation of power, the effects of varying current density on the performance of the MCFC for different fuel and oxidant flow rates are investigated. Figure 16 and Figure 17 demonstrate the variation of fuel cell efficiency with current density at different fuel and oxidant flow rates, respectively.

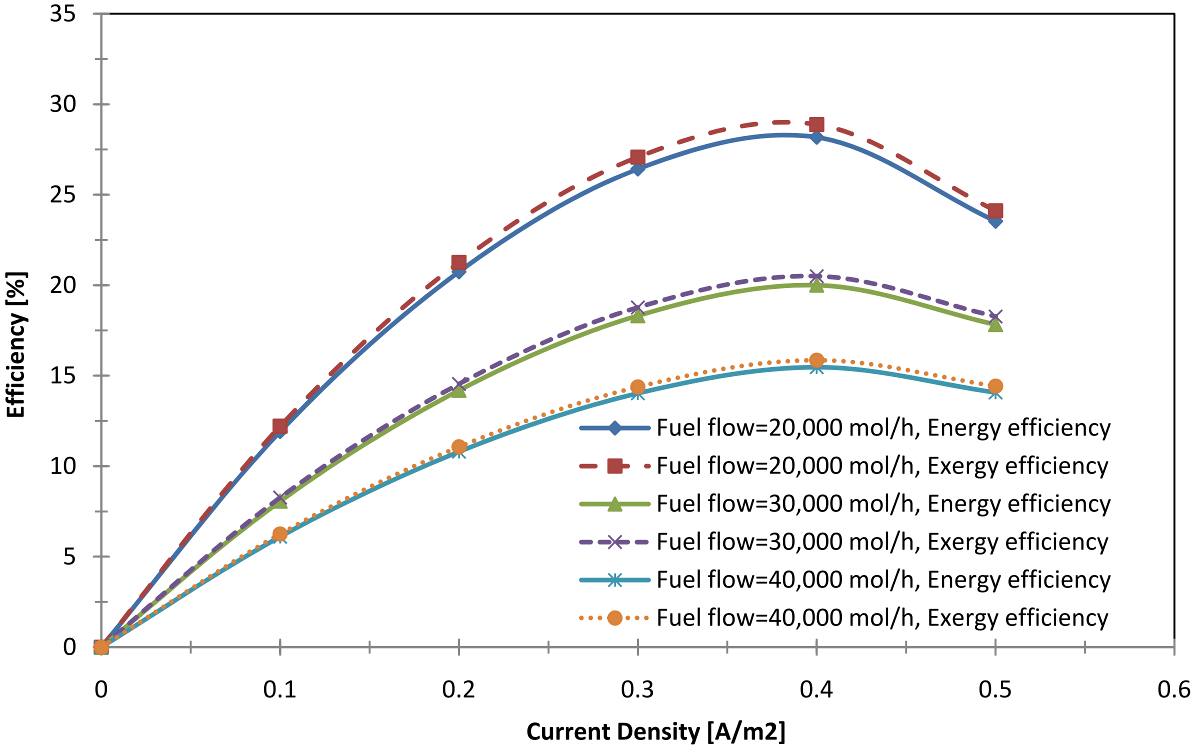

Figure 16: Variation of fuel cell efficiency with current density at different fuel flow rates and constant oxidant flow rate (= 40,000 mol/h).

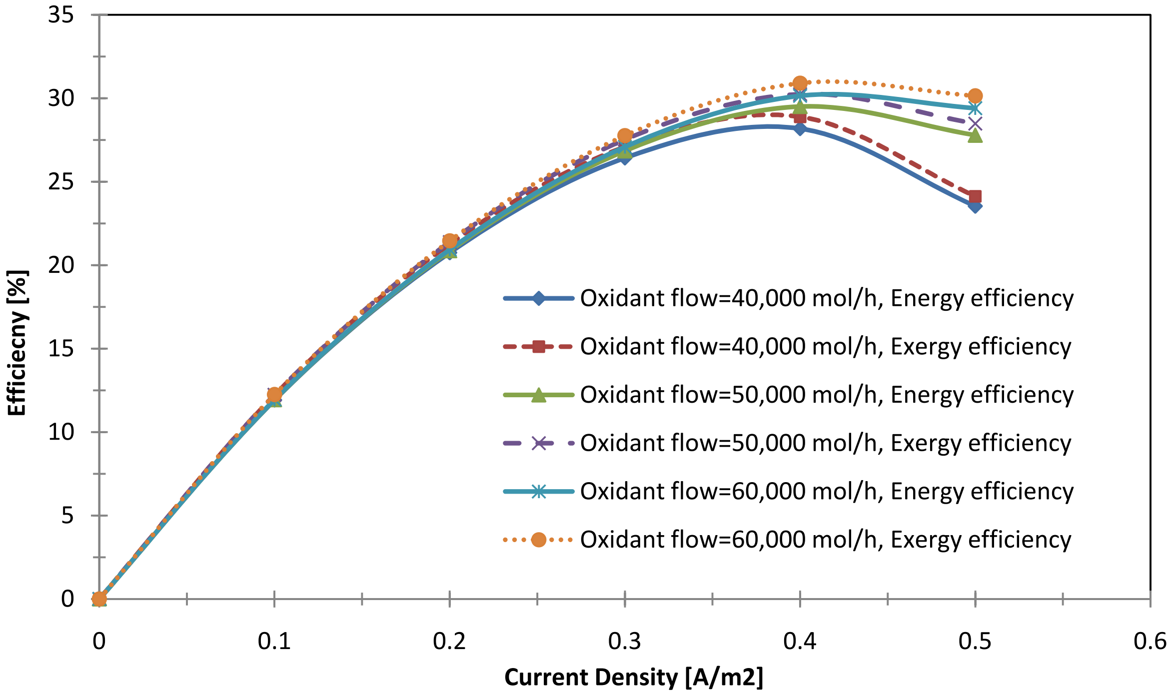

Figure 17: Variation of fuel cell efficiency with current density at different oxidant flow rates and constant fuel flow rate (= 20,000 mol/h).

First, the efficiency of the MCFC increases with current density. After reaching a maximum, it decreases eventually. As mentioned earlier, by defining the efficiency as a static efficiency the plot follows the same trend as that for power. The MCFC power output and efficiency drops abruptly if there is not a sufficient amount of fuel supplied to the fuel cell. Moreover, there is not a noticeable discrepancy between the energy and exergy plots. This is because the heating value and chemical exergy of the input fuel are similar.

9.2 Results of the first case study

This section deals with the results obtained from the first MCFC system analysis.

The proposed analysis is applied to the hybrid system with varying operating pressure, temperature and current density to investigate the performance of the system.

From this study, maximum energy and exergy efficiencies of 57.4 % and 56.2 % are obtained, respectively. The efficiency of the bottoming cycle is calculated as 24.7 %. The energy and exergy efficiencies of the fuel cell are found to be 43.4 %, 42.5 % respectively.

Variation of the fuel cell voltage and irreversible voltage with current density at an operating pressure of 4 atm is shown in Figure 18.

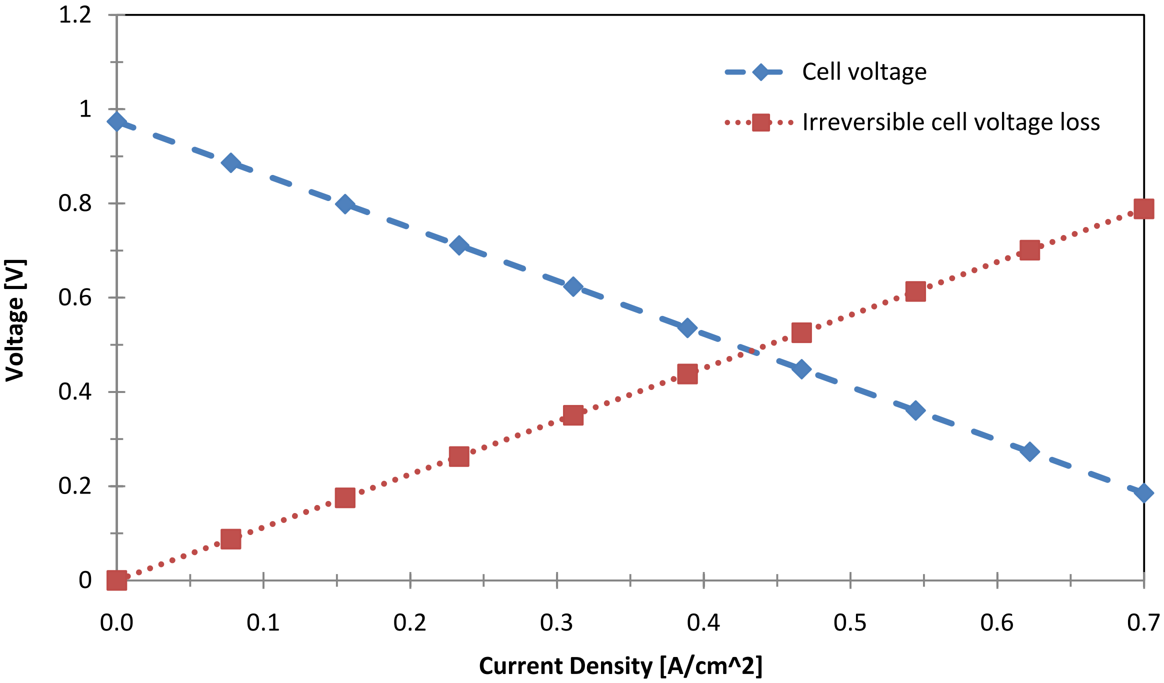

Figure 18: Variation of the fuel cell voltage and irreversible voltage with current density at an operating pressure of 4 atm.

It can be observed from the figure that, with an increase in current density, the cell voltage decreases. Higher current densities increase the irreversibilities in the cell and results in lower voltages. Concentration losses are the main reasons for the low output voltages at high current densities. The similarity between the results obtained from Figure

18 and the results obtained from the last section further proves the validity of this analysis.

Figure 19 shows the variation of power output and overall energy and exergy efficiencies of the system with current density at 4 atm. From the figure it can be seen that both fuel cell power output and overall hybrid system efficiencies initially increase at lower current densities, reach their peaks and finally decrease. The maximum power output is obtained as 418.2 kW at the current density of 0.4667 A/cm^2 for corresponding maximum energy and exergy efficiency of 57.4 % and 56.2 %, respectively.

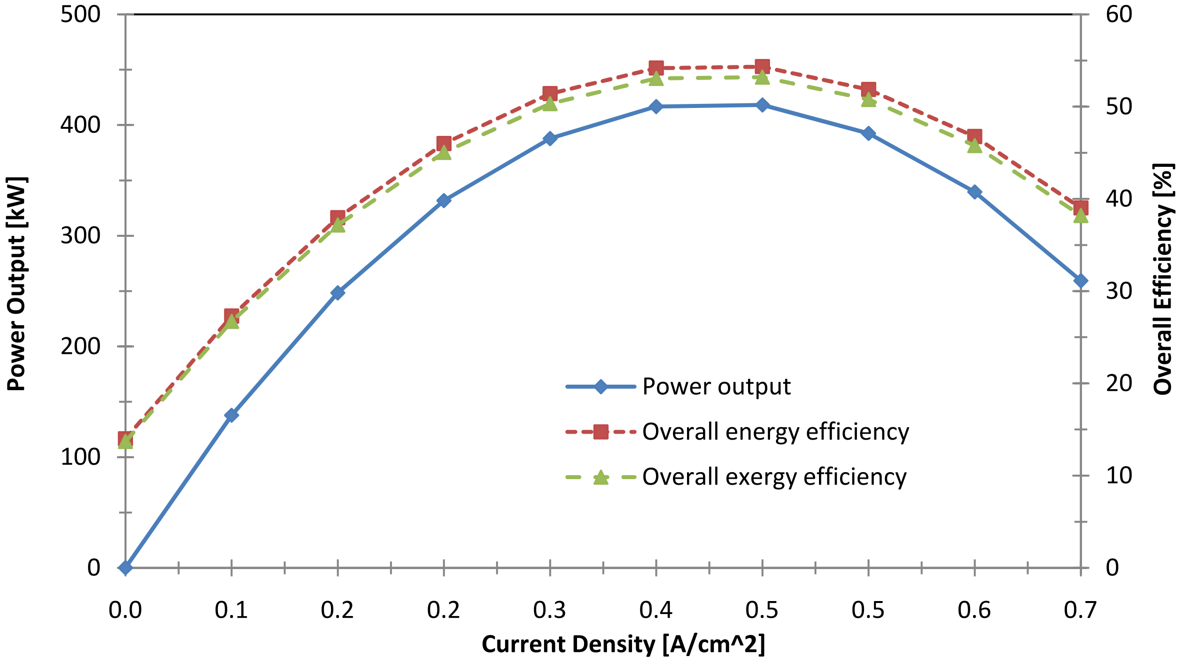

Figure 19: Variation of power output and overall energy and exergy efficiencies of the system with current density at 4 atm.

At lower current densities, the molar flow rate of fuel and the power required by the auxiliary devices are low and, therefore, the efficiency increases to its peak value. Thereafter, the parasitic load and molar consumption of fuel increases at higher current densities and, hence, the efficiency decreases. Moreover, energy efficiencies are higher than exergy efficiencies which is due to the difference between energy and exergy content of the fuel.

Based on the exergy analysis, the fuel cell and the catalytic burner exhibit the maximum exergy destruction and, hence, any exergy improvements should be mainly focused on these compartments. Moreover, the heat exchanger shows a remarkable exergy loss because of a large temperature difference between the streams. The main exergy destructions are in the compartments where chemical reactions take place. Another main source of exergy destruction is from the exit of the heat exchanger. The exergy content of this stream with a fairly high temperature of 280^{o}C can be used for possible cogeneration purposes. Therefore, an additional 215kW of power could be achieved if the exergy of this stream was used in a cogeneration system (e.g. [37]).

Figure 20 summarizes the exergy destruction in different compartments of the hybrid system. Irreversibilities, and thus entropy generation, are the reasons for the exergy destruction. In order to improve the performance of the system, it is essential to minimize the exergy destructions which will result in increasing exergy efficiency. These exergy destructions are primarily affected by the operating conditions within the system and surrounding conditions.

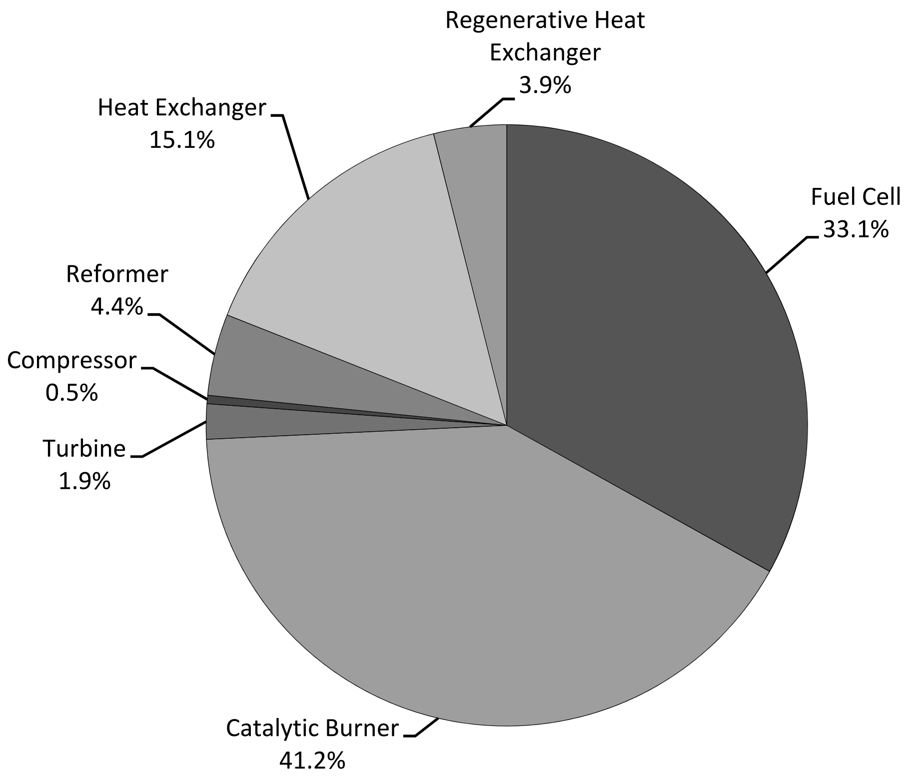

Figure 20: Exergy destruction in different compartments of the hybrid system.

Figure 21 shows the energy and exergy efficiencies of the fuel cell at different operating temperatures. The operating pressure and current density were set at 4 atm and 0.5 A/cm^2 respectively. It can be seen that both energy and exergy efficiencies of the MCFC increase with temperature. This is due to the decrease in irreversibilities of the fuel cell with the increase of temperature reflected by enhanced reaction kinetics. However, increasing the operating temperature is limited by the fuel cell material selection and other operating conditions.

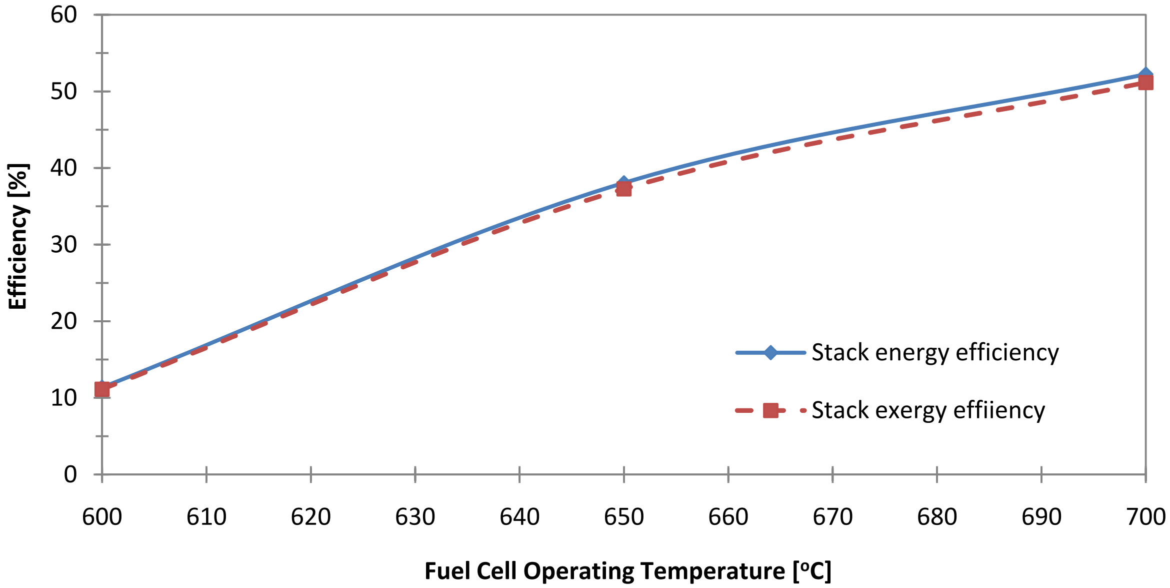

Figure 21: Energy and exergy efficiencies of the fuel cell stack at different operating temperatures.

Figure 22 and Figure 23 exhibit the power output, energy and exergy efficiencies of the fuel cell at different operating pressures, respectively. The operating temperature and current density are set at 650°C and 0.5 A/cm^2, respectively. The power output, energy and exergy efficiencies of the MCFC increase with pressure. This is due to the decrease in irreversible losses, especially anode and cathode overpotentials. Although high pressure operation enhances the performance of the fuel cell, it requires a more powerful compressor, results in a bulky balance of plant and meets limitations to the stack sealing. In fact, the disadvantages of operating at high pressures can be so severe that a low pressure operation is often preferable.

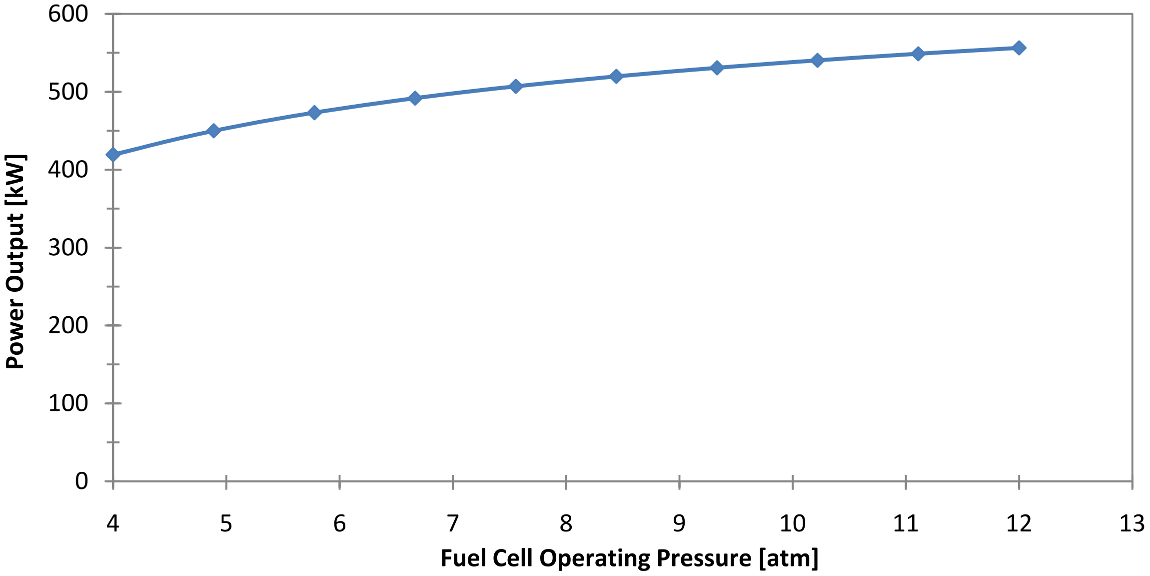

Figure 22: Plot of the fuel cell power output versus the operating pressure.

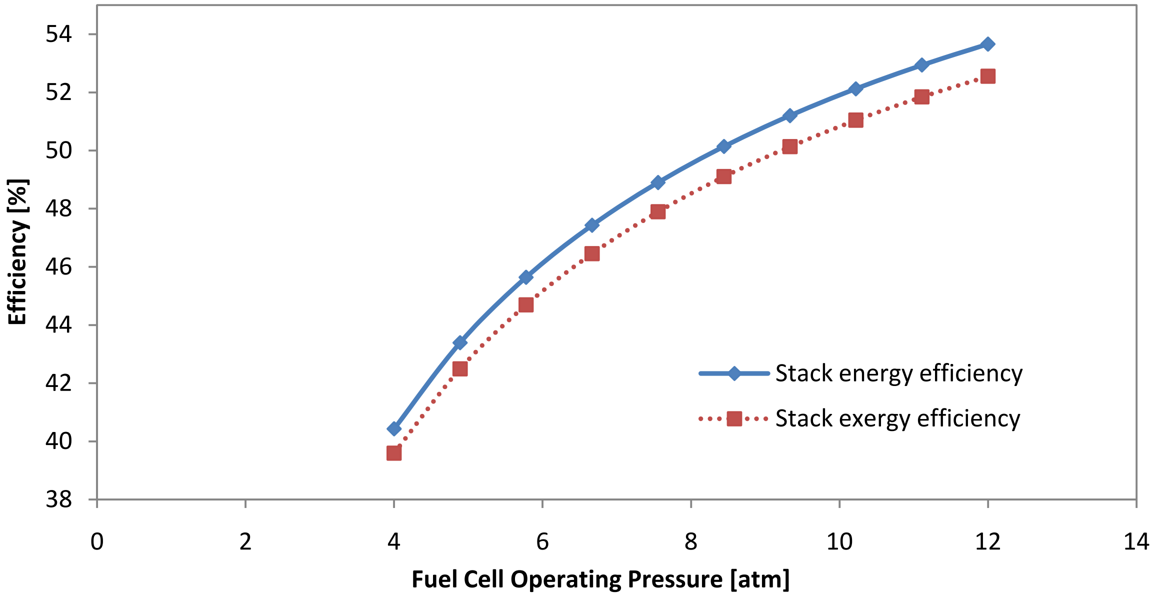

Figure 23: Plot of the fuel cell stack energy and exergy efficiencies versus the operating pressure.

Another approach in improving the overall performance of the combined system is through improving the bottoming cycle efficiency. Table 8 lists the overall energy and exergy efficiency improvements by an enhancement in the bottoming cycle efficiency.

Table 8: Variation of overall energy and exergy efficiencies by varying the bottoming cycle energy efficiency.

Bottoming cycle Energy Efficiency [%]	Overall Energy Efficiency [%]	Overall Exergy Efficiency [%]
6.4	51.7	50.6
7.2	52.1	51.1
8.1	52.6	51.5
8.0	53.0	51.9
9.7	53.4	52.3
10.5	53.9	52.7
11.4	54.3	53.2
12.2	54.7	53.6
13.0	55.1	53.9
13.9	55.6	54.4

The overall system efficiency can also be improved by using the exergy content of stream 2, as shown in Figure 6 . The exergy flow contained in this stream can be used as exergy input into the fuel cell to maintain its operating temperature or can be used for any external co-generation purpose to produce more power output. According to this study, the global exergetic efficiency could be increased by 15 % when the 150 kW exergy wasted at point 2 is used in co-generation power production. Similarly, a maximum energetic efficiency of 75 % for the global system could be achieved upon the usage of the energy loss at point 2.

Finally, considering environmental impact and sustainable development, the system is environmentally benign with very low output emissions. The waste heat generated is assumed to be used efficiently and, therefore, the whole hybrid system helps to improve the sustainability. Increasing the system efficiency leads to even higher sustainability and less environmental impacts. Here, environmental impact is classified as order destruction, source degradation and waste exergy emissions [83].

9.3 Result of the second case study (Enbridge system)

This section deals with the results obtained from the Enbridge MCFC system.

The results from the base case study suggest that an overall energy and exergy efficiency as high as 60 % are achievable. Moreover, a sub-system energy efficiency of 48.09 % and exergy efficiency of 46.82 % (i.e. equations 6.62 and 6.63), bottoming cycle energy and exergy efficiency of 23.19 % and 21.99 %, and fuel cell stack energy and exergy efficiency of 50.56 % and 49.23 % are reached.

Several operating conditions are varied to investigate their effects on the performance of the hybrid system as explained in the rest of this chapter.

9.3.1 Effects of hydrogen utilization

Figure 24 and Figure 25 show the variation of fuel cell power output, fuel cell energy and exergy efficiency, and exergy destruction for a range of hydrogen utilization ratios, respectively.

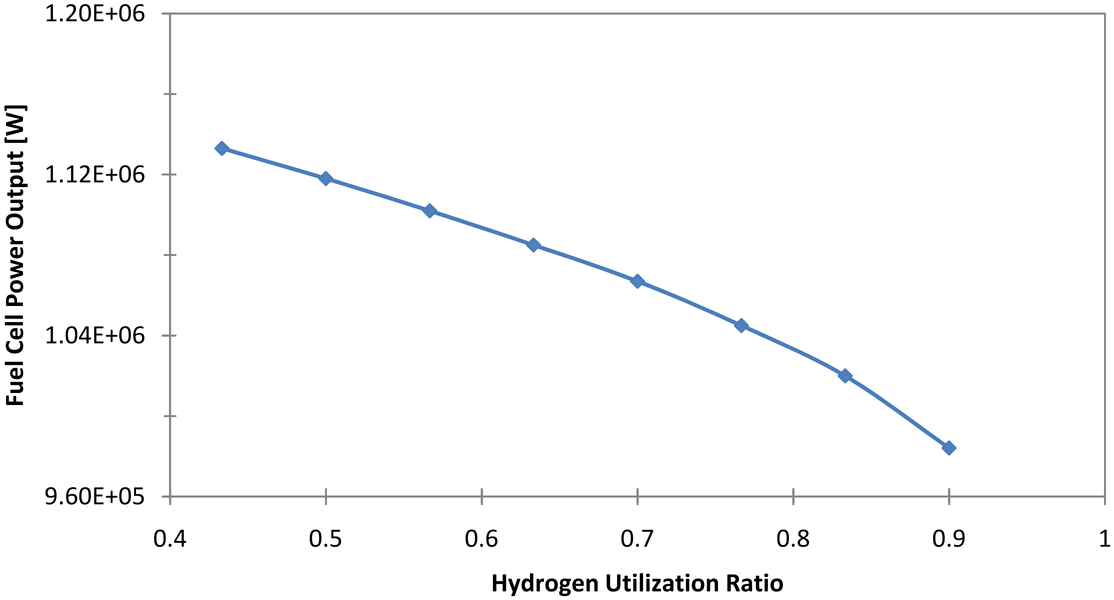

Figure 24: Variation of fuel cell power output versus the hydrogen utilization ratio at constant current.

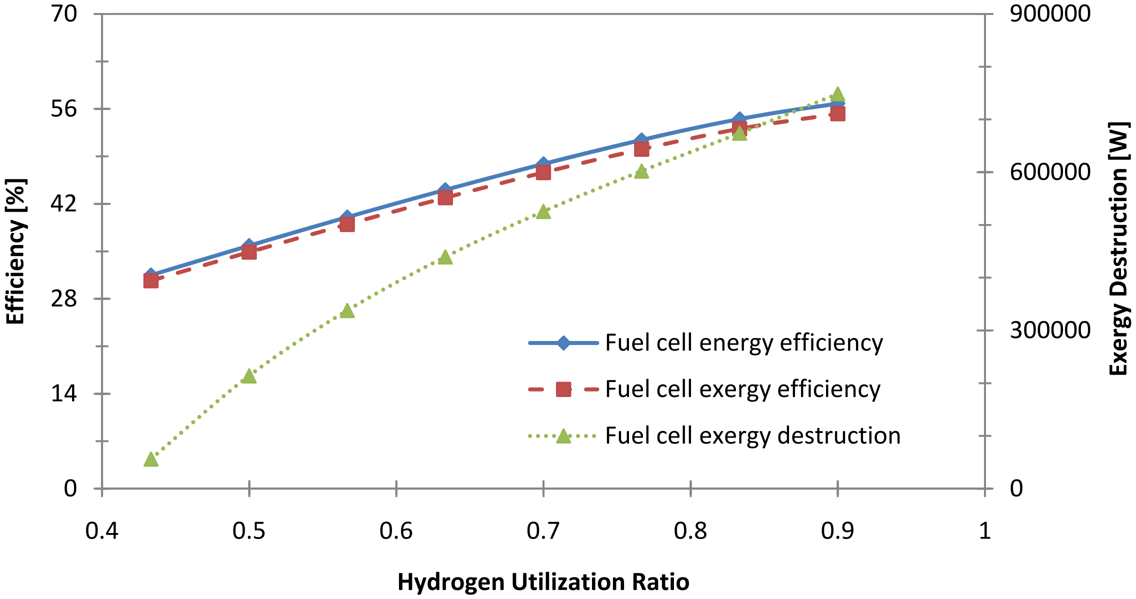

Figure 25: Variation of fuel cell efficiency and exergy destruction versus the hydrogen utilization ratio.

Variation of the overall energy and exergy efficiency of the hybrid system for different hydrogen utilization are illustrated in Figure 26.

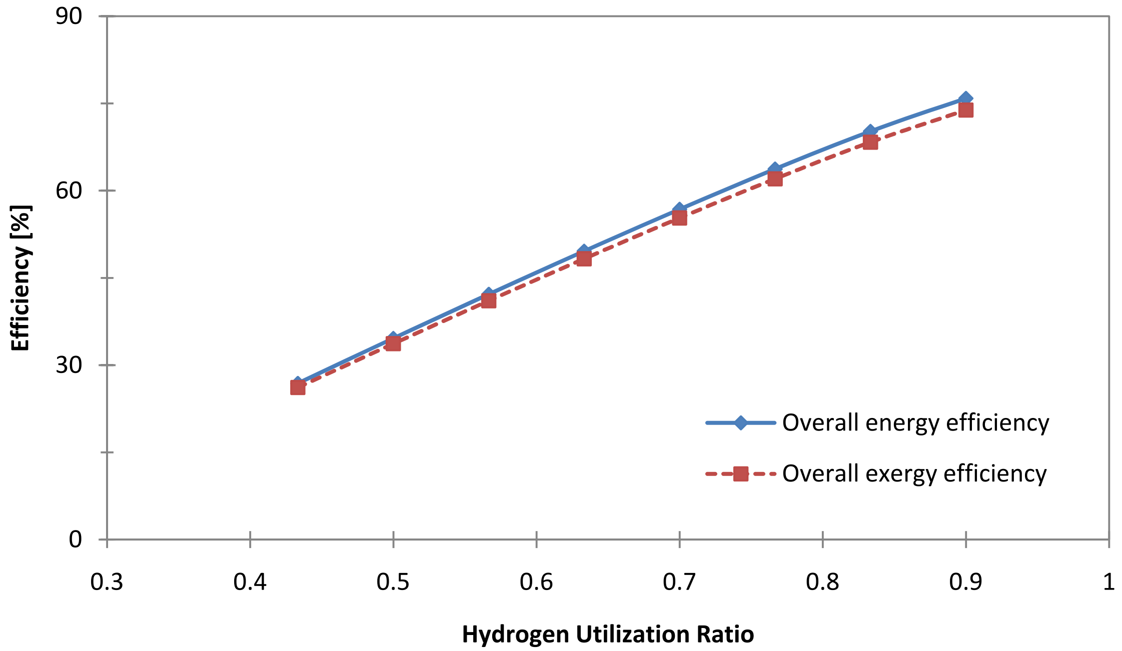

Figure 26: Plot of overall energy and exergy efficiencies versus the hydrogen utilization ratio.

From the figures presented above, increasing the hydrogen utilization (i.e. hydrogen used/ hydrogen supplied) decreases the power output of the fuel cell. However, fuel cell and overall energy and exergy efficiencies increase. Hydrogen usage of the MCFC is a linear function of the current density. Assuming a constant current density, increasing the hydrogen utilization ratio decreases the hydrogen supplied to the system. As a result, the partial pressure and voltage of the fuel cell alter due to the change in the flow rate. Also, the exergy destruction of the fuel cell increases dramatically as more fuel is supplied to the fuel cell but the power output from the fuel cell is limited.

9.3.2 Effects of fuel cell current

Figure 27 is the voltage-current plot of the Enbridge hybrid system. Similar to the previous voltage-current plots, increasing the fuel cell load results in a drop of the fuel cell voltage. The increase of the irreversibilities is the predominant reason for this drop.

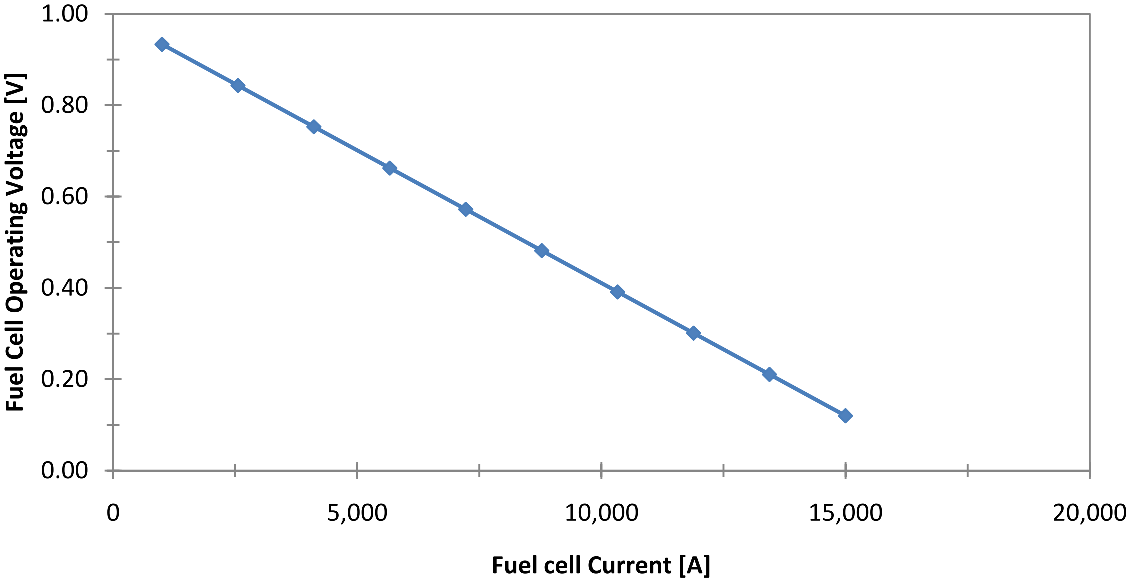

Figure 27: Voltage-current plot of the Enbridge hybrid MCFC system.

Increasing the fuel cell current decreases the overall fuel cell, and subsystem, exergy and energy efficiency. Higher currents require a higher amount of fuel flow rate and, as a result, the dynamic efficiencies decrease. Figure 28, Figure 29 and Figure 30 demonstrate the effects of fuel cell current variation on the system efficiencies. In Figure 29, we stop the simulation at a current of I = 12,000 A. Past this current (i.e. I > 12,000 A), the losses in the compressor dominate the system efficiencies so much so that the overall efficiencies approach zero.

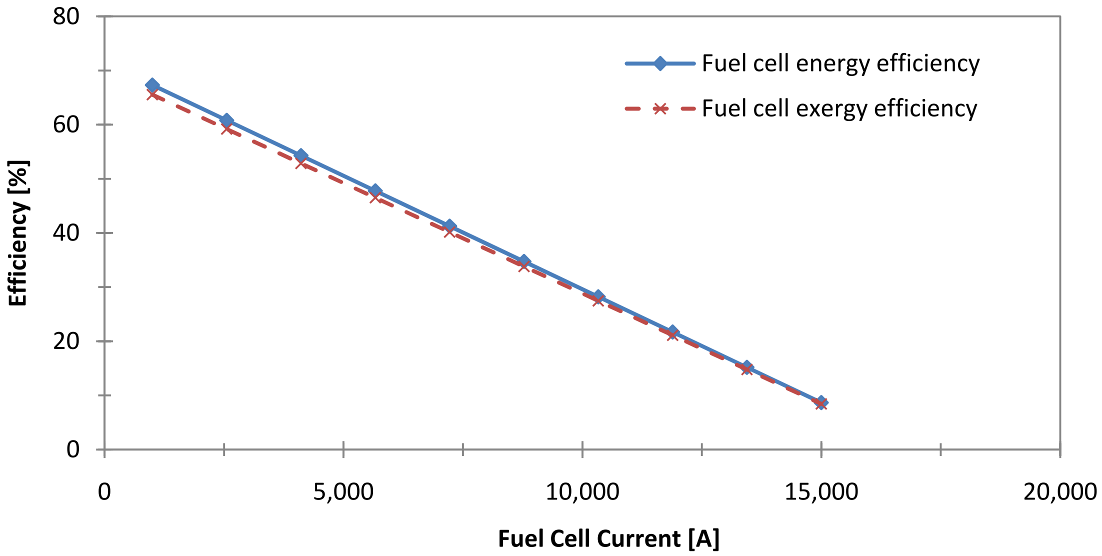

Figure 28: Plot of fuel cell energy and exergy efficiencies against the fuel cell current.

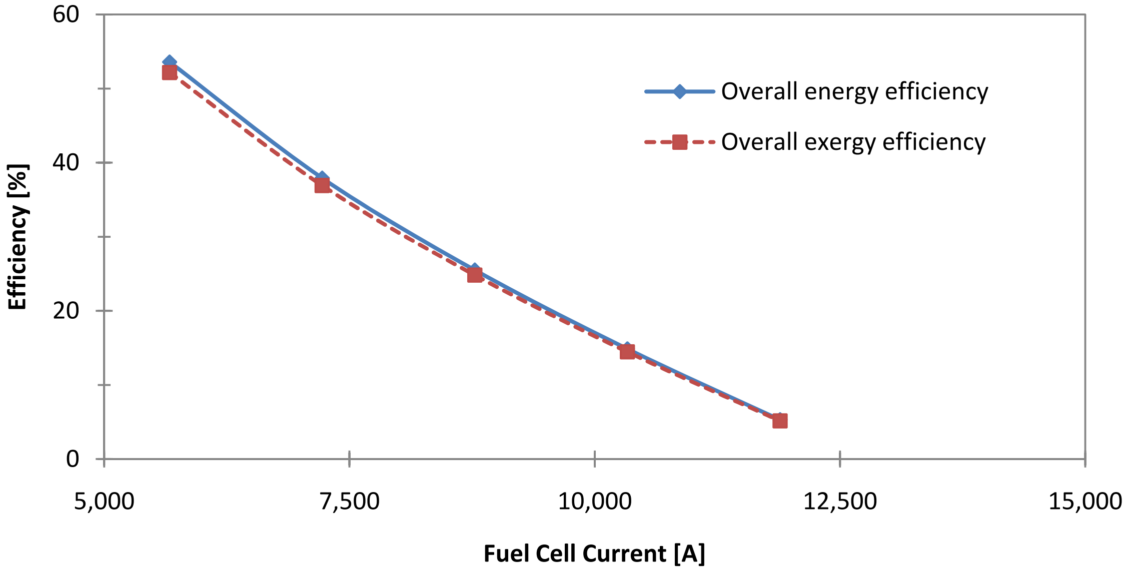

Figure 29: Plot of overall hybrid system energy and exergy efficiencies versus the fuel cell current.

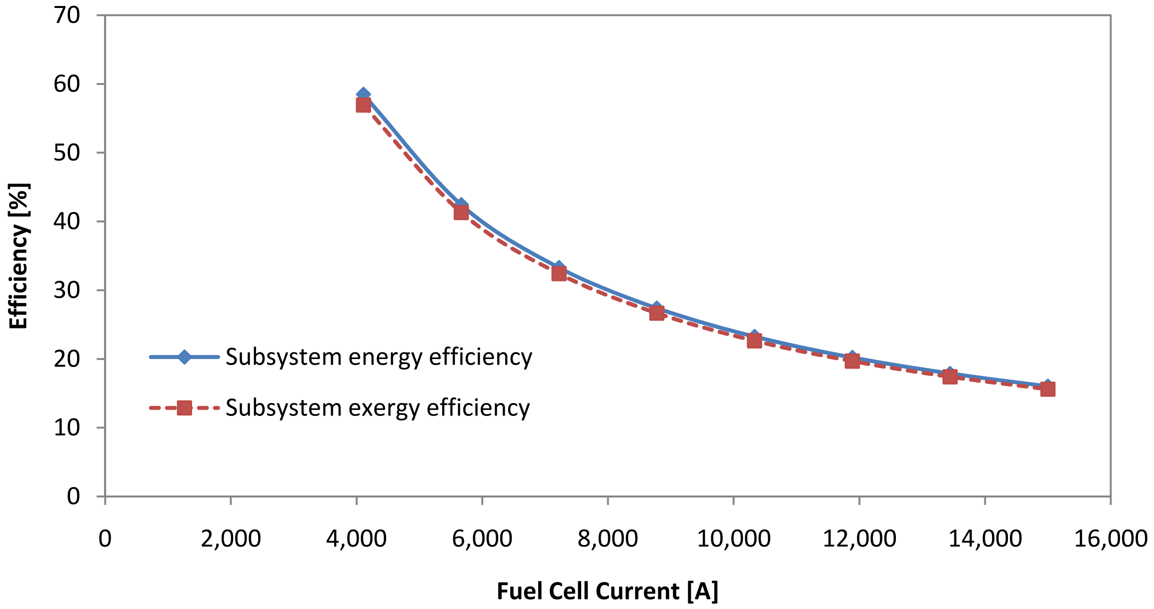

Figure 30: Plot of subsystem energy and exergy efficiencies versus the fuel cell current.

However, increasing the current enlarges the exergy destructions of many components of the hybrid system as shown in Figure 31.

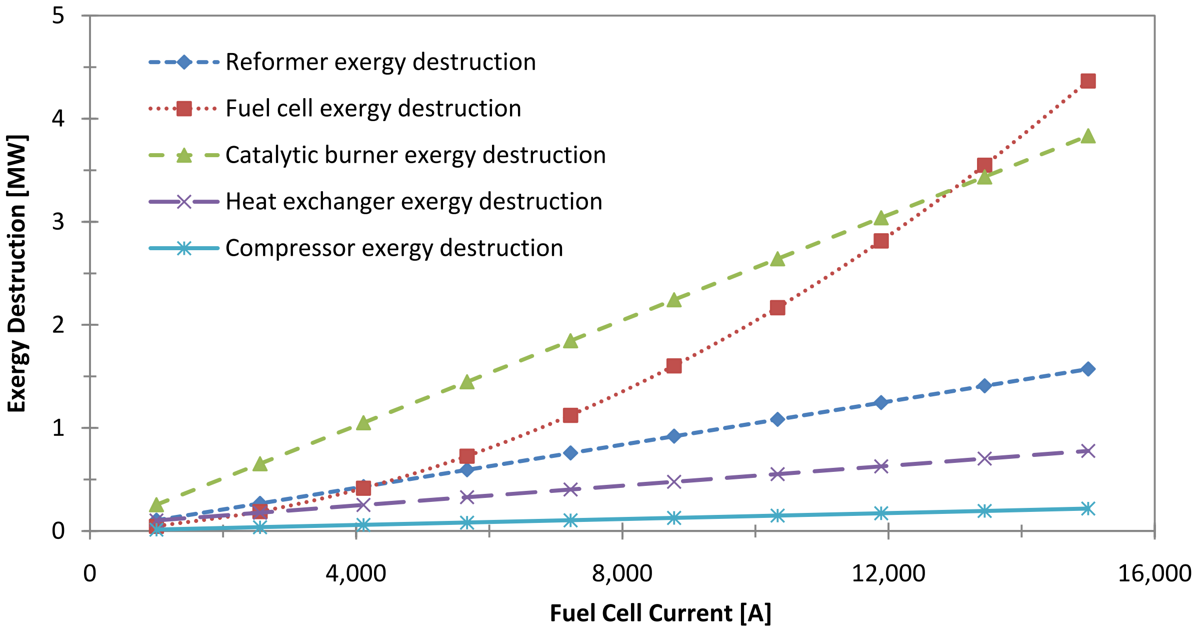

Figure 31: Plot of the exergy destruction of the hybrid system compartments versus the fuel cell current.

In order to increase the fuel cell current, a higher amount of fuel and air are required. Since, more power is required by the compressor to compress the air, the exergy destruction in the compressor increases dramatically. Greater heat loss from the fuel cell and other components of the hybrid system as well as higher fluid friction in pipes destroys even more exergy. Exergy destruction of the hybrid system compartments are not greatly affected by a variation in fuel cell operating temperature or pressure.

In order to increase the fuel cell current, higher fuel and air flow rates would be required for the fuel cell. The variation of the methane and air requirements by increasing the current density is demonstrated in Figure 32. Moreover, Figure 33 demonstrates how the power required by the compressor and the output fuel cell power are increased when higher currents are withdrawn from the fuel cell.

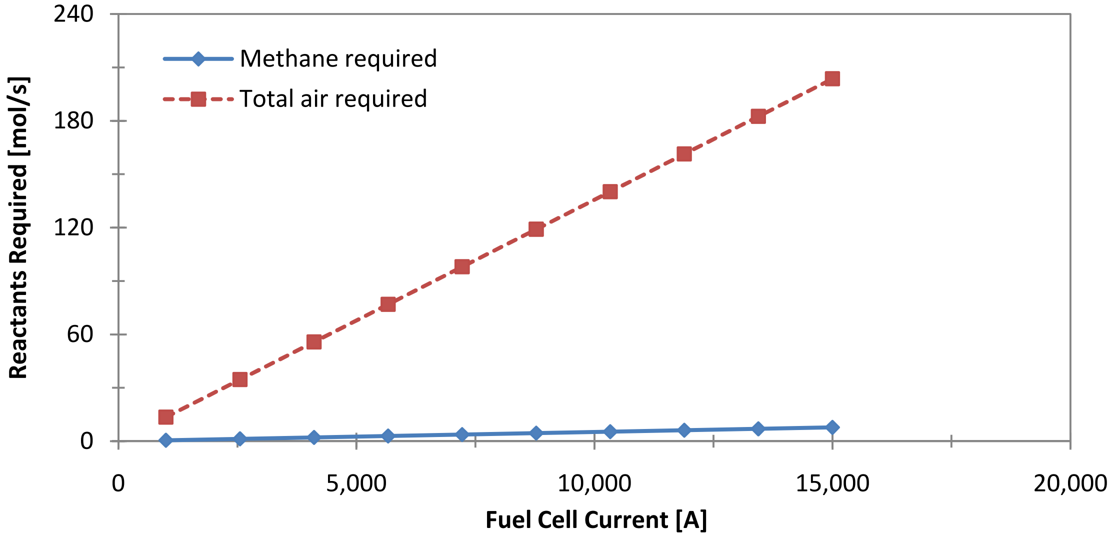

Figure 32: Variation of the molar flow rate of the reactants required versus the fuel cell current.

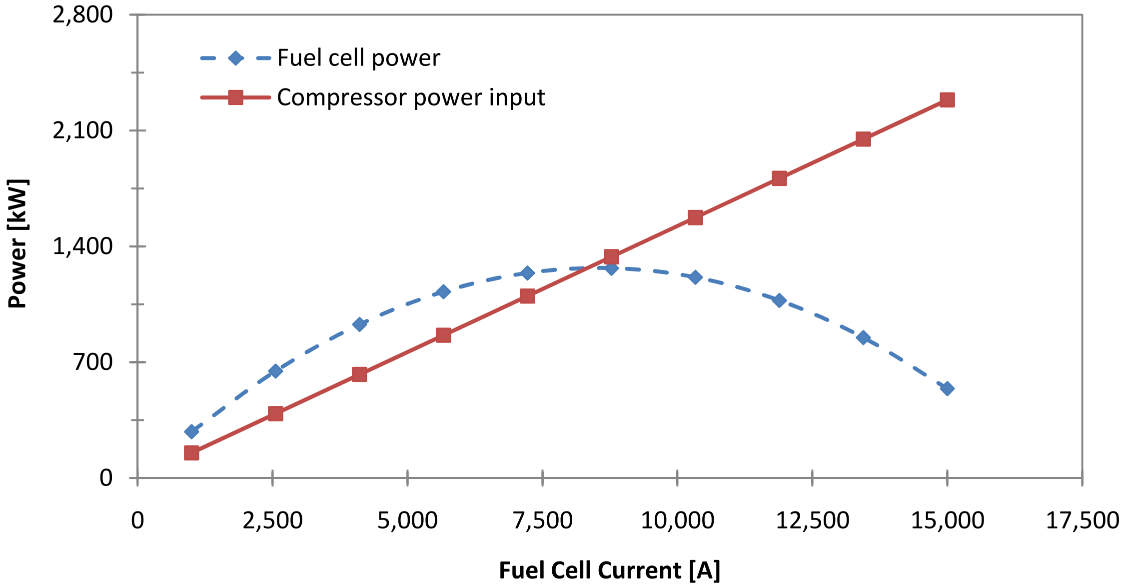

Figure 33: Variation of the compressor power input and fuel cell power output versus the fuel cell current.

From Figure 33, it is not beneficial to run the fuel cell at high current densities. Moreover, operating the fuel cell at its highest power may not be a suitable solution to obtain the best performance from the hybrid system. This is mainly due to the fact that the required compressor power input increases dramatically at high current densities while the fuel cell power may not produce enough power. High system power and efficiency could be maintained by running the fuel cell at low operating pressure and currents.

9.3.3 Effects of fuel cell operating temperature

Variation of the MCFC exergy and energy efficiency and power output for a range of operating temperatures are shown in Figure 34 and Figure 35, respectively. Moreover, its effect on the overall efficiency is shown in Figure 36. Increasing the fuel cell operating temperature improves the reaction kinetics that helps to reduce the MCFC overpotentials.

As a result, the performance of the system is enhanced. In addition, the exergy destruction of the fuel cell is expected to decrease and that is illustrated in Figure 37.

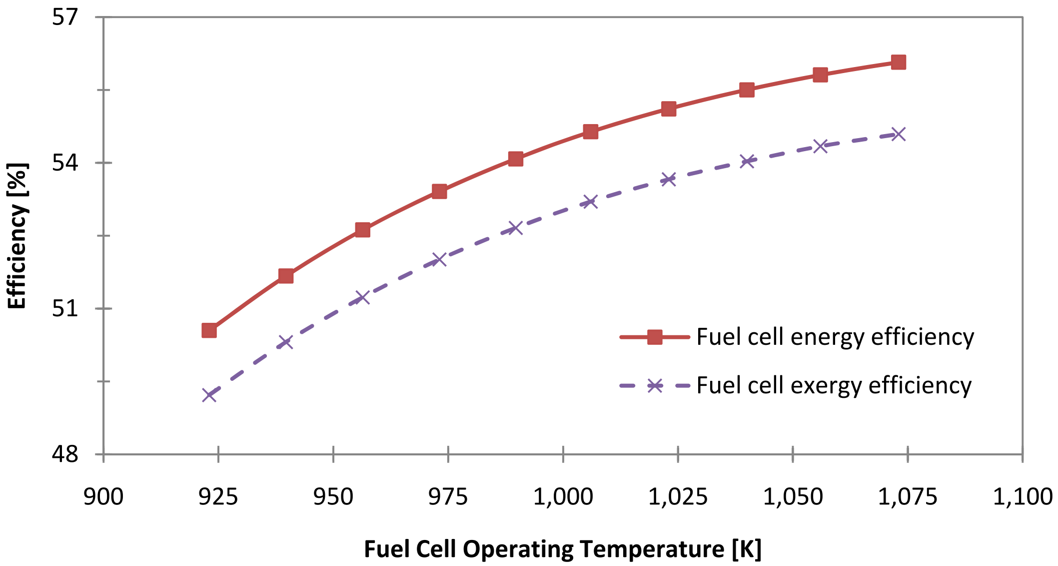

Figure 34: Plot of the fuel cell energy and exergy efficiencies versus the operating temperature.

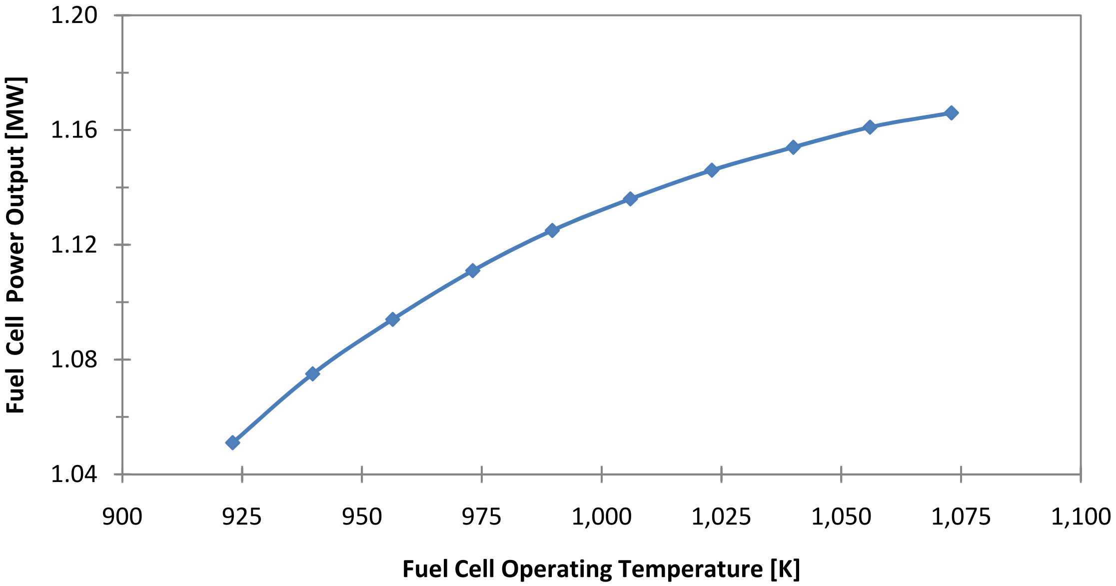

Figure 35: Plot of the fuel cell power output versus operating temperature.

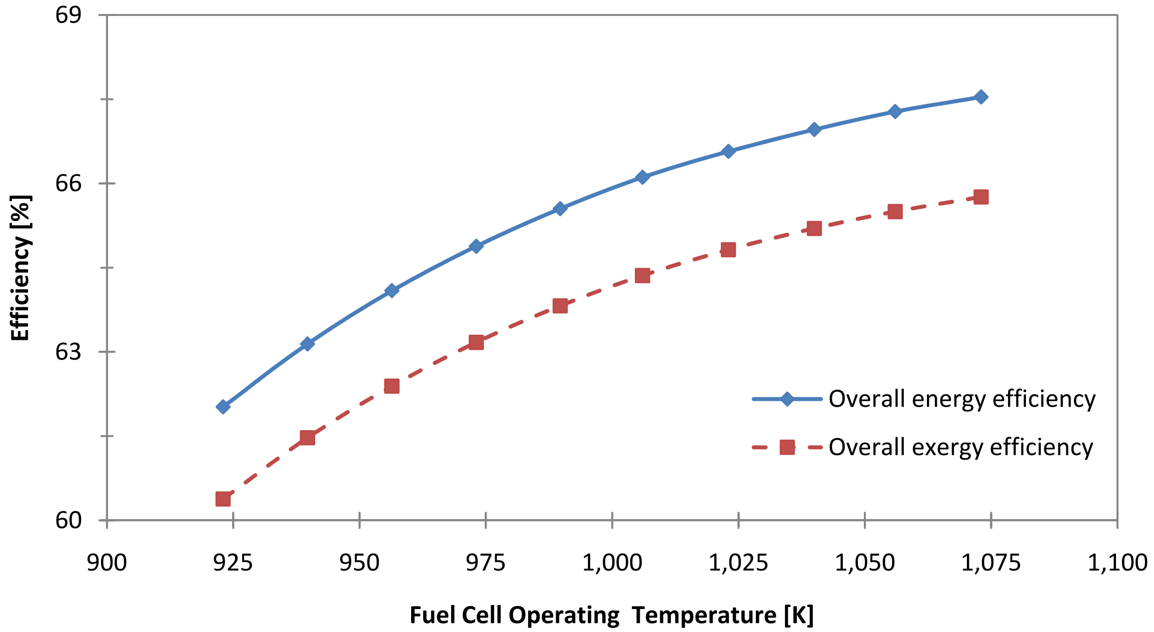

Figure 36: Plot of the overall hybrid system energy and exergy efficiencies versus MCFC operating temperature.

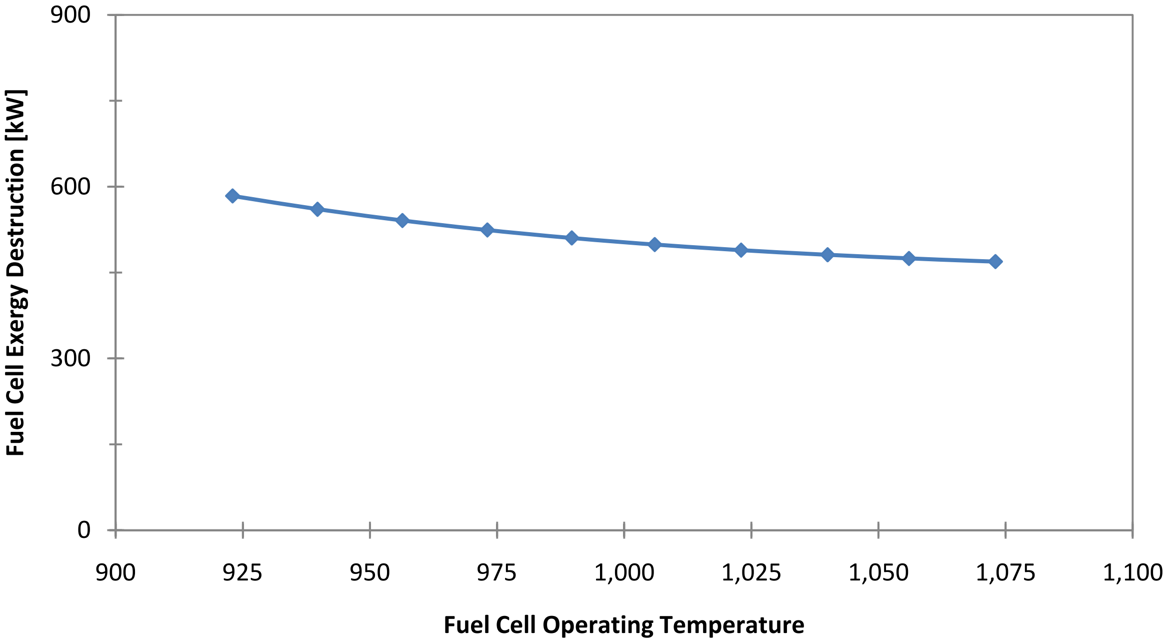

Figure 37: Plot of the fuel cell exergy destruction versus operating temperature.

9.3.4 Effects of fuel cell operating pressure

Figure 38 and Figure 39 illustrate the variation of the fuel cell voltage, irreversible voltage, and energy and exergy efficiency for different fuel cell operating pressures.

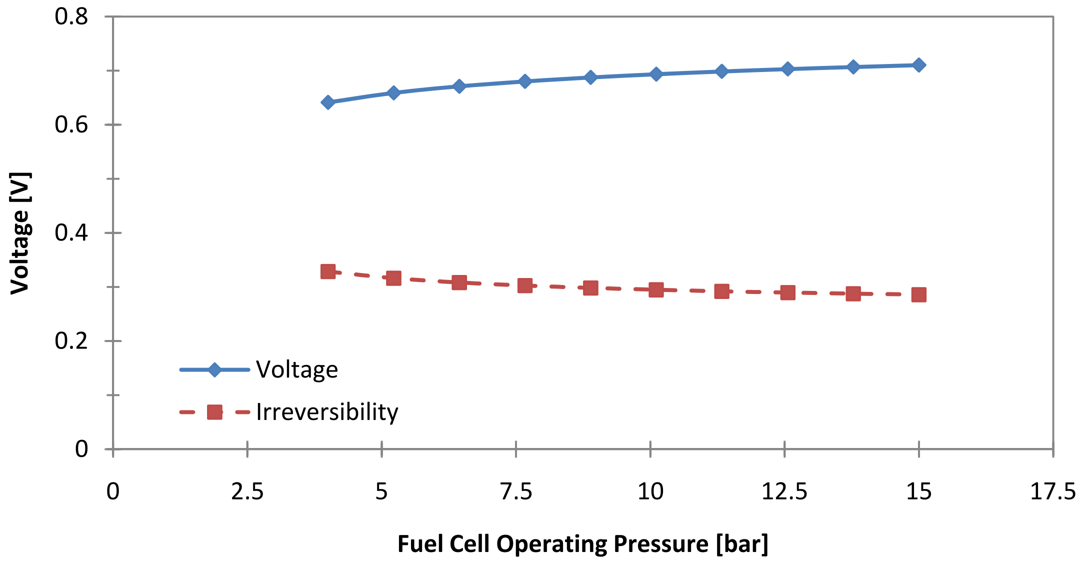

Figure 38: Plot of the fuel cell voltage and irreversible voltage versus operating pressure.

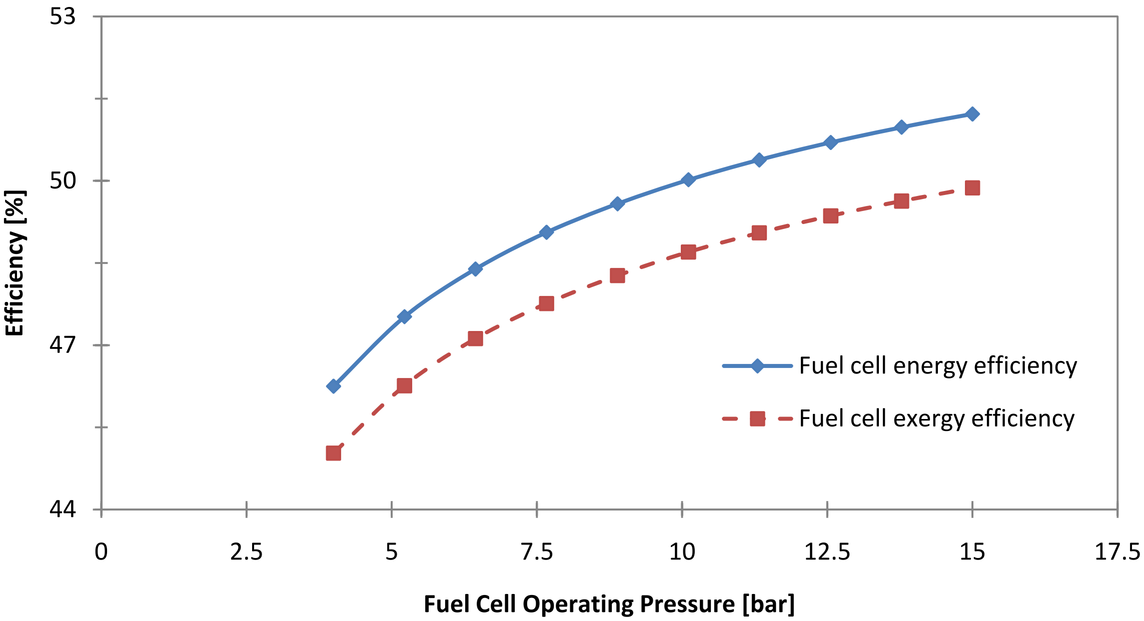

Figure 39: Plot of the fuel cell energy and exergy efficiencies versus operating pressure.

Moreover, the relationship between the fuel cell power output and operating pressure is demonstrated in Figure 40.

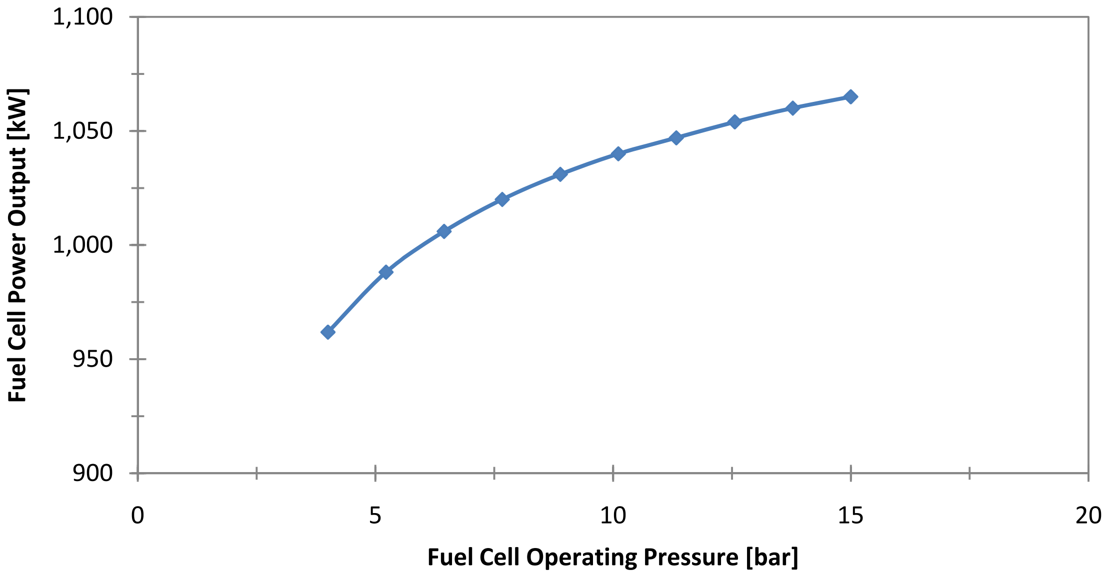

Figure 40: Plot of the fuel cell power output versus operating pressure.

A pattern similar to that of the temperature plots can be seen in these figures. From these graphs, it is clear that increasing the fuel cell operating pressure enhances the performance of the fuel cell. In Figure 38, increasing the operating pressure by a factor of 3 has increases the voltage by at least 0.05 V. In Figure 39 and Figure 40, a dramatic increase in fuel cell efficiency and power output through an increase in operating pressure can be noticed. However, considering the cost issues, fuel cell sealing and power requirement of the compressor at high operating pressures, increasing the operating pressure may not be an economical or beneficial option (e.g. [84, 85]).

9.3.5 Effects of ambient temperature

Figure 41 shows the effects of varying ambient temperature on the mixing chamber, reformer, heat exchanger, compressor and the fuel cell regarding exergy destruction.

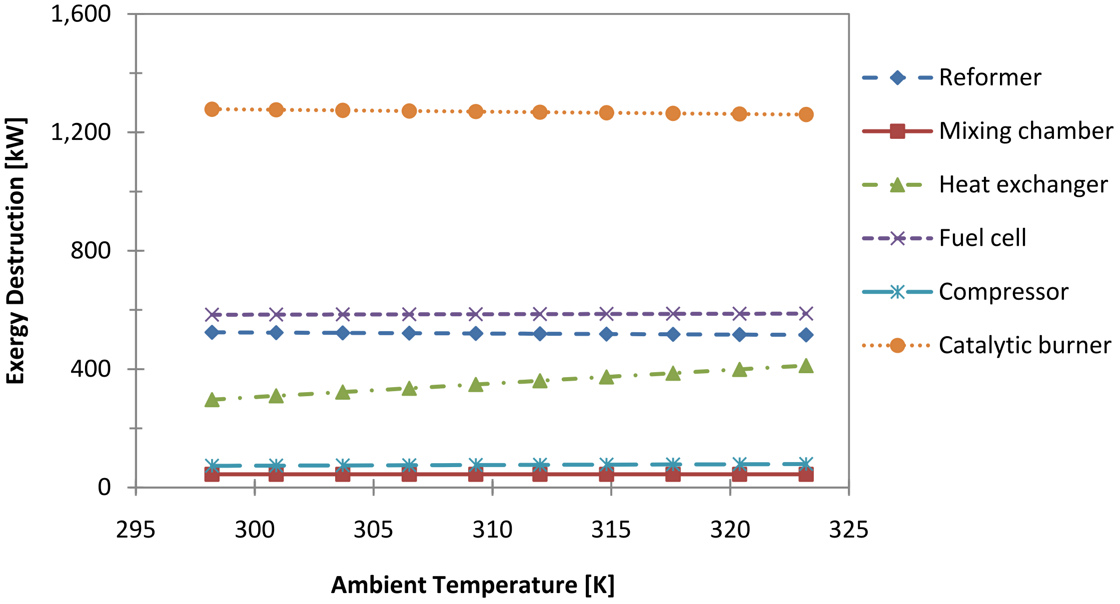

Figure 41: Plot of the exergy destruction of the hybrid system compartments for different ambient temperatures.

As it can be seen from the presented graphs, a variation of ambient temperature does not have a notable effect on the performance of many compartments of the MCFC system. This is mainly because the heat loss from the hybrid system components are assumed to be zero. As a result, the exergetic terms which include both heat and temperature disappear from the balance equations and the graphs show a linear trend.

9.3.6 Effects of ambient pressure

Figure 42 and Figure 43 show the variation of the catalytic burner, reformer and the fuel cell exergy efficiency and exergy destruction for different ambient pressures. Similar to the temperature plots, the variation of pressure does not have a significant effect on the performance of the hybrid system compartments.

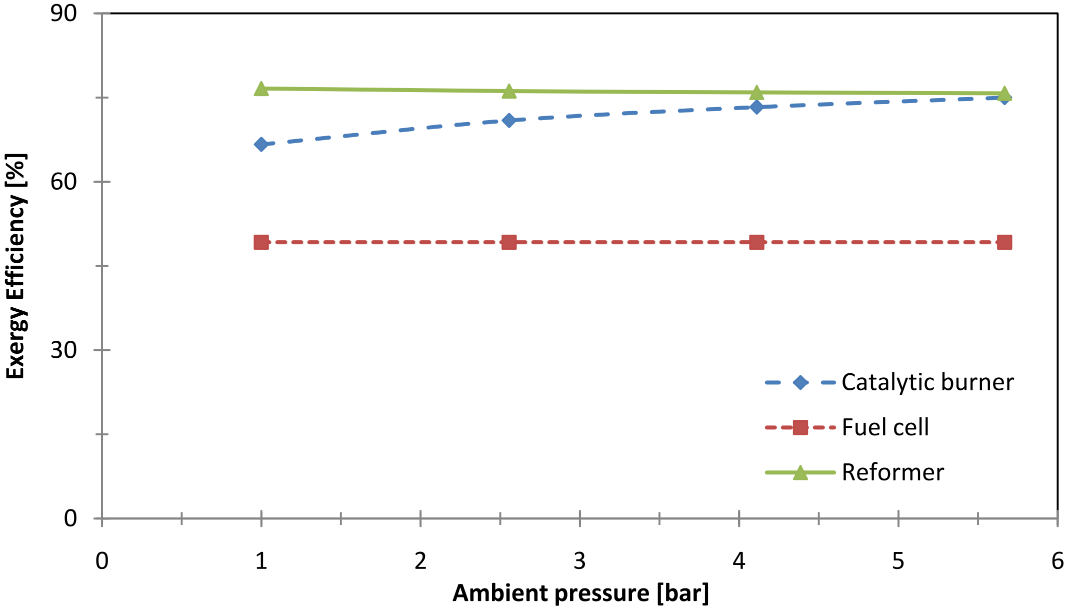

Figure 42: Plot of the exergy efficiency of the hybrid system compartments for different ambient pressures.

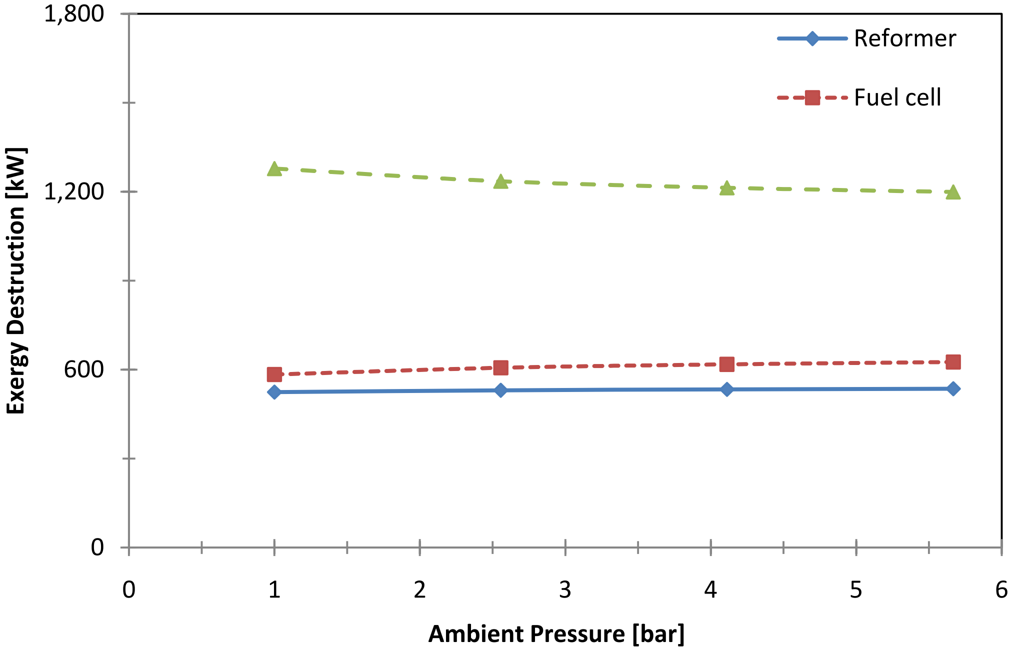

Figure 43: Plot of the exergy destruction of the hybrid system compartments for different ambient pressures.

9.3.7 Exergy destruction

Exergy destruction of the hybrid system components are summarized in Figure 44.

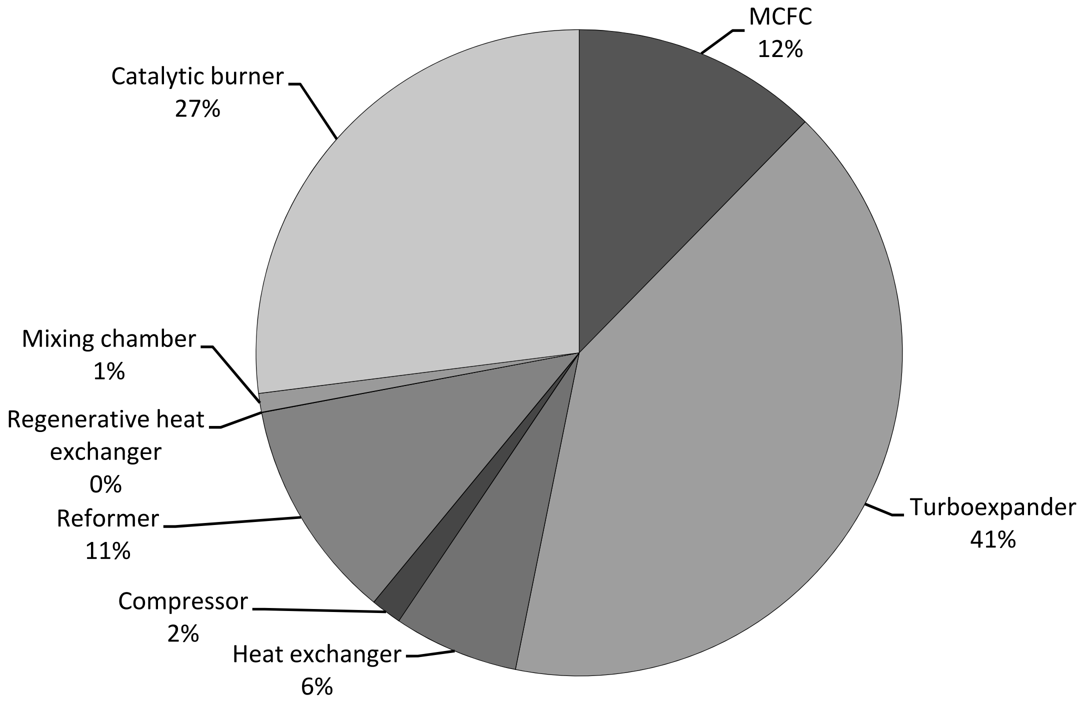

Figure 44: Exergy destruction in different compartments of the Enbridge hybrid system.

It is observed that the turboexpander represents the maximum exergy destruction in the hybrid system studied. This is mainly due to the enormous pressure and temperature drop in the turboexpander. Moreover, components in which chemical reactions occur (i.e. catalytic burner and MCFC) exhibit high exergy destructions.

9.3.8 Heat recovery

Variation of the heat recovery ratio and turboexpander exrgetic efficiency versus the heat recovered in the heat exchanger is shown in Figure 45.

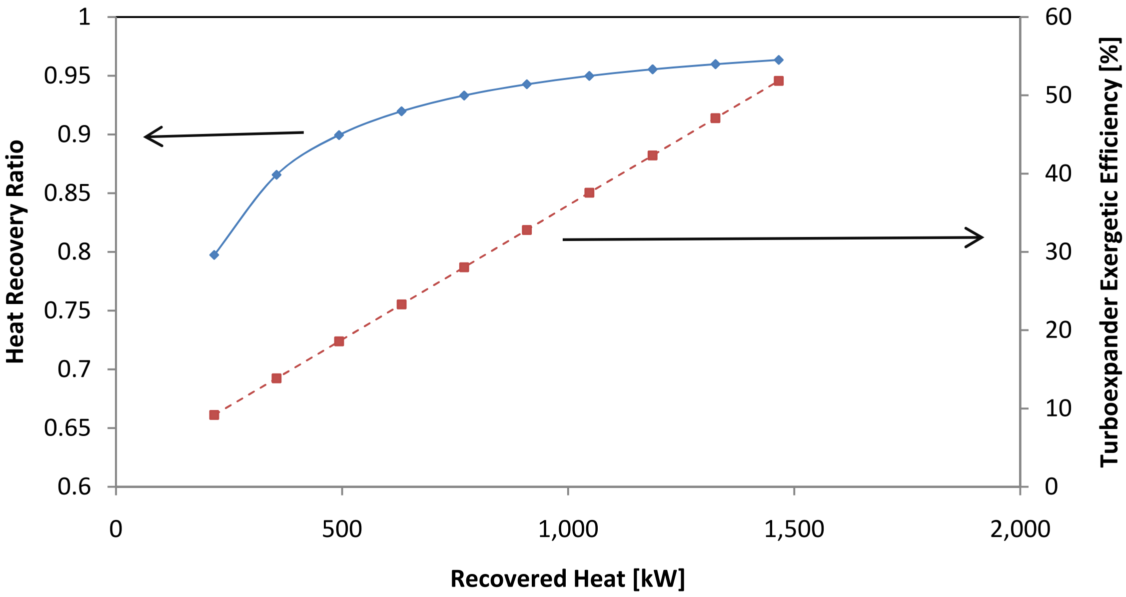

Figure 45: Plot of heat recovery ratio and turboexpander exergy efficiency versus the recovered heat in the heat exchanger

As it can be seen from the presented graph, recovering a higher amount of heat from the fuel cell exhaust enhances the performance of the turboexpander. Heat recovery ratio which shows the effectiveness of the heat exchanger used and also demonstrates the possible performance enhancement that can be achieved from the overall system, increases by an increase in the heat recovery process. The main reason for such improvements is the temperature and exergy increase of the turboexpander inlet stream by utilizing the recovered heat from the fuel cell cathode exhaust.

9.4 Performance optimization

The results obtained from the optimization process are presented here.

Operating temperature, pressure and current density are varied in order to maximize the objective function (i.e. MCFC power output). Moreover, fuel and oxidant flow rates (i.e.

composition) are varied to investigate their effects on the power output and efficiency of the fuel cell. Each analysis is performed for 10 different starting points in order to test the convergence. Figure 46 and Figure 47 demonstrate the convergence plots for different fuel and oxidant flow rates respectively.

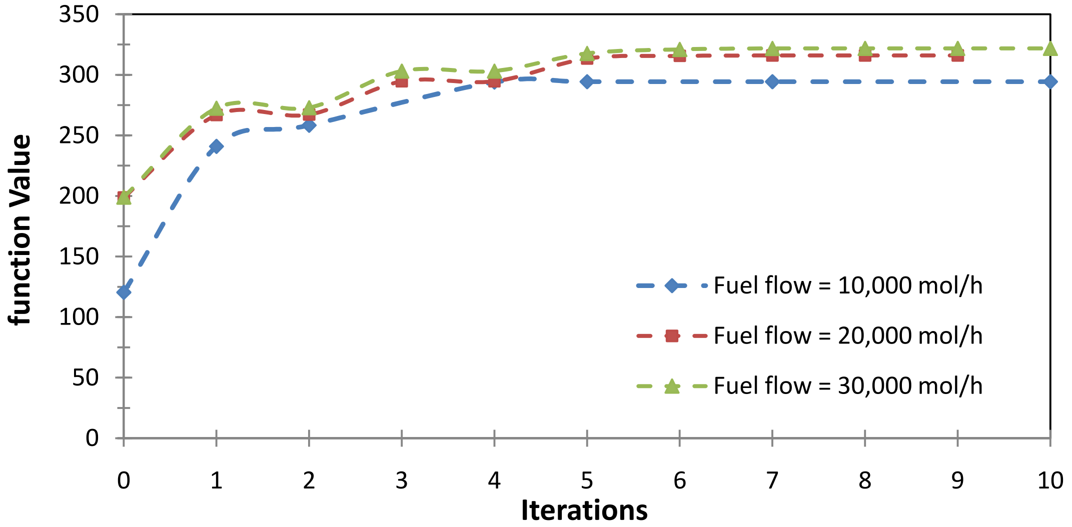

Figure 46: Convergence plot of the optimization process for different fuel flow rates.

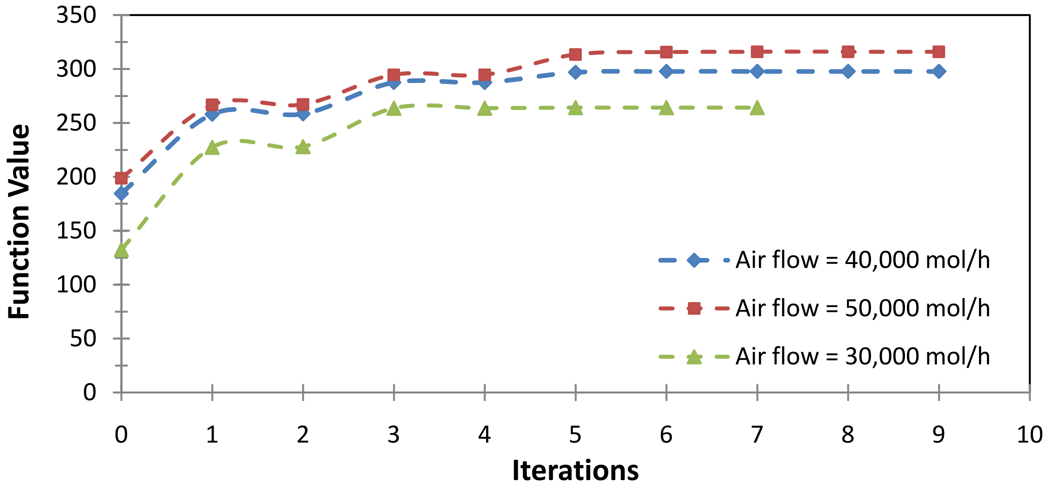

Figure 47: Convergence plot of the optimization process for different air flow rates.

From these graphs, a maximum power output as high as 300 kW is achievable for the MCFC system. In all trial runs, convergence is achieved within about 6 iterations. Global convergence is checked by inspecting the Gradient and Hessian of the objective function at the minimum point [75, 86].

Table 9 is the summary of the results obtained from the optimization process for constant oxidant molar flow rate. Further, Table 10 shows the optimization results when different oxidant flow rates are used in the analysis.

Table 9: Optimization results for constant oxidant molar flow rate.

Fuel flow rate [mol/h]	Oxidant flow [mol/h]	Pressure [atm]	Temperature [K]	Current [A]	Maximum power output [kW]	Directional derivative
10000	40000	10	973.15	4997.67	294.34	1.16E-06
20000	40000	10	973.15	4697.17	297.85	1.44E-07
30000	40000	10	973.15	4947.86	321.90	7.64E-10

Table 10: Optimization results for constant fuel flow rate.

Oxidant flow rate [mol/h]	Fuel flow [mol/h]	Pressure [atm]	Temperature [K]	Current [A]	Maximum power output [kW]	Directional derivative
30000	20000	10	973.15	3895.40	264.20	8.26E-06
40000	20000	10	973.15	4697.17	297.85	1.44 E-7
50000	20000	10	973.15	5128.86	316.04	3.01E-07

The effects of varying the operating temperature and pressure on the fuel cell exergy efficiency at different fuel cell currents are illustrated in Figure 48 and Figure 49, respectively.

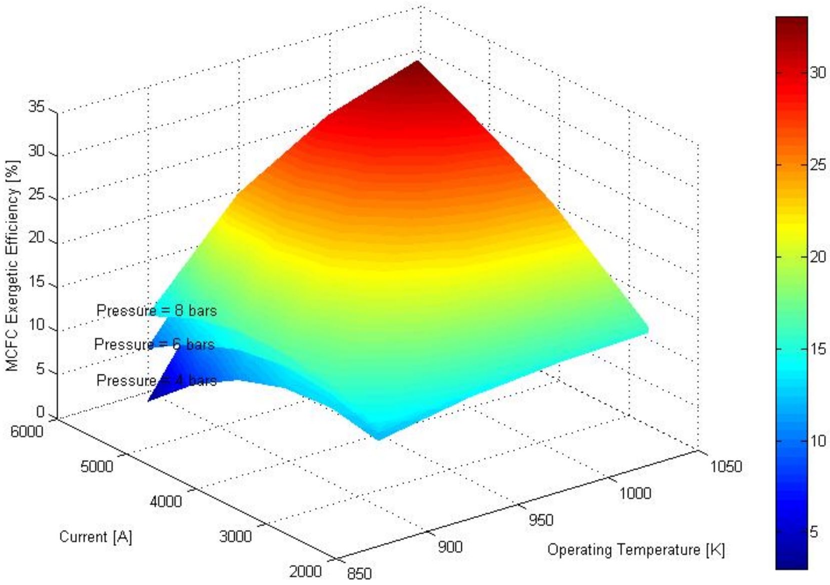

Figure 48: Plot of the MCFC exergetic efficiency versus operating temperature and current for different operating pressures.

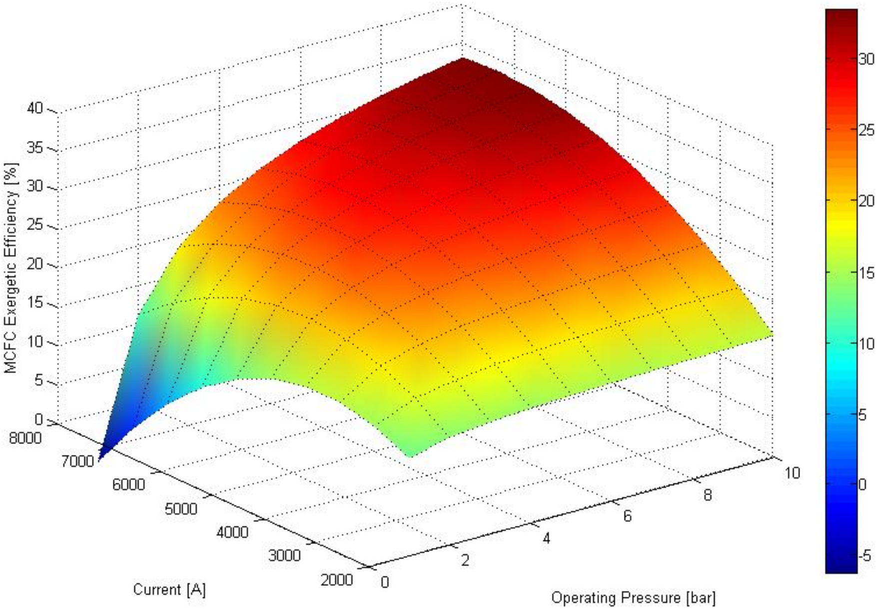

Figure 49: Plot of the MCFC exergetic efficiency versus operating pressure and current for constant operating temperature.

Higher exergetic efficiencies could be achieved by increasing the operating pressure and temperature of the fuel cell. However, as discussed before, because of the nature of the materials used in the MCFC, operation difficulties and cost issues, an excessive increase of fuel cell operating pressure and temperature must be avoided.

9.5 Cost analysis

Figure 50, Figure 51 and Figure 52 demonstrate the variation of revenue, operating cost, potential savings and net income during the operational life time of the hybrid system for electricity costs of 6 (currently paid in Ontario by residential customers), 11 (current wind incentive in Ontario) and 22 (average residential price in Germany) cent/kWh, respectively.

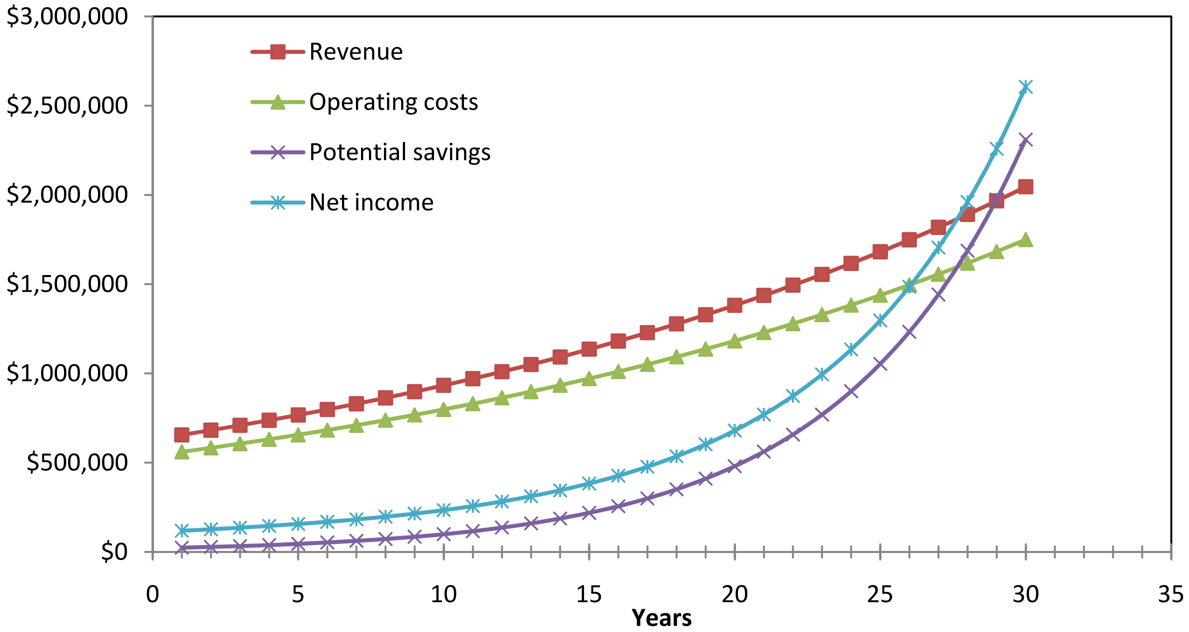

Figure 50: Plot of the revenue, operating cost, potential savings and net income of Enbridge system versus its operational time (using the current price of electricity in Ontario, Canada).

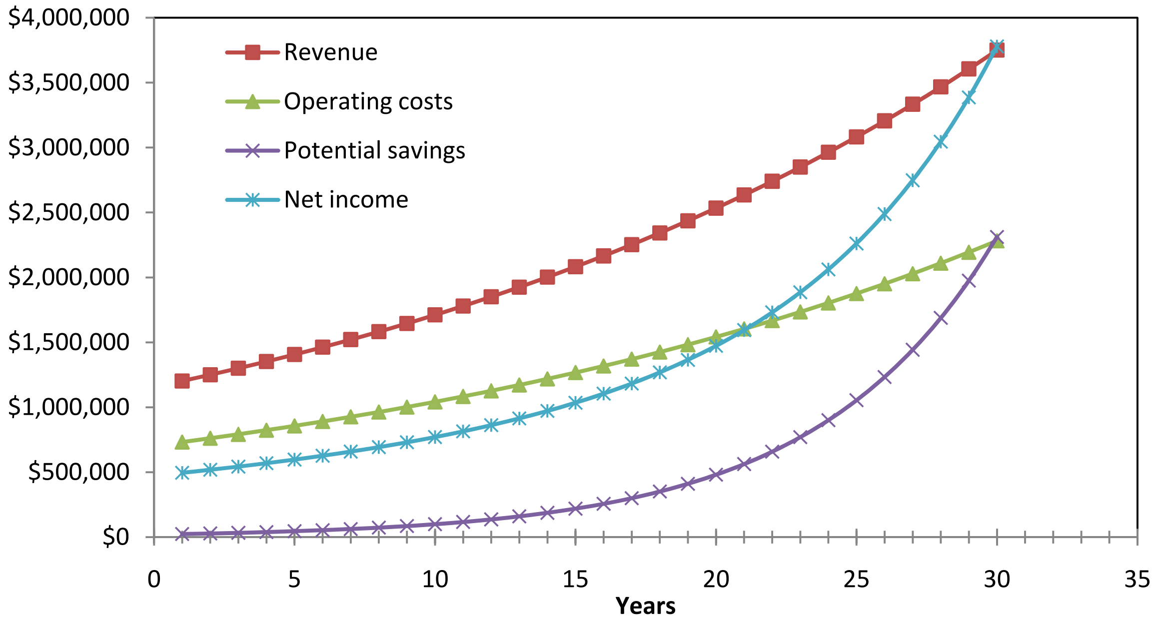

Figure 51: Plot of the revenue, operating cost, potential savings and net income of Enbridge system versus its operational time (using the price of electricity supplied from wind energy).

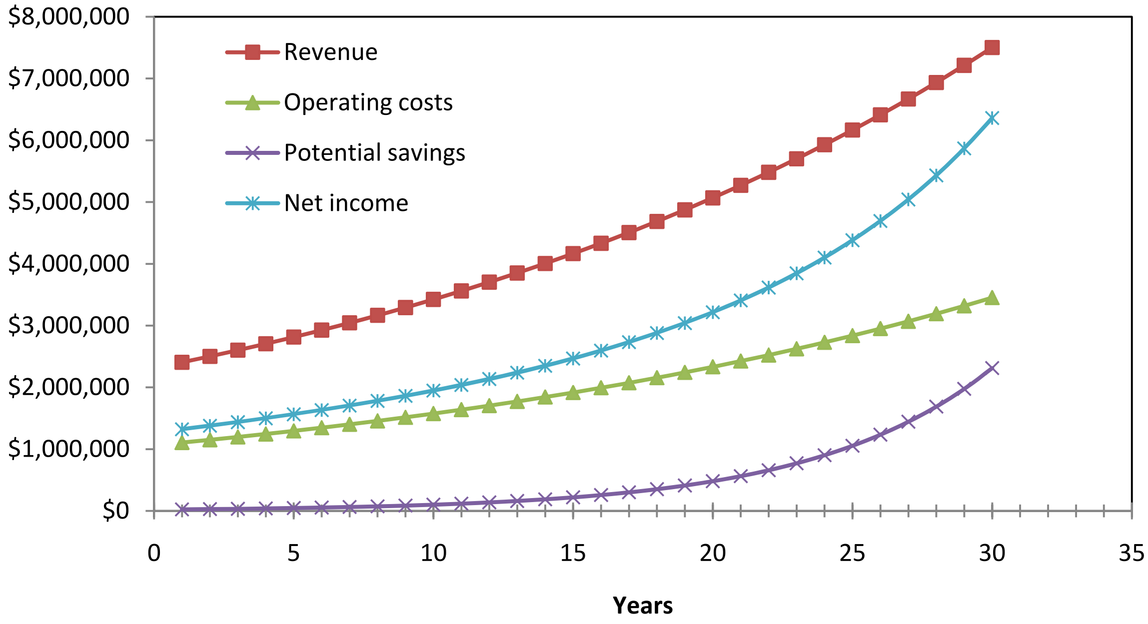

Figure 52: Plot of the revenue, operating cost, potential savings and net income of Enbridge system versus its operational time (using the electricity price in Germany).

Furthermore, the variation of the accumulative income of the hybrid system for different electricity costs are presented in Figure 53, Figure 54 and Figure 55.

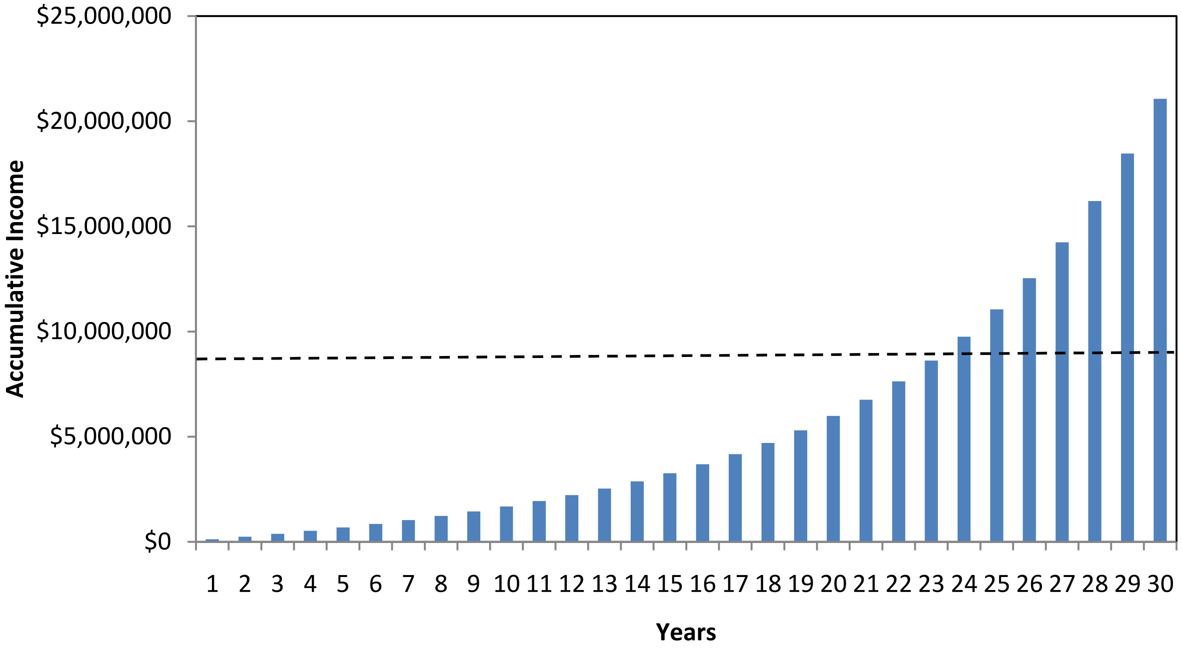

Figure 53: Plot of the accumulative income of Enbridge system versus its operational time (using the current price of electricity in Ontario, Canada).

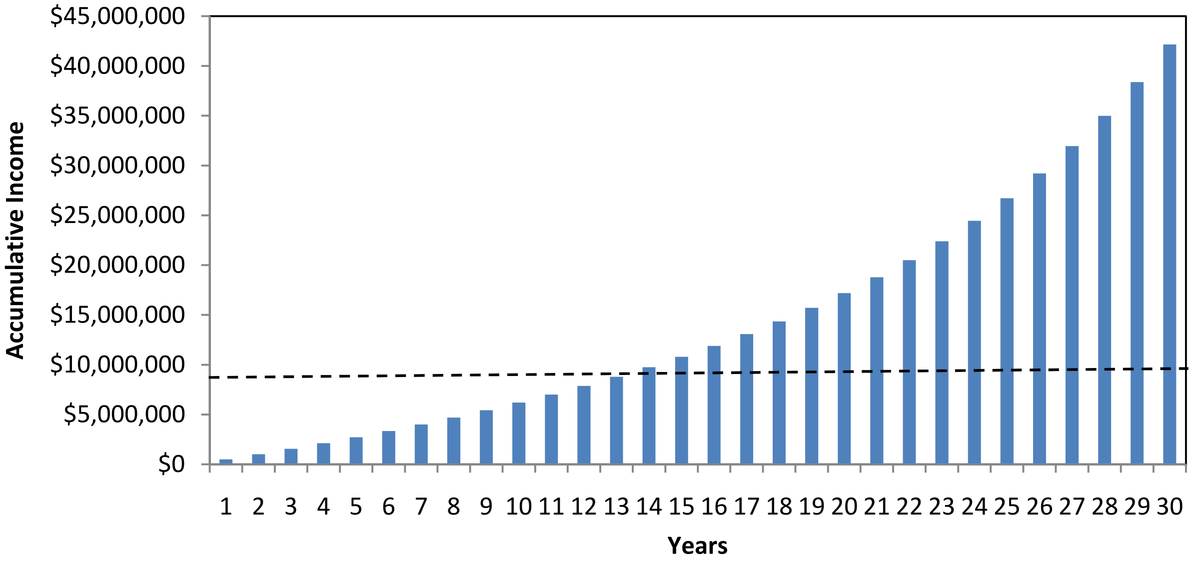

Figure 54: Plot of the accumulative income of Enbridge system versus its operational time (using the price of electricity supplied from wind energy).

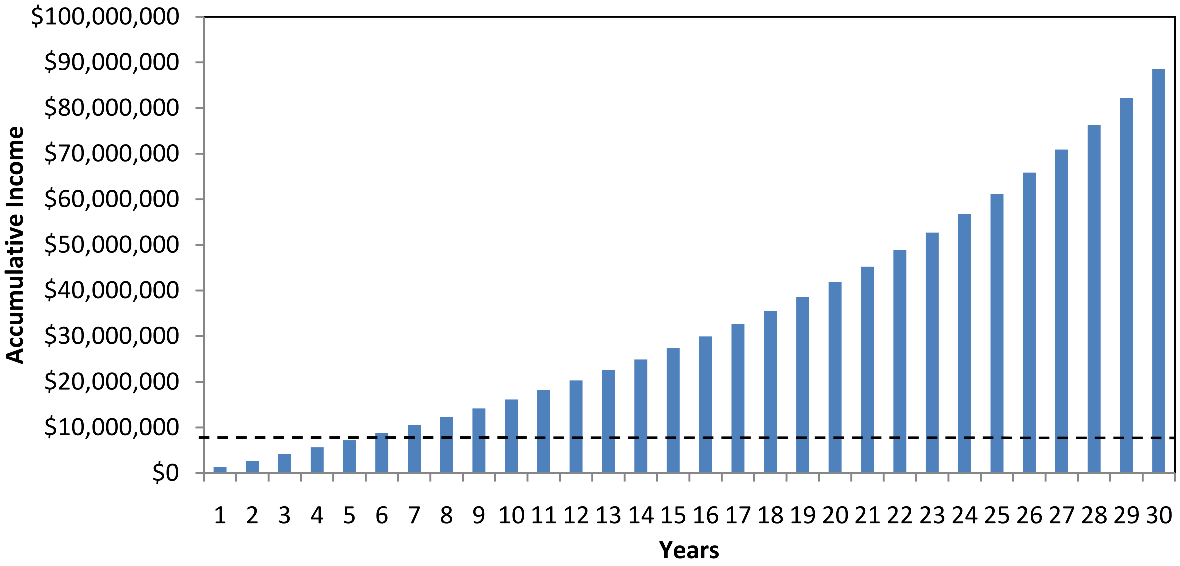

Figure 55: Plot of the accumulative income of Enbridge system versus its operational time (using the electricity price in Germany).

From the plots, depending on the price of the electricity sold, a payoff period of about 10 years is expected. Potential additional revenues which mainly include carbon offsets have a major contribution to the overall income. With present concerns regarding CO_2 production, potential savings through carbon offsets may become a leading advantage of such systems in the near future in comparison to conventional power plants.

Notwithstanding the volatile price of electricity and gas which is not included in this cost analysis, the Enbridge hybrid MCFC system seems to be a promising solution for future supply of energy. For example, from the accumulative income plots it is clear that only 5 years of operational time would be needed to payoff this project if it was in Germany. The payoff period would be 13 years if the electricity price is equivalent to that of wind sources. With the current price of electricity in Ontario, this project will be profitable just after 23 years of operation. This figure will be significantly improved if one considers the contribution of the actual annual revenue from natural gas sold to customers and potential MCFC efficiency improvements over the next 20 years or so.

9.6 Validation

The results obtained from the case studies, optimization and cost analysis are consistent with those of the literature. Figure 56 demonstrates the variation of voltage against the current density for different studies. As it can be seen from the presented graph, the polarization plots of the case studies follow a linear trend similar to the literature which validates the results obtained in this thesis.

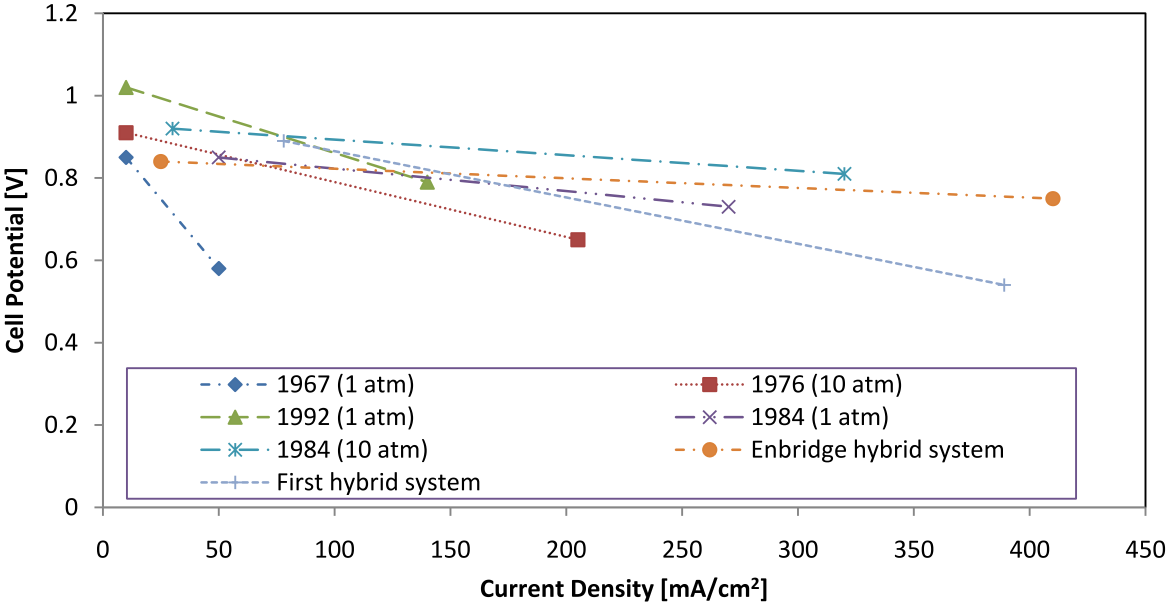

Figure 56: Validation of the polarization curves for the two case studies

In addition, fuel cell stack and overall efficiency calculations also suggest that the results are in a very good agreement to other performance analyses in this area. Moreover, the cost analysis of the Enbridge system predicts an amortization period close to company estimates.

Chapter 10: CONCLUSIONS AND RECOMMENDATIONS

10.1 Conclusions

The energy, exergy, optimization and cost analyses of the MCFC hybrid systems reported in this study allow several conclusions to be drawn.

- Mass, energy and exergy balance equations have helped to understand the systems as well as defining their efficiencies.
- A parametric study has been performed to investigate the variation of system performance for different operating conditions.
- Overall energy and exergy efficiencies as high as 60 % are achievable.
- The cost analysis indicated that the amortization of the Enbridge hybrid system may take up to 15 years of operational time depending on the price of electricity and natural gas sold. However, this figure varies for different electricity and natural gas prices. Moreover, carbon offsets can make a paramount contribution to the overall savings of future MCFC hybrid systems.
- Reducing the exergy destruction of the power plant components and increasing the energetic and exergetic efficiencies, results in reduced emissions, less environmental impact and enhanced sustainability.

10.2 Recommendations

This thesis calls for further thermodynamic analysis of such systems in order to gain the necessary knowledge needed to optimize the performance of hybrid fuel cell systems. Furthermore, pinch analysis and heat transfer improvements could be analyzed to enhance the efficiency of hybrid fuel cell systems.

Finally, through the availability of data from the Enbridge hybrid MCFC system over time (the Enbridge system will begin to provide data in 2009), a comprehensive cost analysis and optimization of the system will be possible. This thesis provides the foundations for such applied analysis.

References

1. Dincer I., Rosen M. A. (2005),'Thermodynamic aspects of renewables and sustainable development', *Renewable and Sustainable Energy Reviews*, (9), pp. 169-189.

2. Dincer I. (2000),'Renewable energy and sustainable development: a crucial review', *Renewable and Sustainable Energy Reviews*, (2), pp. 157-175.

3. Anon, "World Energy Council Technical Report", *Global energy perspectives to 2050 and beyond*, London, 1995.

4. Singh R. (1999),'Will developing countries spur fuel cells surge?', *Chemical Engineering Progress*, pp. 59-66.

5. Sundmacher K., Kienle A., Pesch H. J., Berndt J. F., Huppmann G. (2007). *Molten Carbonate Fuel Cells: Modeling, Analysis, Simulation, and Control* First ed.: Wiley-VCH.

6. Bischoff M. (2006),'Molten carbonate fuel cells: A high temperature fuel cell on the edge to commercialization', *Journal of Power Sources*, (160), pp. 842-845.

7. Dicks A. L. (2004),'Molten carbonate fuel cells', *Current Opinion in Solid State & Material Science*, (8), pp. 379-383.

8. Selman J. R. (2006),'Molten-salt fuel cells—Technical and economic challenges', *Journal of Power Sources*, (160), pp. 852-867.

9. Tomczyk P. (2006),'MCFC versus other fuel cells—Characteristics, technologies and prospects', *Journal of Power Sources*, (160), pp. 858-862.

10. Szargut J., Morris D.R., Steward F.R. (1988). *Exergy Analysis of Thermal, Chemical, and Metallurgical Processes*, New York: John Benjamins Publishing Co.

11. Rosen M.A., "The development and application of a process analysis methodology and code based on exergy, cost, energy and mass", Toronto: University of Toronto, 1986.

12. Granovskii M., Dincer I., Rosen M. A. (2007),'Exergetic life cycle assessment of hydrogen production from renewables', *Journal of Power Sources*, (167), pp. 461-471.

13. Kazim A. (2004),'Exergy analysis of a PEM fuel cell at variable operating conditions', *Energy Conversion & Management*, (45), pp. 1949-1961.

14. Xianglin L., Yaling H., Benhao Y., Zheng M., Xiaoyue L. (2008),'Exergy flow and energy utilization of direct methanol fuel cells based on a mathematic model', *Journal of Power Sources*, (178), pp. 344-352.

15. Hussain M. M., Dincer I., Li X., "Energy and exergy analysis of an integrated SOFC power system", *Proceedings of the Symposium on Thermal and Fluids Engineering*, London, Canada, 1-4 June, 2004, pp. 1080-1090.

16. Kanoglu M., Dincer I., Rosen M. A. (2007),'Understanding energy and exergy efficiencies for improved energy management in power plants', *Energy Policy*, (35), pp. 3967-3978.

17. Dincer I., Sahin A.Z. (2004),'A new model for thermodynamic analysis of a drying process', *International Journal of Heat and Mass Transfer*, (47), pp. 645-652.

18. Wolf T. L., Wilemski G. (1983),'Molten carbonate fuel cell performance model', *Journal of the Electrochemical Society*, (130), No. 1, pp. 48-55.

19. Arato E., Bosio B., Costa P., Parodi F. (2000),'Optimisation of the cell shape for industrial MCFC stacks', *Journal of Power Sources*, (86), pp. 302-308.

20. Bosio B., Costamagna P., Parodi F. (1999),'Modeling and experimentation of molten carbonate fuel cell reactors in a scale-up process', *Chemical Engineering Science*, (54), pp. 2907-2916.

21. Park H. K., Lee Y. R., Kim M. H., Chung G. Y., Nam S. W., Hong S. A., Lim T. H., Lim H. Ch. (2002),'Studies of the effects of the reformer in an internal-reforming molten carbonate fuel cell by mathematical modeling', *Journal of Power Sources*, (104), pp. 140-147.

22. Standaert F., Hemmes K., Woudstra N. (1996),'Analyitical fuel cell modeling', *Journal of Power Sources*, (63), pp. 221-234w.

23. Standaert F., Hemmes K., Woudstra N. (1998),'Analytical fuel cell modeling; non-isothermal fuel cells', *Journal of Power Sources*, (70), pp. 181-199.

24. Yoshiba F., Ono N., Lzaki Y., Watanabe T., Abe T. (1998),'Numerical analyses of the internal conditions of a molten carbonate fuel cell stack: comparison of stack performance for various gas flow types', *Journal of Power Sources*, (7), pp. 328-336.

25. Yoshiba F., Abe T., Watanabe T. (2000),'Numerical analysis of molten carbonate fuel cell stack performance:diagnosis of internal conditions using cell voltage profiles', *Journal of Power Sources*, (87), pp. 21-27.

26. Arato E., Bosio B., Costa P., Parodi F. (2001),'Preliminary experimental and theoretical analysis of limit performance of molten carbonate fuel cells', *Journal of Power Sources*, (102), pp. 74-81.

27. Koh J. H., Kang B. S., Lim H. Ch. (2000),'Effect of various stack parameters on temperature rise in molten carbonate fuel cell stack operation', *Journal of Power Sources*, (91), pp. 161-171.

28. Koh J. H., Kang B. S., Lim H. Ch. (2001),'Analysis of Temperature and Pressure Fields in Molten Carbonate Fuel Cell Stacks', *The American Institute of Chemical Engineers*, (47), No. 9, pp. 1941-1956.

29. Koh J. H., Kang B. S. (2001),'Theoretical study of a molten carbonate fuel cell stack for pressurized operation', *International Journal of Energy Research*, (25), pp. 621-641.

30. Koh J. H., Kang B. S., Lim H. Ch. (2002),'Consideration of numerical simulation parameters and heat transfer models for a molten carbonate fuel cell stack', *Chemical Engineering Journal*, (87), pp. 367-379.

31. Li Z., Huaxin L., Baolian Y., Huamin Z., Zhigang Sh., Pingwen M., Mojie Ch. (2006),'A study on the start-up and performance of a kW-class molten carbonate fuel cell (MCFC) stack', *Electrochimica Acta*, (51), No. 26, pp. 5698-5702.

32. Freni S., Maggio G., Cavallaro S. (1996),'Ethanol steam reforming in a molten carbonate fuel cell: a thermodynamic approach', *Journal of Power Sources*, (62), pp. 67-73.

33. Varbanov P., Klemes J., Shah R. K., Shihn H. (2006),'Power Cycle Integration and Efficiency Increase of Molten Carbonate Fuel Cell Systems', *Journal of Fuel Cell Science and Technology*, (3), pp. 375-383.

34. Bocci E., Orecchini F., Carlo Di A. (2006),'MCFC and microturbine power plant simulation', *Journal of Power Sources*, (160), pp. 835-841.

35. Lunghi P., Ubertini S., Desideri U. (2001),'Highly efficient electricity generaiton through a hybrid molten carbonate fuel cell-closed loop gas turbine', *Energy Conversion & Management*, (42), pp. 1657-1672.

36. Lobachyov K. V., Richter H. J. . (1997),'Addition of Highly Efficient Bottoming Cycles for the /Vth-Generation Molten Carbonate Fuel Cell Power Plant', *Journal of Energy Resources Technology*, (119), pp. 103-108.

37. De Simon G., Parodi F., Fermeglia M., Taccani R. (2003),'Simulation of process for electrical energy production based on molten carbonate fuel cells', *Journal of Power Sources*, (115), pp. 210-218.

38. Kang B. S., Koh J. H., Lim H. Ch. (2002),'Effects of system configuration and operating condition on MCFC system efficiency', *Journal of Power Sources*, (108), pp. 232-238.

39. Lunghi P., Bove R., Desideri U. (2003),'Analysis and optimization of hybrid MCFC gas turbines plants', *Journal of Power Sources*, (118), pp. 108-117.

40. Braun R. J., Gaggioli R. A., Dunbar W. R. (1999),'Improvements of a Molten Carbonate Fuel Cell Power Plant via Exergy Analysis', *Journal of Energy Resources Technology*, (121), pp. 227-285.

41. Sugiura K., Naruse I. (2002),'Feasibility study of the co-generation system with direct internal reforming-molten carbonate fuel cell (DIR-MCFC) for residential use', *Journal of Power Sources*, (106), pp. 51-59.

42. Silveira J. L., Leal E. M., Ragonha Jr. L. F. (2001),'Analysis of a molten carbonate fuel cell: cogeneration to produce electricity and cold water', *Energy*, (26), pp. 891-904.

43. Leal E. M., Silveira J. L. (2002),'Study of fuel cell co-generation systems applied to dairy industry', *Journal of Power Sources*, (106), pp. 102-108.

44. Li X. (2005). *Principles of Fuel Cells*, 1st ed.: Taylor & Francis.

45. Larminie J., Dicks A. (2003). *Fuel Cell System Explained*, 2nd ed.: Wiley.

46. Durante G., Vegni S., Capobianco P., Golgovici F. (2005),'High temperature corrosion of metallic materials in molten carbonate fuel cells environment', *Journal of Power Sources*, (152), pp. 204-209.

47. Capobianco P., Guarnone P., Leonini M., Torazza A., "High temperature corrosion in molten carbonate fuel cells for power generation", *International AIM/NACE conference*, Venice, 2000, pp. 189-196.

48. Bergman B., Lagergren C., Lindbergh G., Schwartz S., Zhu B. (2001),'Contact corrosion resistance between the cathode and current collector plate in the molten carbonate fuel cell', *Journal of Electrochemical Society*, (148), pp. A38-A43.

49. Makkus R. C., Sitters E. F., Nammensma P., Huijsmans J. P. P., "MCFC electrolyte behaviour: Li/K vs. Li/Na carbonate", *Fourth International Symposium on Carbonate Fuel Cell Technology*, Netherlands, 1997, pp. 344-352.

50. Mohn H., Wendt H. (1995),'Molecular thermodynamics of molten salt evaporation. 4. The evaporation of molten carbonates in atmospheres containing CO2 and water vapor', *Zeitschrift Für Physikalische Chemie* (192), No. 1, pp. 101-119.

51. Nishimura T., Fujita Y., Urushibata H., Sasaki A., *Fuel Cell Seminar*, 1996, pp. 363-366.

52. Higaki J., Nagashima J., Terada S., *Fuel Cell Seminar*, 1998, pp. 146-149.

53. Wolfenstine J., Sperry C. D., Goretta K.C., Routbort J. L., Lanagan M. T., Bloom I., Kaun T. D., Krumpelt M. (1997),'Elevated-temperature creep strength of $LiFeO_2$, $LiCoO_2$ and NiO-5(at.%)Li_2O', *Materials Letters*, (31), pp. 251-254.

54. Oh I. H., Yoon S. P., Lim T. H., Nam S. W., Hong S. A., Lim H Ch. (1996),' Effect of the structural changes of the Ni-Cr anode on the molten carbonate fuel cell performance', *Denki Kagaku*, (64), No. 6, pp. 497-507.

55. Basu S. (2007). *Recent Trends in Fuel Cell Science and Technology*, First ed.: Springer.

56. Yuh C. Y., Selman J. R. (1991),'The polarization of Molten Carbonate Fuel Cell Electrodes, I. Analysis of Steady-State Polarization Data', *Journal of Electrochemical Society*, (138), pp. 3642-3648.

57. Chan S. H., Low C. F., Ding O. L. (2002),'Energy and exergy analysis of simple solid-oxide fuel-cell power systems ', *Journal of Power Sources*, (103), pp. 188-200.

58. Cengel Y.A., Boles M. A. (2001). *Thermodynamics: An Engineering Approach*, Forth ed.: Mcgraw-Hill College.

59. Xiang J. Y., Cali M., Santarelli M. (2004),'Calculation for physical and chemical exergy of flows in systems elaborating mixed-phase flows and a case study in an IRSOFC plant', *International Journal of Energy Research*, (28), pp. 101-115.

60. Chase M. W.,(1998) NIST-JANAF Thermodynamical Tables,Forth ed., Journal of Physical Chemistry Reference Data, Monograph 9 pp. 1-1952

61. Riveo R., Garfias M. (2006),'Standard chemical exergy of elements updated', *Energy*, (31), pp. 3310-3326.

62. Sato N. (2004). *Chemical Energy and Exergy: An Introduction to Chemical Thermodynamics for Engineers*, 1st ed.: Elsevier Science.

63. Stefan, "http://exergoecology.com/", 2007.

64. Morris D. R., Szargut J. (1986),'Standard chemical exergy of some elements and compounds on the planet earth', *Energy*, (8), No. 11, pp. 733-755.

65. Dincer I., Rosen M. A. (2007). *Exergy, Energy, Environment and Sustainable Development*, First ed.: Elsevier.

66. Sonntag R. E., Borgnakke C., Van Wylen G. J. (2003). *Fundamentals of Thermodynamics*, Sixth ed.: John Wiley & Sons Inc.

67. Massie D. D., Boettner D. D., Massie C. A. (2005),'Residential experince with proton exchange membrane fuel cell systems for combined heat and power', *Journal of Fuel Cell Science and Technology*, (2), No. 4, pp. 263-267.

68. Wu J. Y., Wang R. Z., Xu Y. X. (2002),'Dynamic analysis of heat recovery process for a continuous heat recovery adsorption heat pump', *Energy Conversion & Management*, (43), pp. 2201-2211.

69. Angelino G., Invernizzi C., Iora P. (2008),'Closed versus open cycle energy recovery from solid oxide fuel cells', *Journal of Power and Energy*, (222), No. 4, pp. 371-379.

70. Klein S. A., Engineering Equation Solver, Commercial V8.158 F-Chart Software Software, 2003

71. Moran M. J., Shapiro H. N. (2007). *Fundamentals of Engineering Thermodynamics* Sixth ed.: Wiley.

72. Bejan A., Tsastsaronis G., Moran M. (1995). *Thermal Design and Optimization*, 1st ed.: Wiley-Interscience.

73. "http://hydrogen.pnl.gov/cocoon/morf/hydrogen": Hydrogen Analysis Resource Center, 2006.

74. Keenan J. H., Kaye J. (1984). *Gas Tables*: John Wiley & sons Inc.

75. Antoniou A., Lu W.S. (2007). *Practical Optimization: Algorithms and Engineering Applications*, New York: Springer.

76. "http://www.cs.ubc.ca/~ascher/542/chap11.pdf": The University of British Columbia.

77. "http://navier.engr.colostate.edu/": Colorado state university, 2008.

78. "www.bloomberg.com/energy": Bloomberg, 2008.

79. "www.directenergy.com/EN/Ontario": Direct Energy, 2008.

80. "http://www.statcan.ca/menu-en.htm": Statistics Canada, 2008.

81. "http://www.oeb.gov.on.ca/OEB": Ontario Energy Board, 2008.

82. "www.stromprecise.de/strom.php", 2008.

83. Dincer I. (2002),'The role of exergy in energy policy making', *Energy Policy*, (30), pp. 137-149.

84. Hirschenhofer J. H., Stauffer D. B., Engelman R. R., "Fuel Cell Handbook ": Pearsons Corporation, 1998.

85. Blomen L., Leo J. M. J., Mugerwa M. (1993). *Fuel Cell Systems*, New York: Plenum Publishing.

86. Nocedal J., Wright S. J. (2006). *Numerical Optimization*, second ed.: Springer.